

12

20000801203

NSWC TR 85-114

AD-A166 808

DTIC  
ELECTE  
APR 24 1986  
S D

**FRAGMENT AND DEBRIS HAZARDS  
FROM ACCIDENTAL EXPLOSIONS**

BY J. C. HOKANSON, L. M. VARGAS, M. G. WHITNEY, P. K. MOSELEY, J. W. CARDINAL  
(SOUTHWEST RESEARCH INSTITUTE)

FOR NAVAL SURFACE WEAPONS CENTER  
RESEARCH AND TECHNOLOGY DEPARTMENT

13 JULY 1981

Approved for public release; distribution is unlimited.

DTIC FILE COPY



**NAVAL SURFACE WEAPONS CENTER**

Dahlgren, Virginia 22448-5000 • Silver Spring, Maryland 20903-5000

Reproduced From  
Best Available Copy

86-4 24 003

UNCLASSIFIED

SECURITY CLASSIFICATION OF THIS PAGE (When Data Entered)

REPORT DOCUMENTATION PAGE		READ INSTRUCTIONS BEFORE COMPLETING FORM
1. REPORT NUMBER NSWC TR 85-114	2. GOVT ACCESSION NO. <i>AD-A166 808</i>	3. RECIPIENT CATALOG NUMBER
4. TITLE (and Subtitle) FRAGMENT AND DEBRIS HAZARDS FROM ACCIDENTAL EXPLOSIONS		5. TYPE OF REPORT & PERIOD COVERED Final Report 09-05-80 - 07-05-81
7. AUTHOR(s) J. C. Hokanson      P. K. Moseley L. M. Vargas        J. W. Cardinal M. G. Whitney		6. PERFORMING ORG. REPORT NUMBER 02-6247
9. PERFORMING ORGANIZATION NAME AND ADDRESS Southwest Research Institute 6220 Culebra Road San Antonio, Texas 78284		8. CONTRACT OR GRANT NUMBER(s) N60921-80-C-0267
11. CONTROLLING OFFICE NAME AND ADDRESS Naval Surface Weapons Center (Code R15) 10901 New Hampshire Avenue Silver Spring, MD 20903-5000		10. PROGRAM ELEMENT, PROJECT, TASK AREA & WORK UNIT NUMBERS NIF, O, O, R15JK
14. MONITORING AGENCY NAME & ADDRESS (if different from Controlling Office)		12. REPORT DATE 13 July 1981
		13. NUMBER OF PAGES 111
		15. SECURITY CLASS. (of this report)  UNCLASSIFIED
		15a. DECLASSIFICATION/DOWNGRADING SCHEDULE
16. DISTRIBUTION STATEMENT (of this Report) Approved for public release, distribution unlimited.		
17. DISTRIBUTION STATEMENT (of the abstract entered in Block 20, if different from Report)		
18. SUPPLEMENTARY NOTES <i>fr. back</i> <i>(Naval Ordnance Hazards Analysis and Risk Management)</i>		
19. KEY WORDS (Continue on reverse side if necessary and identify by block number) Fragment                      Debris Density;                      Navy Ships; Debris                              Prediction Methodology; <del>Reinforced Concrete</del> Explosion Hazards              NOHARM                              Hazardous Fragment; Fragmentation;                      Internal Explosions;                      Hazardous Debris; Trajectory;                              Hazard Criteria		
20. ABSTRACT (Continue on reverse side if necessary and identify by block number) The objective of this program was to provide the necessary methodologies and data required to begin implementation of the NOHARM system. This program was divided into three tasks: (1) perform a comprehensive review of the technical literature, (2) develop new methodologies for predicting the debris environment resulting from internal explosions in reinforced concrete structures, and (3) develop a master plan to derive the fragment/debris input data required for implementation of the Explosives Hazards Model of NOHARM. The Task 1 effort resulted in the identification of 102 useful reports and papers. <u>A bibliographic</u>		

UNCLASSIFIED

SECURITY CLASSIFICATION OF THIS PAGE (When Data Entered)

20. (CONT.)

listing was prepared and included as part of this report. The Task 2 effort resulted in a model for estimating the number of fragment/debris missiles per unit of ground surface area which exceed specified impact energy levels. The Task 3 effort resulted in a scale model test program and similitude analysis which can be used to generalize the test results. Keywords:

UNCLASSIFIED

## FOREWORD

This report documents the results of an analytical program performed by the Southwest Research Institute (SwRI). The program was intended to provide some of the necessary methodologies and data required to begin implementation of the Naval Ordnance Hazards Analysis and Risk Management (NOHARM) System during the 1980-81 timeframe. NOHARM is a software system developed by the Naval Civil Engineering Laboratory (NCEL) (W. Keenan, Program Manager). It is designed to provide information required to assess and manage the risks to personnel and property exposed to hazards associated with the handling of naval ordnance.

This effort was performed by Southwest Research Institute (J. C. Hokanson, principal investigator) for the Naval Surface Weapons Center (NSWC) under Contract Number N60921-80-C0267. Dr. J. M. Ward (NSWC) was the contract monitor. Dr. L. Huang (NCEL) monitored the NSWC effort performed under Contract N68305-80-WR00101.

This report does not reflect the official view or final judgement of NSWC. Its main purpose is to publish the review of technical literature and the SwRI approach for the predictive methodologies and master test plan for estimating debris hazard environments from reinforced concrete structures subjected to internal explosion loading.

The technical work was completed in July 1981 and, therefore, does not reflect any of the advances in fragment and debris hazard prediction methodologies which have been developed since July 1981.

Approved by:

*H. S. Ham*  
H. S. HAISS, Acting Head  
Energetic Materials Division



1/11

Accession For	
NTIS CRA&I	<input checked="" type="checkbox"/>
DTIC TAB	<input type="checkbox"/>
Unannounced	<input type="checkbox"/>
Justification	
By _____	
Distribution/ _____	
Availability Codes	
Dist	Available d/or Special

CONTENTS

<u>Chapter</u>		<u>Page</u>
1	INTRODUCTION . . . . .	1
2	REVIEW OF EXISTING DEBRIS AND FRAGMENT PREDICTION METHODOLOGIES . . . . .	3
3	ACCEPTABLE HAZARD HANDLING ARC CRITERIA . . . . .	39
4	DEBRIS HAZARDS METHODOLOGY DEVELOPMENT PLAN . . . . .	63
5	RECOMMENDED MODEL TESTS . . . . .	75
6	ANALYSIS OF TEST DATA . . . . .	81
	REFERENCES . . . . .	89
	APPENDIX A--BIBLIOGRAPHY . . . . .	A-1

## ILLUSTRATIONS

<u>Figure</u>		<u>Page</u>
1	SCALED CURVES FOR FRAGMENT/DEBRIS RANGE PREDICTION . . . . .	17
2	CUMULATIVE PROBABILITY DISTRIBUTION, DEBRIS WEIGHT (LB) . . . . .	26
3	CUMULATIVE PROBABILITY DISTRIBUTION, DEBRIS RANGE (FT) . . . . .	31
4	DEBRIS CUMULATIVE PROBABILITY DISTRIBUTION, NONDIMENSIONAL RANGE, $\bar{R}$ . . . . .	32
5	FLOW CHART FOR PREDICTING THE FRAGMENT AND DEBRIS ENVIRONMENT AROUND EXPLOSIONS . . . . .	43
6	MISSILE MAP FOR A TYPICAL DIVIDING WALL TEST . . . . .	50
7	MASS DISTRIBUTION FOR A DIVIDING WALL TEST . . . . .	51
8	DRAG AREA ESTIMATION CURVE FOR CONCRETE FRAGMENTS . . . . .	53
9	DEFINITION OF VERTICAL PLANE USED TO ESTIMATE THE VERTICAL DEBRIS DENSITY . . . . .	54
10	MAXIMUM RANGE ENVELOPE FOR 90 GM (0.20 LB) DEBRIS . . . . .	56
11	DRAWING OF MEASURED DEBRIS DENSITY OF BUILDING AND CRATER MATERIAL DURING MODEL TESTS . . . . .	65
12	TEST SETUP . . . . .	78
13	THE LARGEST DEBRIS VELOCITY AS A FUNCTION OF THE IMPULSE FACTOR FOR THREE-SIDE-SUPPORTED PANELS . . . . .	82
14	THE LARGEST DEBRIS RANGE AS A FUNCTION OF THE IMPULSE FACTOR FOR THREE-SIDE-SUPPORTED PANELS . . . . .	83
15	NUMBER OF DEBRIS MISSILES PRODUCED AS A FUNCTION OF THE IMPULSE FACTOR FOR THREE-SIDE-SUPPORTED PANELS . . . . .	84
16	LARGEST RECOVERED MASS AS A FUNCTION OF THE IMPULSE FACTOR FOR THREE-SIDE-SUPPORTED PANELS . . . . .	85
17	DEBRIS MASS DISTRIBUTION FOR A CANTILEVERED WALL . . . . .	86
18	DEBRIS MASS DISTRIBUTION FOR CANTILEVERED DIVIDING WALLS AS A FUNCTION OF BLAST LOADING . . . . .	87

## TABLES

<u>Table</u>		<u>Page</u>
1	METHODOLOGIES FOR PREDICTION OF FRAGMENT MASS . . . . .	4
2	METHODOLOGIES FOR PREDICTION OF FRAGMENT WEIGHT . . . . .	6
3	METHODOLOGIES FOR PREDICTION OF NUMBER OF FRAGMENTS . . . . .	7
4	METHODOLOGIES FOR PREDICTION OF FRAGMENT VELOCITY . . . . .	10
5	METHODOLOGIES FOR PREDICTION OF FRAGMENT RANGE AND TRAJECTORY . . . . .	13
6	METHODOLOGIES FOR PREDICTION OF FRAGMENT DISTRIBUTION . . . . .	18
7	DETERMINATION OF DEBRIS INITIAL VELOCITY . . . . .	20
8	"GASEX" COMPUTER CODE METHODOLOGY . . . . .	21
9	PROCEDURE TO DETERMINE THE HAZARDOUS DEBRIS DENSITY . . . . .	24
10	METHODOLOGY FOR PREDICTION OF DEBRIS RANGE . . . . .	33
11	METHODOLOGY OF PREDICTING DEBRIS DISTRIBUTION . . . . .	35
12	HAZARDOUS FRAGMENT CRITERIA . . . . .	40
13	ALLOWABLE VELOCITIES FOR CERTAIN MASSES USING THE HAZARDOUS FRAGMENT CRITERIA . . . . .	41
14	GENERAL SUMMARY FOR A TYPICAL DIVIDING WALL TEST . . . . .	49
15	NUMBER OF CONCRETE FRAGMENTS RECOVERED BY MASS IN THE SIX RECOVERY ZONES . . . . .	52
16	CALCULATIONS OF THE HAZARDOUS DEBRIS DENSITY IN THE HORIZONTAL PLANE . . . . .	58
17	NUMBER OF HAZARDOUS DEBRIS IN THE VERTICAL PLANE . . . . .	61
18	PARAMETERS TO BE VARIED DURING MODEL TESTING . . . . .	68
19	PARAMETERS TO BE HELD CONSTANT DURING MODEL TESTING . . . . .	69
20	MEASURED PARAMETERS OR DEBRIS CHARACTERISTICS . . . . .	70
21	MODEL LAW FOR DIVIDING WALL FRAGMENTATION . . . . .	72
22	FULL-SCALE RANGE OF VARIATION TO BE APPLIED TO PARAMETERS IN TABLE 18 DURING MODEL TESTING . . . . .	74
23	PRELIMINARY TEST PLAN . . . . .	76

CHAPTER 1

INTRODUCTION

This report presents the results of an analytical program intended to provide necessary methodologies and data required to begin implementation of the Naval Ordnance Hazards Analysis and Risk Management (NOHARM) system. This effort was conducted for the Naval Surface Weapons Center (NSWC), White Oak, under Contract Number N60921-80-C-0267. NOHARM is a software system designed to provide information required to assess and manage the risks to personnel and property exposed to hazards associated with the handling of naval ordnance. The primary objective of the NOHARM system is to identify unsafe (unacceptable risk) conditions in ordnance handling. A secondary goal is to determine the optimum strategy for mitigating risks once they are discovered. To achieve these objectives, NOHARM must have the capability to estimate the explosive hazards associated with ordnance operations, predict the human and economic risks from possible explosions and fires, assess those risks to identify unsafe conditions, and assist in the selection of optimum techniques for risk mitigation. As such, the software will consist of three distinct modules: the Explosives Hazards Model (EHM), the Risk Prediction Model (RPM), and the Risk Mitigation Model (RMM). This report is concerned only with the EHM. The EHM is intended to produce several primary outputs which are required by the other two modules. These outputs are:

- o The probability per year of all possible yields of explosions and fires from transactions and storage of naval ordnance.
- o The maximum credible yield from such accidents.
- o The identification of particular ordnance transactions which are major causes of fire and explosion.
- o The estimation of the blast, fragment, and debris environment associated with explosions in the naval ordnance handling system.

This report is concerned only with the estimation of the fragment and debris environment around accidental explosions in naval facilities. This project consisted of three tasks: a comprehensive review of the technical literature, the development of a new methodology for predicting the debris environment from internal explosions in reinforced concrete structures, and the development of a master plan to derive the input data required for full implementation of the EHM of NOHARM.

The objective of Task 1, literature review, was to prepare a bibliography on the primary fragment hazard from accidental detonations of Navy weapons, and

the debris hazard from accidental explosions both in reinforced concrete buildings and in ships.

The review of the literature on fragment/debris characteristics was conducted with the aid of three computerized information retrieval systems. To supplement the computerized scan of the literature, the report files at Southwest Research Institute (SwRI) were examined. J. M. Ward at NSWC also contributed many references to pertinent reports. Finally, we examined the proceedings of the Department of Defense Explosive Safety Board (DDESB) meetings for the past 12 years. Through this exhaustive scan of the literature, 102 useful reports and papers were identified. A bibliographic listing of these reports was prepared and is included as Appendix A of this report.

The objective of Task 2 was to develop a methodology for predicting the fragment and debris environments from accidental explosions within reinforced concrete structures. The model developed provides a technique for the estimation of the number of fragments (emanating from the weapon) and the number of debris missiles (emanating from the concrete structure) per square foot of ground surface area which exceed specified energy levels on impact. The methodology is presented in a form suitable for eventual conversion to a computer code. However, certain critical input parameters are not currently available, so development of the computer code is restricted to only those situations for which experimental data are available.

The methodology presented parallels a similar methodology developed by J. M. Ward for predicting the fragment hazard associated with the accidental detonation of weapons, specifically a pallet load of Mk 82 bombs. His methodology, which is an application of concepts developed by F. B. Porzel for the Naval Explosive Safety Improvement Program (NESIP), was developed for the special case of an explosion in the open field providing for both high and low trajectories of the debris or fragments. This feature is important in the establishment of acceptable hazard arcs. In this report we have included this concept in the estimation of hazards for both fragments and debris missiles.

Task 3 was intended to develop a master plan which could be used by the Government to provide necessary methodologies and data required to implement the NOHARM system for fragment and debris effects. The objective of this task was to identify gaps in the current state-of-the-art of predicting the fragment and debris environment from accidental explosions of naval ordnance.

During this project we have established that major data gaps exist in the prediction of structural failure patterns, in the estimation of internal loading on the buildings, and in the prediction of initial conditions used to calculate debris trajectories. Much weapon effectiveness data are available and are useful for establishing fragment effects (from the weapons case). However, not much data for the debris effects (from the surrounding structures) are available.

Currently, to predict the debris hazards for a particular situation, tests must be conducted to provide the requisite data. This report presents a scale model test program and similitude analysis which may be used to generalize the test results.

## CHAPTER 2

## REVIEW OF EXISTING DEBRIS AND FRAGMENT PREDICTION METHODOLOGIES

This technical literature was reviewed to identify existing methodologies to define the hazards associated with the accidental detonation of weapons within and outside of different classes of structures. Of particular interest was the explosion of naval weapons within reinforced concrete structures and ships. In the following paragraphs, the methodologies identified during this effort are described for bomb fragments and for debris from ships and reinforced concrete. In this report we will use the term fragment to refer to pieces of the weapon and the term debris to refer to pieces of the structure emanating from the explosion.

The review of the literature on fragment/debris characteristics was conducted in several stages. The COMPENDEX (Computerized Engineering Index) and the National Technical Information Service (NTIS) data bases were scanned using the Lockheed DIALOG information retrieval system. Additionally, a search was initiated on the Defense Technical Information Center (DTIC) data base. To supplement the computerized scan of the literature, the report files of several people at SwRI were examined. J. M. Ward also contributed many references to pertinent reports. Finally, we examined the proceedings of the DDESB meetings for the past 12 years. Through this exhaustive scan of the literature, useful reports and papers were identified. A bibliographic listing of these reports is contained in Appendix A.

## BOMB FRAGMENT METHODOLOGIES

Existing methodologies for predicting the behavior of bomb fragments have been reviewed. This research resulted in identifying methodologies for the determination of each of the following parameters: mass, weight, number, size, velocity, range and trajectory, distribution, and impact probability. A summary of the methodologies found for the determination of each fragment parameter is presented in the following paragraphs. Tables are included to give specific methodologies and the source from which they were taken.

Fragment Mass

The most extensive treatment of bomb fragment masses is a statistical study conducted by Hekker and Pasman.<sup>1</sup> An equation derived by Weibull is presented which predicts the probability that a mass,  $x$ , is greater than a given mass,  $\bar{m}$ . This equation is used by the authors to derive the mean fragment mass,  $m$ . This term,  $\bar{m}$ , is a function of  $m_0$ , which is also the average mass but is calculated differently by researchers as shown in Table 1. It is important to distinguish between  $\bar{m}$  and  $m_0$  and also to realize that other researchers such as Mott use

TABLE 1. METHODOLOGIES FOR PREDICTION OF FRAGMENT MASS

PARAMETER	METHODOLOGY	DESIGNATION	REFERENCE
Probability	$P(x>m) = \exp[-(m/m_0)^\lambda]$ $m_0, \lambda \text{ are functions of material and geometry}$	Weibull	(1)
Mean Mass	$\bar{m} = \int_0^\infty x dP(x>x) = m_0 \Gamma(1+1/\lambda)$ $x = 0$ <p>where: <math>\Gamma</math> = Euler Gamma Function</p>		(1)
Average Mass	$m_0 = C_G \left(\frac{t}{d_i}\right)^2 \left(t+d_i\right)^3 \left(1 + \frac{1}{2\mu}\right)$ $m_0 = C_L t c_i^{1/3} \left(\frac{1}{1+2/\mu}\right)$ $m_0 = C_M t^5 d_i^{-4/3} (t+d_i)^2$ $m_0 = C_B \frac{d_o^3}{v_o^2} \text{ or } C_9 \frac{d_o^2}{v_o^2}$ <p>where: <math>v_o</math> = initial fragment velocity  <math>t</math> = wall thickness  <math>d_i, d_o</math> = diameters  <math>\mu</math> = metal to high explosive ratio  <math>C</math> = coefficient, function of metal and high explosive</p> $\mu^{1/2} = B t^{5/6} d_i (1+t/d_i)$ <p>where: <math>B</math> = constant  <math>d_i</math> = inside diameter  <math>t</math> = thickness</p> $\mu^{1/2} = \frac{A t (d_i+t)^{3/2}}{d_i} \sqrt{1 + \frac{1}{2} \left(\frac{C}{M}\right)}$ <p>where: <math>C/M</math> = mass ratio  <math>A</math> = constant</p> $\bar{m} = C_m \left(\frac{t d_i^{1/3}}{1+2C/H}\right)$ <p>where: <math>t</math> = thickness  <math>d_i</math> = inside diameter  <math>C_m</math> = material constant</p>	Gurney and Sarmousakis Lindeman Mott Weiss	(1) (1) (1) (1)
		Mott	(6)
		Gurney and Sarmousakis	(6)
		Magis	(2)

$\mu$  in place of  $m_0$  whereas Hekker and Pasman use  $\mu$  to symbolize the ratio of metal-to-high explosive mass.

Each of the possible average mass equations presented by Hekker and Pasman was tested statistically using the F-test with experimental data derived from tests on ring-type cylindrical shells. Their results indicated that the formulae of Gurney-Sarmousakis and Mott are the most applicable under the conditions tested. A note is made by the authors, however, that completely different results could be obtained with an increase in the number of experiments, or from a change in the  $\lambda$ -value.

The literature reviewed for this project indicates that the formulae of Mott and Gurney-Sarmousakis are the present day standard for calculating the average fragment mass. There does exist an alternative to these two equations, the Magis equation, which was used by Randers-Pehrson,<sup>2</sup> and is presented in Table 1.

#### Fragment Weight

Some of the articles considered concern themselves with fragment weight, rather than fragment mass. Obviously this represents only a minor change in variable definition (by a factor of the acceleration of gravity). The U.S. Army Technical Manual 5-1300<sup>3</sup> and other Army work use an equation for primary fragment weight based on Mott's equation. The Swedish researchers, Ericksson and Arvidsson,<sup>4</sup> also use a variation of the Mott equation to determine the total weight of all fragments with a weight  $m$ , greater than a specified  $m_1$ . This equation differs dramatically from others encountered in that it includes the influence of the percentage of carbon present in the steel shell casing on the fragment weight. Fragment weight methodologies are given in Table 2.

#### Number of Fragments

Various approaches available for calculating the number of fragments with a mass greater than a given mass are presented in Table 3. A number of these are presented by Hekker and Pasman<sup>1</sup> and are incorporated into their statistical analysis, which has been previously discussed. The Mott equation, or variations thereof, is by far the most commonly used method in this category and appears many times. Johnson and Moseley<sup>5</sup> have presented 2D and 3D variations on Mott's formula, while Sternberg<sup>6</sup> defined a fragment range for the Mott equation and developed other equations for the number of fragments, which are valid where the Mott formula is not. Krauklis and Bedford<sup>7</sup> present the Payman method of analysis along with modifications on Mott and Payman. Porzel,<sup>8</sup> after discussing Mott's general equation, proposes a prediction equation for the number of fragments, based on the idea that fragmentation is controlled by fragment length, rather than by mass or area.

#### Fragment Size

The standard method for predicting fragment size (area) is a formula which is a function of the fragment's mass and the shape factor, or ballistic density.<sup>5</sup> This equation, given below, is the only method used to determine fragment size.

TABLE 2. METHODOLOGIES FOR PREDICTION OF FRAGMENT WEIGHT

PARAMETER	METHODOLOGY	LIMITS OF APPLICABILITY	DESIGNATION	REFERENCE
Primary Fragment Weight	$W_f = C \left[ \ln \left( \frac{W_c}{2C} \right) \right]^2$ $C = \left[ B t^{5/6} d_i^{1/3} (1+t/d_i) \right]^2$ <p>where: <math>W_f</math> = weight of next to largest fragment  <math>B</math> = constant  <math>t</math> = casing thickness  <math>d_i</math> = inside diameter  <math>W_c</math> = casing weight</p>		Hott	(16)
Largest Fragment Weight	$W_f = \left( M_A \ln \left[ \frac{8W_c}{M_A} \right] \right)^2$ <p>where: <math>M_A = C</math>, defined as above  <math>W_c</math> = casing weight</p>			(3)
Total Weight $> m_1$	$M = M_0 \exp(-\gamma m_1)$ <p>where: <math>M</math> = total weight of all fragments with weight <math>&gt; m_1</math>  <math>M_0</math> = total weight of shell case, kg.  <math>\gamma</math> = fragmentation number: <math>\text{kg}^{-1}</math>  and  <math display="block">\gamma = \gamma_0 \exp(-26.4\phi - 15.8d/\phi)</math>  where: <math>\phi</math> = outer diameter, meters  <math>d</math> = shell case thickness, meters  <math>\gamma_0</math> varies with HE and shell case material and is tabulated for various Z C steel compositions</p>	$m_1 > 0.5 \times 10^{-3} \text{ kg}$		(4)

TABLE 3. METHODOLOGIES FOR PREDICTION OF NUMBER OF FRAGMENTS

PARAMETER	METHODOLOGY	LIMITS OF APPLICABILITY	DESIGNATION	REFERENCE
Number of Fragments	$N(>u) = \left( \frac{M_T}{m_0} \right) \exp(-2m/m_0)^{1/2}$ where: $M_T$ = total mass $m_0$ = average fragment mass		Mott	(25)
	$N(>u) = N_0 \exp(-m/u)^\gamma$ where: $N_0$ = constant $u$ = average mass $\gamma = 1, 1/2, 1/3$ , depends on $u$		Mott	(9)
	$N(>u) = N_0 \exp(-L/L_1)$ where: $N_0$ = constant $L_1$ = proportionality constant $L$ = length	$\gamma = 1/3$	Porral	(9)
	$N(>u) = N_0 \cdot P(x \geq u)$ where: $P(x \geq u)$ = Probability of mass $x$ being greater than $\geq u$ and $N_0 = \frac{M}{m} = \frac{M}{m_0 \cdot (1+1/\lambda)}$ where: $M$ = total mass other items are defined in Table 1		Hakkar and Pasman	(1)
	$N_0 = 1.10Ld_0^{2/3}t^{-2/3}$		Cook	(1)
	$N_0 = C_6 \frac{d_0}{d_0} \cdot \frac{M}{d_0} \cdot \frac{2u + 2}{2u(u+1)}$		Justrow	(82)
	$N_0 = C_7 \frac{t}{d_0} \left( 1 - \frac{t}{d_0} \right) \cdot \frac{M}{ud_0^2 K_0}$		Gabeaud	(1)
	where: $t$ = wall thickness $d_1, d_0$ = diameters $u$ = metal to high explosive ratio $C$ = coefficient, function of metal and high explosive.			
	$N(>u) = N_0 \exp(-(m/u)^{1/2})$	2-Dimensional	Mott	(6)
	where: $N_0 = M/2u$ = total number of fragments $2u$ = average fragment mass $M$ = total case mass			
	$N(>u) = N_0 \exp(-(m/u)^{1/3})$	3-Dimensional	Mott	(5)
	$\ln N_f = \ln \left[ \frac{3W_c}{N_A} \right] - \frac{W_f^{1/2}}{N_A}$			(3)
	where: $N_f$ = number of fragments larger than $W_f$ $W_f$ = weight of primary fragment $W_c$ = total weight of cylindrical portion of casing $N_A$ is defined in Table 2.			



$$m = kA^{3/2}$$

where

k = ballistic density

A = presented area

m = mass

### Fragment Velocity

An extensive number of reports containing fragment velocity prediction equations were reviewed as part of this program and a list of prediction equations is given in Table 4. The Gurney equation, which is applicable to cylinders, is the most widely accepted method for predicting fragment initial velocity. Several variations of the Gurney equation have been developed and are also included in Table 4. Randers-Pehrson<sup>2</sup> modified the Gurney equation to predict the nonsteady state velocity of a fragment. He also modified the Gurney equation to account for an open-ended cylinder. Variations of the Gurney equation also exist for spheres and steel-core cylinders, and are shown in Table 4.<sup>9</sup> The maximum initial velocity for a fragment from a cylinder, sphere, and a steel-cored cylinder is given in U.S. Army TM 5-1300.<sup>3</sup> This manual also gives an equation to calculate the striking velocity of a fragment on a target for small fragments up to several ounces in weight. The initial fragment velocity (based on experimental photographic velocity), fragment mass, and the drag coefficient can also be determined in an equation found in another U.S. Army publication.<sup>10</sup> Lacher<sup>11</sup> presents an equation for fragment velocity as a function of drag factor and range.

The only equation found to predict secondary fragment velocities appeared in a U.S. Army Corps of Engineers publication.<sup>12</sup> Shape factors are given for different geometries, and ranges of applicability are also shown.

### Fragment Range and Trajectory

The methodologies encountered for the prediction of fragment range and trajectory are given in Table 5. Zaker<sup>13</sup> solves the equation of motion for a fragment by separating the problem into a gravity-free solution and a perturbed solution. Schreyer and Romesberg<sup>14</sup> give equations for calculating the accelerations in the x and y direction for two sets of conditions: first, assuming no fragment lift and second, assuming both fragment lift and drag. The latter is incorporated into the FRISB computer code, which is used at SwRI and referred to later in this report.

The initial trajectory angle can be found using the Taylor equation for steady state conditions which is referenced in numerous reports. Randers-Pehrson<sup>2</sup> has modified the steady state Taylor equation to account for nonsteady state conditions.

Various authors give relationships between fragment range and velocity which are shown in Table 5,<sup>15</sup> along with validity criterion and any assumptions made. Fugelson and Rathmann<sup>16</sup> present a range equation which is a function of the initial launch angle and the ratio of the terminal free-fall velocity of the fragment to its initial velocity. A graphical method for

TABLE 4. METHODOLOGIES FOR PREDICTION OF FRAGMENT VELOCITY

PARAMETER	METHODOLOGY	LIMITS OF APPLICABILITY	DESIGNATION	REFERENCE
Velocity	$V^2 = 2Z/(N/C + (n+2))$ <p>where: <math>Z</math> = Gurney constant  <math>N/C</math> = weight ratio  <math>n</math> = 1, 2, or 3, depending on geometry</p>		Gurney	(25)
	$V_0 = \sqrt{2Z} \sqrt{\frac{c/m}{1 + 1/2 c/m}}$ <p>where: <math>Z</math> = Gurney constant  <math>c/m</math> = mass ratio</p>	Steady-State	Gurney	(2)
	$V = V_0 \left( 1 - \exp\left(-\frac{t-T}{\tau}\right) \right)$ <p>where: <math>V</math> = instantaneous velocity  <math>V_0</math> = ultimate velocity  <math>T</math> = time at which detonation front reaches the element  <math>\tau</math> = time constant of acceleration</p>	Non-Steady-State		
	$V_0 = \sqrt{2Z} \sqrt{\frac{F(s) \cdot c/m}{1 + \frac{1}{2} F(s) \cdot c/m}}$ <p>where: <math>F(s) = 1 - (1 - \min\{s/2R, L, L-s\})^2</math></p> <p>and <math>s</math> = initial axial location  <math>L</math> = charge length  <math>R</math> = charge radius</p>	Open-Ended Cylinder	Modified Gurney	(2)
Velocity	$V_0 = \sqrt{2Z} \sqrt{\frac{c/m}{1 + 0.6 c/m}}$	Sphere	Gurney	(6)
	$\bar{v} = \sqrt{\frac{a \cdot D}{D}}$ <p>where: <math>a = C_D \rho k m^{-1/3}</math> = drag factor</p> <p><math>\bar{v}</math> = average velocity = <math>\frac{\text{distance traveled (total)}}{\text{time traveled}}</math></p> <p><math>C_D</math> = drag coefficient  <math>\rho</math> = air density  <math>k</math> = shape factor  <math>m</math> = fragment mass  <math>D</math> = distance  <math>v</math> = velocity at distance <math>D</math></p>			(15)
	$V = 2D \sin(\alpha/2)$ <p>where: <math>D</math> = detonation velocity  <math>\alpha</math> = angle to horizontal  <math>V</math> = velocity in direction of detonation</p>			(12)
	$V = V_g (N/C + A)^{-1}$ <p>where: <math>V_g</math> = Gurney velocity  <math>A</math> = arbitrary dimensionless constant</p>			(12)

TABLE 4. (CONT.)

PARAMETER	METHODOLOGY	LIMITS OF APPLICABILITY	DESIGNATION	REFERENCE
Velocity	$v_o = v_p \left( \exp \left( \frac{ar}{m^{1/3}} \right) - 1 \right) \left( \frac{m^{1/3}}{ar} \right)$ <p>where: <math>v_o</math> = initial velocity  <math>v_p</math> = photographic velocity  <math>a = 12\rho C_D k^{-2/3}</math> = drag factor  <math>\rho</math> = air density  <math>C_D</math> = drag coefficient  <math>k = \pi A^{-2/3}</math> = fragment shape factor  <math>r</math> = distance traveled</p>	Experimental data		(14)
Velocity (Primary Fragment)	$v_o = \sqrt{2E} \left[ \frac{W/W_c}{1+3W/5W_c} \right]^{1/2}$ $v_o = \sqrt{2E} \left[ \frac{W/W_c}{1 + \frac{(3+a)W}{6(1+a)W_c}} \right]^{1/2}$ <p>where: <math>W</math> = explosive weight  <math>W_c</math> = casing weight  <math>a = \frac{d_{co}}{d_c}</math>  <math>d_c</math> = inside casing diameter  <math>d_{co}</math> = core diameter</p>	Sphere  Steel-Cored Cylinder		(16)  (16)
Velocity (Secondary Fragment)	$v_{os} = \frac{A_p R_s g_s}{M} \left[ 0.556 \left( \frac{R_e}{R} \right) + 2.75 \left( \frac{R_e^2}{R} \right) \right]$ <p>where: <math>A_p</math> = presented area of secondary fragment  <math>R_e</math> = radius of spherical charge  <math>M</math> = mass of secondary fragment  <math>R</math> = range of secondary fragment  <math>g_s</math> = secondary fragment shape factor  <math>= 2/3</math>, sphere  <math>= 7/4</math>, side on cylinder  <math>= 1</math>, end on cylinder or plane</p>	$1.5 \leq R/R_e \leq 6.0$ $0.18 \frac{\text{lb sec}}{\text{in.}^3} \leq \frac{M v_o}{A_p R_s g_s} \leq 2.0 \frac{\text{lb sec}}{\text{in.}^3}$		(16)

TABLE 4. (CONT.)

PARAMETER	METHODOLOGY	LIMITS OF APPLICABILITY	DESIGNATION	REFERENCE
Velocity (Maximum Initial)	$v_{o \max} = 1.414 \sqrt{2E}$	Cylinder		(3)
	$v_{o \max} = \sqrt{5/3} \sqrt{2E}$	Sphere		(3)
	$v_{o \max} = \sqrt{2E} \sqrt{\frac{6(1+a)}{3+a}}$	Steel-Cored Cylinder		(3)
	where: $a = \frac{d_{co}}{1.6d_i}$			
	and $d_{co}$ = core diameter			
	$d_i$ = inside casing diameter			
Velocity (Striking)	$v_s = v_o \exp \left[ -0.004 R_f / W_f^{1/3} \right]$	Small fragments up to several ounces in weight		(3)
	where: $v_s$ = striking velocity			
	$v_o$ = initial fragment velocity			
	$R_f$ = distance traveled by fragment			
	$W_f$ = weight of primary fragment			

TABLE 5. METHODOLOGIES FOR PREDICTION OF FRAGMENT RANGE AND TRAJECTORY

PARAMETER	METHODOLOGY	LIMITS OF APPLICABILITY	DESIGNATION	REFERENCE
Direction (Angle)	$\sin \delta = \frac{v}{2U}$ <p> <math>\delta</math> = direction relative to normal to surface  <math>U</math> = rate of detonation wave  <math>v</math> = velocity </p>	Steady-State	Taylor	(2)
	$\sin \delta = \frac{v_0}{2U} - \frac{v_0' \tau}{2} - \frac{(v_0' \tau)^2}{5}$ <p> <math>v_0'</math> = derivative of <math>v_0</math>, initial velocity with respect to distance along the surface  <math>\tau</math> = time constant of acceleration </p>	Non-Steady-State	Modified Taylor	(2)
Velocity (as a function of range)	$v = V \exp(-R/L)$ <p>           where: <math>v</math> = velocity  <math>R</math> = range  <math>L</math> = distance in which fragment velocity drops to 1/e of its initial value, <math>V</math> </p> $L = \frac{2(km)^{1/3}}{C_D \rho_A}$ <p> <math>k</math> = shape factor  <math>m</math> = mass  <math>\rho_A</math> = air density  <math>C_D</math> = drag coefficient </p>	Constant Drag No Gravity		(25)
Range (As a function of velocity)	$R = \left[ 7920 \left( \frac{v}{1000} \right)^{0.275} \right]^\gamma \left[ 0.18 \left( \frac{1000}{v} \right)^{0.275} - 1 \right]$			(20)
	where: $v$ = ejection velocity $\gamma = A/W$	$2 < \gamma < 20 \text{ in.}^2/\text{lb}$ $3000 < v < 10,000 \text{ ft/sec}$		
	$\text{SAFE RANGE} = KW_{TE}^{1/3}$ <p>           where: <math>K</math> = proportionality constant (ft/lb)<sup>1/3</sup>  <math>W_{TE}</math> = total explosive weight (lb) </p>			

TABLE 5. (CONT.)

PARAMETER	METHODOLOGY	LIMITS OF APPLICABILITY	DESIGNATION	REFERENCE
Range	$r_{max} = 0.5140 - 1.0358 \ln c$ <p>where: <math>c = \frac{\text{fragment terminal free fall velocity}}{\text{fragment initial velocity}}</math></p> <p>assuming <math>r(\alpha_0, c) = r_{max}(c) f(\alpha_0)</math></p> <p>where: <math>\alpha_0 =</math> initial launch angle to the horizontal</p> <p>letting <math>\epsilon = 0.02</math></p> $f(\alpha_0) = \frac{3\sqrt{3}}{2} \sqrt{\epsilon} (1-\epsilon) \left[ 1 + \bar{\lambda} \left( \epsilon - \frac{1}{3} \right)^2 \right] = h(\epsilon)$ <p>where: <math>\bar{\lambda} = 3.25, \epsilon &lt; 1/3</math>  <math>\bar{\lambda} = 2.00, \epsilon &gt; 1/3</math>  <math>\epsilon = \sin^2 \alpha_0</math></p> <p>other approximations</p> $a_f = 90 \left[ 1 - \exp \left( - \frac{\epsilon}{0.175} \right) \right]$ $\frac{v_f}{c} = \left( \frac{1}{c} - 1.9 \right) \exp \left( - \frac{\epsilon}{0.01} \right) + 1.6 \exp \left( - \frac{\epsilon}{0.06} \right) - 0.7 \exp \left( - \frac{\epsilon}{0.14} \right) + 1$			(21)
	GRAPHICAL METHOD (see Figure 1.) generated using FRISB computer code.			(22)
Solutions to Equations of Motion	$\frac{d^2 \bar{x}}{dt^2} + 3v \frac{d\bar{x}}{dt} + g \sin \alpha = 0$ $\frac{d^2 \bar{y}}{dt^2} + 3v \frac{d\bar{y}}{dt} + g \cos \alpha = 0$ <p>where: <math>\bar{x}</math> and <math>\bar{y}</math> are local coordinates tangent and normal to trajectory</p> <p><math>v =</math> speed in path  <math>g =</math> acceleration of gravity  <math>\alpha =</math> angle between <math>\bar{x}</math> axis and horizontal  <math>\delta =</math> aerodynamic drag coefficient</p> <p>solutions:</p> $\frac{\bar{x}}{g} = \{ \log(1+u) \} / \delta$ $\frac{\bar{y}}{g} = v_0 / (1+u)$ <p>where <math>u = 3v_0 t</math></p> $\frac{\bar{x}}{g} = - (g/2) t^2 \sin(\beta\alpha/3) / (1+u)$ $\frac{\bar{y}}{g} = \frac{(-g/2) t^2 \cos \alpha}{2} \{ (u(1+u/2) - \log(1+u)) \}$ $\frac{\dot{\bar{x}}}{g} = \frac{-gt \sin \alpha}{(1+)^2} (1+u(1+u/3))$ $\frac{\dot{\bar{y}}}{g} = -gt \cos \alpha (1+u/2) / (1+u)$			(17)
				(17)

TABLE 5. (CONT.)

PARAMETER	METHODOLOGY	LIMITS OF APPLICABILITY	DESIGNATION	REFERENCE
Solutions to Equations of Motion (con't)	Global Displacements:			
	$\Delta x = \bar{x} \cos \alpha - \bar{y} \sin \alpha$ $\Delta y = \bar{x} \sin \alpha + \bar{y} \cos \alpha$	$t \ll (8g)^{-1/2}$		(21)
	Rotation of Trajectory Tangent:			
	$\Delta \alpha = \tan^{-1} \left( \frac{\dot{y}}{\dot{x}} \right)$			
	$\ddot{x} = - \frac{A_D C_D \rho}{2m} v_x^2 \cos \alpha$ $\ddot{y} = -g - \frac{A_D C_D \rho}{2m} v_y^2 \sin \alpha$	No Lift		(18)
	<p>where: <math>\rho</math> = air density  <math>g</math> = acceleration of gravity  <math>A_D</math> = drag area  <math>C_D</math> = drag coefficient  <math>\alpha</math> = angle between horizontal and tangent to trajectory  <math>v_x, v_y</math> = velocity components  <math>m</math> = mass</p>			
	$\ddot{x} = - \frac{A_D C_D \rho}{2m} (\dot{x}^2 + \dot{y}^2) \cos \alpha$ $- \frac{A_L C_L \rho}{m} (\dot{x}^2 + \dot{y}^2) \sin \alpha$ $\ddot{y} = -g - \frac{A_D C_D \rho}{2m} (\dot{x}^2 + \dot{y}^2) \sin \alpha$ $+ \frac{A_L C_L \rho}{m} (\dot{x}^2 + \dot{y}^2) \cos \alpha$	Lift and Drag	FRISB Equations	(18)
	<p>where: <math>A_L</math> = lift area  <math>C_L</math> = lift coefficient  Other symbols as above.</p>			

predicting fragment range is contained in NASA Contractor Report 3023,<sup>17</sup> and is shown in Figure 1. This set of curves was developed by performing a model analysis to generate dimensionless parameters which describe ranges for selected cases, and then the results were plotted to form the curves. It should be noted that, in generating these curves, several initial trajectory angles were used in the analysis to obtain the maximum range for the respective fragments.

#### Fragment Distribution

Fragment distribution methodologies reviewed are given in Table 6. Klein,<sup>18</sup> assuming a Mott analysis, derives a formula for the total number of fragments per unit solid angle. An expression for angular fragment distribution is given by Johnson and Moseley<sup>5</sup> while Fugelso, et al.<sup>19</sup> derive a formula for the fragment density in terms of the range and azimuth. An expression for zonal fragment density is used by the U.S. Army in their publication.<sup>10</sup> For large range fragment densities, Fugelso, et al.,<sup>19</sup> present a formula which is a function of the angle of incidence at impact and the ground range.

#### Fragment Impact Probability

The literature search conducted for this program resulted in only one formula for predicting the probability that a fragment would impact a particular target.<sup>18</sup> This formula, given below, appeared in numerous publications in different forms.

$$P = 1 - \exp(-qA_T) \quad (2)$$

where

$A_T$  = target area

$q$  = areal fragment density

#### DEBRIS FROM EXPLOSIONS IN NAVY SHIPS

The literature search indicates that methodologies for predicting debris characteristics from explosions inside Navy ships and submarines are very limited. No methodologies were found to predict the number of debris fragments which would result from an explosion in a ship or submarine. Some model tests have been performed at NSWC where debris data bases were created which include debris of particular masses and sizes recovered.<sup>20,21</sup> To date, the data bases have not been statistically analyzed to establish prediction equations or schemes. The only report located which presents analytical predictions of debris characteristics for Navy ships or submarines is an SwRI report on debris hazards from an explosion in a torpedo tender workshop.<sup>22</sup> However, the breakup pattern assumed resembles a pressure vessel explosion and this assumption must be considered before applying the methods described in the report. Tests done since publication of that work show that explosions in torpedo workshops usually involve detonation of several warheads which result in a different breakup than assumed in the SwRI report. It is still feasible that gaseous explosion products could build up sufficient pressure in a ship to cause an explosion similar to a pressure vessel rupture, but one needs to analyze what type of explosion is possible before predicting debris characteristics using the methods contained in the SwRI report (not verified by test). Although the

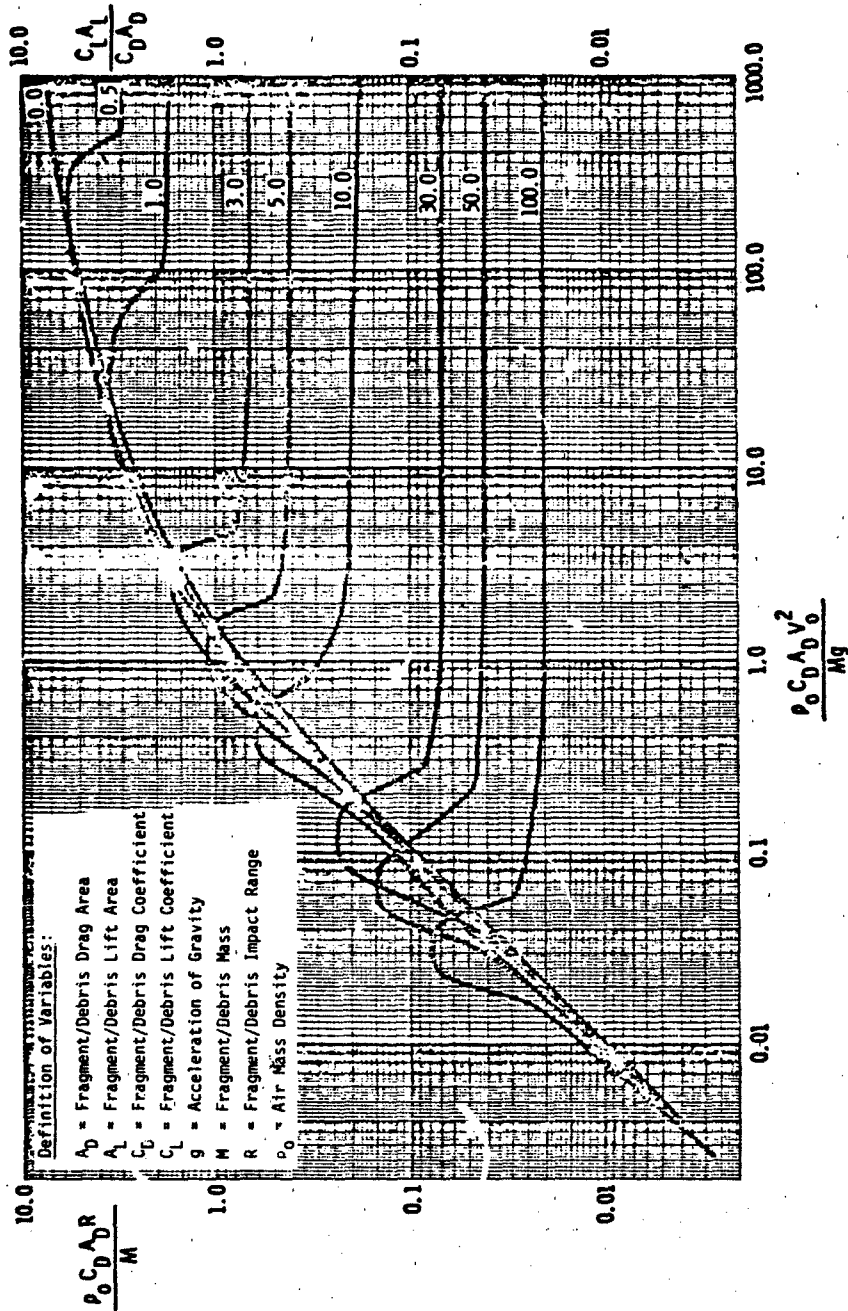


FIGURE 1. SCALED CURVES FOR FRAGMENT/DEBRIS RANGE PREDICTION

TABLE 6. METHODOLOGIES FOR PREDICTION OF FRAGMENT DISTRIBUTION

PARAMETER	METHODOLOGY	LIMITS OF APPLICABILITY	DESIGNATION	REFERENCE
Fragment Density	$q = (Q_0/R^2) \exp(-2m/a_0)^{1/2}$ <p>where: <math>q</math> = areal fragment density  <math>R</math> = distance  <math>Q_0</math> = total number of fragments/unit solid angle</p>			(23)
	$Q_1(R) = Q(R)/\sin \theta_f$ <p>where: <math>Q_1(R)</math> = fragment density at <math>R</math> for isotropic target  <math>Q(R)</math> = fragment density at <math>R</math> on ground  <math>\theta_f</math> = angle of incidence at impact</p>	Large Ang.		(23)
Angular Fragment Density	$N = 2\pi \int_{\theta_1}^{\theta_2} \rho(\theta) \sin\theta d\theta$ <p>where: <math>N</math> = number of fragments contained in polar zone  <math>\rho(\theta)</math> = number of fragments per steradian in polar zone between <math>\theta_1</math> and <math>\theta_2</math>, obtained from arena tests</p> $\theta_1 = \left( \frac{R^2}{A_{ti}} \right)^{1/2}$ <p>where: <math>\rho</math> = fragment density for each zone <math>\theta_1</math>  <math>n_1</math> = number of fragments in each zone  <math>R</math> = perpendicular distance from munition centerline to recovery panels  <math>A_{ti}</math> = area of each zone projected onto a sphere of radius <math>R</math>.</p>			(6)
Number of Fragments Beyond $R$ , Fragment Density	<p>Consider a slice of a unit hemisphere and an infinitesimal element of azimuth <math>\phi</math>. The number of fragments which fall beyond <math>R</math> is given by:</p> $N(R, \phi) = \left[ \int_0^{\pi/2} \cos\alpha d\alpha \int_{\theta_1}^{\pi} f(\alpha) d\alpha \right] \Delta\phi$ <p>where: <math>\theta_1 = R/\sin\alpha</math></p> <p>Consider an infinitesimal <math>\Delta R</math>; then the number of fragments in the small area <math>R\Delta R\Delta\phi</math> is:</p> $n(R, \Delta R, \Delta\phi) = \Delta R\Delta\phi \left( \frac{\partial N}{\partial R} \right)$ <p>Therefore the fragment density at range <math>R</math> is</p> $q(R, \phi) = \frac{1}{R} \left( \frac{\partial N}{\partial R} \right)$ <p>This expression can then be approximated.</p>			(14)

applications are limited, the methodologies will be presented since they are the only ones revealed in the literature search.

### Debris Velocity

The velocity of debris from a bulkhead or deck in a tender workshop is determined in a stepwise manner consisting of three basic phases. The first phase consists of the initial impulsive loading from the blast wave. The second phase involves the expansion of the gases produced by the products of the explosion. The final phase occurs as the debris is further accelerated by the venting of the gases around it as it leaves the ship and begins its trajectory.

The extent of damage and a breakup pattern are established for a 680 kg (1500 lb) charge weight by examining the loading on individual members in the bulkheads and decks immediately surrounding the charge. The report<sup>22</sup> concludes that these bulkheads and decks will either remain intact or break into large pieces with the explosion of 680 kg (1500 lb) of high explosive in the tender workshop. Therefore, the additional momentum obtained by the structural elements due to gas expansion of the combustion products is maximized since the gas is assumed not to escape between debris fragments. The average reflected impulse imparted to an entire exposed bulkhead/deck is determined at the location of the average distance of the bulkhead/deck from the charge. The procedure to determine the initial velocity of debris once the impulse has been determined is presented in Table 7. The first step is the simple calculation of velocity due to the impulsive loading on the structure. Kinetic energy is then calculated in the second step. The strain energies (S.E.) are determined for all structural elements in the exposed bulkhead/deck individually, added together, and subtracted from the kinetic energy. The adjusted initial velocity,  $V_0$ , is then determined as shown in the second step in Table 7. The third step in the procedure is the determination of the increase in velocity due to the expansion of the gaseous explosion products. A small computer program, GASEX, is used to solve simultaneously the equations of motion and the pressure equations for all bulkheads/decks surrounding the tender workshop where the charge is located. The sequence followed by the computer code is outlined in Table 8.

As the final step in the velocity prediction method, the computer code EDCYL is used to obtain the increase in velocity due to venting of the gaseous explosion products around the debris as they begin their trajectories. This code is a modification of a program developed by SwRI for NASA<sup>22</sup> to determine the velocity of fragments from a bursting cylindrical pressure vessel. A complete description of the program can be found in Reference 22. The initial velocity determined from the blast loading, gas expansion, and gas venting is next used to calculate the range that the debris travels from the ship.

### Debris Range

Maximum debris ranges for a specific initial velocity and mass (with a prescribed area) are determined by assuming appropriate launch angles as input to the computer code FRISB developed by Baker, et al.<sup>23</sup> Several probable breakup patterns are considered in the analytical report.<sup>22</sup> The arena data described in References 20 and 21 can be used to compare with analytical predictions so they can be supported or modified.

TABLE 7. DETERMINATION OF DEBRIS INITIAL VELOCITY

## Stepwise Method:

1. Impulsive loading

$$V = \frac{IA}{M}$$

where I = reflected specific impulse

A = area of bulkhead/deck

M = mass of bulkhead/deck.

2. Since kinetic energy of each structural element is

$$\text{K.E.} = 1/2 MV^2,$$

use adjusted initial velocity

$$V_o = \left[ \frac{2(\text{K.E.} - \text{S.E.})}{M} \right]^{1/2}$$

where S.E. = strain energy.

3. Computer code GASEX to obtain increase in velocity due to expansion of the gaseous explosion products.
4. Computer code BOXCYL to obtain increase in velocity due to venting of gaseous explosion products.

TABLE 8. "GASEX" COMPUTER CODE METHODOLOGY

1. Input the area, mass, initial velocity, and initial position from the center of the explosion of each of the six bulkheads/decks.
2. Input the initial volume and pressure  $p$  of the torpedo workshop.
3. Input atmospheric pressure  $p_0$  which is constant, a start time of zero, and the time increment  $\Delta t$  between calculations.
4. Calculate the position of each bulkhead/deck at time  $(t + \Delta t)$  from

$$X_i(t + \Delta t) = [p(t) - p_0] \frac{A_i (\Delta t)^2}{2 M_i} + v_i(t) \Delta t + X_i(t)$$

[Note that  $\Delta t$  is assumed to be so small that  $p(t)$  is essentially constant during the time interval between  $(t)$  and  $(t + \Delta t)$ ].

5. Calculate the velocity of each bulkhead/deck at time  $(t + \Delta t)$  from

$$v_i(t + \Delta t) = [p(t) - p_0] \frac{A_i (\Delta t)}{M_i} + v_i(t)$$

[Same note as in 4 above].

6. Calculate a new volume  $V(t + \Delta t)$  from

$$V(t + \Delta t) = \sum_{i=1}^6 [x_i(t + \Delta t) - x_i(t)] M_i + V(t)$$

TABLE 8. (CONT.)

7. Calculate the new internal pressure at time  $(t + \Delta t)$  from

$$p(t + \Delta t) = \frac{p(t) V(t)^{\gamma}}{V(t + \Delta t)^{\gamma}} \quad (40)$$

8. If  $p(t + \Delta t) < p_0$  then stop the calculations.
9. If the longitudinal bulkheads have reached the position of the shell, then stop the calculations.
10. Set  $t = t + \Delta t$ ,  $x_i(t) = x_i(t + \Delta t)$ , and  $v_i(t) = v_i(t + \Delta t)$ .
11. Go to 4 above and continue.

Debris Mass and Size

No reliable prediction methodologies have been located for determining debris mass or size. In an NSWC report<sup>21</sup> an experimental average mass was determined in model tests of explosions in nuclear attack submarines to establish safe handling arcs around the submarines during pierside topping off operations. All that is presented, however, are experimental data used to determine the arc distances.

Debris Distribution

All reports studied are concerned with the quantity-distance criteria of determining hazardous debris patterns by establishing the numbers of debris/fragments of kinetic energy equal to or greater than 80J (58 ft-lb) per 55.7 m<sup>2</sup> (600 ft<sup>2</sup>). The two experimental papers<sup>20,21</sup> present plots of areal density, with Reference 20 plotting the distribution by density per 55.7 m<sup>2</sup> (600 ft<sup>2</sup>). Kulesz, et al.,<sup>22</sup> presents debris density using the same criteria for several breakup scenarios. The density is determined following the procedure in Table 9. It should be noted here that this procedure was based on specific assumptions about the breakup of a portion of a particular ship. The angle  $\theta$  is governed by the extent of damage along a ship's length.

## DEBRIS METHODOLOGIES FOR REINFORCED CONCRETE STRUCTURES

Reinforced concrete (R/C) structures are widely used as high explosive (HE) storage magazines, HE manufacturing facilities, test facilities, and other structures. Many structures are designed to contain\* an accidental detonation of its contents using design methods such as those specified in TM5-1300.<sup>3</sup> For large quantities of HE it may be impractical to design for containment, particularly for operations which are considered low risk such as magazine storage, aircraft shelters, packaging buildings, and other areas where no machining, pressing, or other potentially hazardous activities with HE are being performed. If there exist large distances between a building containing HE (with operations at any risk level) and other occupied areas then the structure may not be designed to contain an accident. The definition of what constitutes a dangerous situation for debris is not universally determined; however, the DDESB has set a standard of not more than one fragment per 55.7 m<sup>2</sup> (600 ft<sup>2</sup>) with an impact energy of 80J (58 ft-lb) or more.

The problem of determining expected debris hazard to other occupied areas from an explosion in an R/C building has been approached using analysis of test and accident data to obtain statistical fits for debris parameters (initial velocity, range, distribution, etc.) and empirical methods which apply equations of motion to calculate debris parameters. Methodologies for debris from R/C structures include the following categories:

\*Containment--design of a structure to withstand an explosion and mitigate debris and blast hazards to other occupied areas. This may include permanent deformation of the wall without collapse.

TABLE 9. PROCEDURE TO DETERMINE THE HAZARDOUS DEBRIS DENSITY

1. Arc Length =  $R\theta$

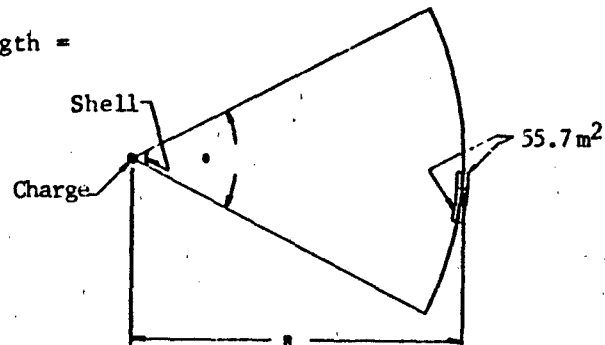
where R is the radius of a sector out from the charge.

R is actually the sum of the range of a fragment and the distance from the center of the explosion to the origin of the fragment (like the shell or bulkhead on a ship).

2. No. of  $55.7 \text{ m}^2$  squares along arc length =

$$(\text{arc length}) / \sqrt{55.7}.$$

The diagram to the right further illustrates this concept.



3. No. of  $55.7 \text{ m}^2$  squares covered by one debris

$$\text{fragment } (\geq 1) = (\text{width of debris}) / \sqrt{55.7}.$$

4. Effective number of  $55.7 \text{ m}^2$  squares covered =

$$N_e = (\text{number of debris})(\text{number of } 55.7 \text{ m}^2 \text{ squares covered by one debris fragment}).$$

5. Debris/ $55.7 \text{ m}^2$  =

$$\frac{N_e}{\text{No. of } 55.7 \text{ m}^2 \text{ squares along arc length.}}$$

- o Debris Size or Mass and Quantity
- o Initial Velocity
- o Launch Angle
- o Range
- o Distribution
- o Final Velocity
- o Drag Effects

This section of the report will review methodologies for each of the previously listed categories individually and describes one report which combined methodologies in several categories for a complete analysis to predict the debris hazard from an explosion inside an R/C structure. Also, a list of available debris data bases will be given and discussed.

#### Debris Size, Mass, and Quantity

Data bases from scaled tests and accident investigations indicate that debris size from an R/C structure can range from very small pieces up to entire parts of a building such as a wall or roof. This wide range of debris sizes as a percent of the total building area lends itself to a statistical fit. Kulesz, et al.,<sup>24</sup> conducted a search of DDESB accident reports containing debris data and performed a statistical analysis of debris weight. The accident data included data from seven accidents, and one result of the analysis is a plot of cumulative probability distribution of debris weight for three energy levels (see Figure 2). All buildings in the data base, except one, were primarily reinforced concrete. This review of methodologies could find no correlation between debris weight and range for a given energy level and it is suggested that debris weight could be assumed log normally distributed within a given debris range. Figure 2 shows that approximately 30 percent of the debris is 0.454 kg (1.0 lb) or less and approximately 75 percent of the debris is 4.54 kg (10 lb) or less for the energy levels indicated. A 4.54 kg (10 lb) cube of concrete is approximately a 12.7 cm<sup>2</sup> (5.0 in.) cube, hence 75 percent of the debris will be relatively small. From Figure 2, debris weighing 22.7 kg (50 lb) and up comprises only approximately 10 percent of the total debris. The report noted that the three curves on Figure 2 are nearly parallel, and standard deviations are almost equal for all log normal distributions. This could indicate that it may be possible to derive a scale factor from the energy ratios and the magnitudes which are related to the mean of the distribution.

Ahlers<sup>25</sup> studied an accidental explosion at the Pantex Ordnance Plant in 1960 and described debris size distribution. Although this report does not give a debris hazard methodology, Ahlers made several observations from the Pantex data base including:

- o Larger debris did not have as great a range as smaller debris.
- o At all distances, less than 6 percent of the total debris was greater than 1.36 kg (3.0 lb). At ranges larger than 366 m (1200 ft), no debris above 0.45 kg (1.0 lb) was found; at intermediate ranges of 183 to 366m (600 to 1200 ft), the percentage of debris above 1.36 kg (3.0 lb) is greater than that at distances shorter than 183 m (600 ft).

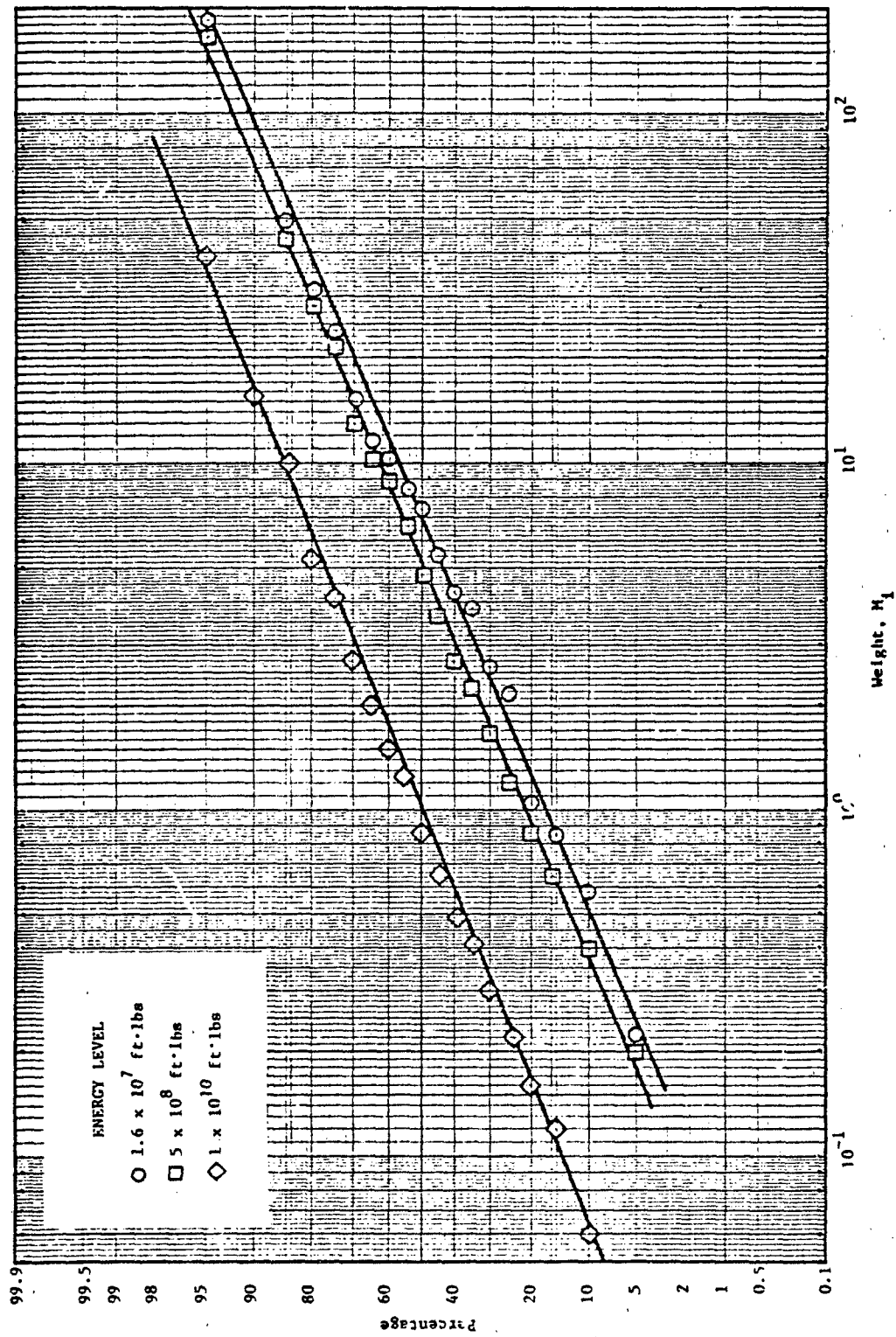


FIGURE 2. CUMULATIVE PROBABILITY DISTRIBUTION, DEBRIS WEIGHT (LB)

- o The largest concrete fragment weighed 1814 kg (4000 lb) and was found approximately 45.7 m (150 ft) from explosion center, all other debris was approximately 90.7 kg (200 lb) or less.
- o There were no concrete fragments above 1.3 kg (3.0 lb) found at ranges greater than 274 (900 ft), which could suggest an optimum design point for debris hazards, provided this is characteristic of explosions in R/C structures in general.

Vargas, Hokanson, and Rindner<sup>26</sup> conducted a study to determine fragmentation characteristics of reinforced concrete and masonry dividing walls subjected to close-in blast effects. The study included a model analysis and a series of model tests on 1/6 scale cantilevered and three-side supported R/C walls and full-scale concrete block masonry walls. An extensive amount of data were collected. A model analysis was conducted, and the results guided the data presentation. The conclusions drawn from this useful experimental effort included:

- o Debris emanating from the interior of the panel comprises 40 percent of the number of concrete fragments produced in any test. Debris originating from the outside face (facing the recovery area) comprises another 40 percent of the concrete fragments. The remaining 20 percent of the concrete fragments are produced from the acceptor (charge side) of the panel.
- o Debris produced in these kinds of experiments can be classified as either "chunky" or "pancake" in shape. The average range of "chunky" concrete fragments is generally 20 to 50 percent greater than the average range of the "pancake" concrete fragments on a given test.

Based on the statistical distribution of debris range, mass, and velocity, the following conclusions can be drawn:

- o Mass and range distributions in the format of Mott Distributions for arena fragmentation tests were prepared. The resulting distributions for debris range and mass are qualitatively similar, and similar observations were drawn. If all other parameters are held constant, more concrete fragments at each mass level and more concrete fragments at each range level are produced when:
  - a. the total impulse applied to the panel is increased,
  - b. the panel compressive strength is decreased,
  - c. the reinforcement spacing is increased, or
  - d. the number of supporting edges is increased.

Initial Velocity

The velocity of individual concrete fragments due to shock loading varies and depends on: (1) the magnitude of the excess impulse defined as the blast impulse minus the flexural impulse capacity of the element (area under the resistance-time curve), (2) the mass of the debris, (3) the location of the concrete fragment prior to collapse, (4) the interaction between the debris during their flight, and (5) the strength and time history of the compressive stress wave transmitted through the R/C wall or roof as the blast wave is reflected. Although the velocities of individual concrete fragments differ, the average translational velocity,  $V_i$ , of the debris after complete failure can be approximated from the excess impulse,  $i_e$ , and the momentum of the wall or roof after collapse. The equation below<sup>3</sup> provides a means of estimating the debris velocities from the blast impulse and a knowledge of the R/C geometry.

$$i_a^2 = C_u \left( \frac{P_H d_c^3 f_{ds}}{H} \right) + C_f d_c^2 v_i^2 \quad (3)$$

where

$i_a$  = applied unit blast impulse

$P_H$  = reinforcement ratio in the horizontal direction

$d_c$  = distance between the centroids of the compression and tension reinforcement

$f_{ds}$  = dynamic design stress for the reinforcement

$H$  = span height

$v_i$  = maximum velocity of the post-failure debris

$C_u$  = impulse coefficient

$C_f$  = post-failure debris coefficient

A simpler expression widely used is a momentum balance that ignores strain energy and equates applied specific impulse times area with kinetic energy as:

$$v_i = \frac{i A}{m} \quad (4)$$

where:

$A$  = area of applied impulse

$i$  = applied specific impulse

Vargas, et al.,<sup>26</sup> discussed earlier, present plots of the largest debris velocity as a function of impulse factor. The report concludes:

- o There existed a wide range of velocities and launch angles in every test. The majority of the debris particles were observed leaving the wall in a direction perpendicular to the original surface, and moving with a velocity at or near the maximum observed velocity. Late in the event, other debris particles were observed which traveled at off-normal trajectories and at somewhat lower velocities.
- o The largest velocity appeared to be independent of the reinforcing bar (rebar) spacing but dependent on total impulse, effective wall thickness, and the restraint conditions (the panels supported on three sides had higher velocities than those supported on one edge, all else equal). Some effect of concrete compressive strength below 27.6 MPa (4000 psi) was observed.
- o Debris velocities for masonry walls were lower than those for R/C walls.

Debris generated from completely or partially enclosed R/C structures which collapse due to shock loading can undergo acceleration from the quasi-static or gas phase of the blast loading as well as the shock phase. To account for this acceleration and its contribution to debris velocity, Kulesz, et al.,<sup>22</sup> used a computer program called GASEX to calculate the acceleration due to gas phase for an explosion in a torpedo tender. Typically each wall and roof are treated as a panel with initial velocity due to shock loading. The quasi-static pressure is entered as initial pressure. In a time step fashion the panels are allowed to move, a new volume and internal pressure are calculated, and time step repeated until internal pressure is atmospheric. The GASEX program is explained in more detail in Table 8. Debris originating from a particular wall or roof will have the same velocity as that for the wall or roof panel used in GASEX. Similar programs called BOXCYL and CYLIN can be used which take into account volume change and pressure venting relief between concrete fragments.<sup>23</sup> Debris can be generated from completely or partially enclosed R/C structures which do not collapse due to shock loading but do collapse due to the quasi-static loading. To account for this, the structure is treated as a pressure vessel which ruptures and breaks into panels that are accelerated due to the expanding gas. Reference 27 used this procedure in an R/C aircraft shelter by running the program called CYLIN.

#### Launch Angle

The angle between the initial velocity vector of a concrete fragment and the ground is called the launch angle of the fragment. Although debris from an R/C surface may take on a wide range of launch angles, the predominate angles are approximately normal to the surface. This conclusion was suggested by Vargas, et al.,<sup>26</sup> where the predominate launch angle of the higher velocity debris was normal to the test panel surface. Merz<sup>28</sup> reports that debris dispersal tends to be normal to the building surface. Moseley and Whitney<sup>27</sup> performed an analysis on an R/C Norwegian aircraft shelter while concurrent model tests (1/20 and 1/100 scale) were being performed. The analysis used launch angles for debris in the analysis which were close to perpendicular to

each surface. These launch angles were obtained through review of films of the model tests which indicated a wide range of launch angles from each surface but a predominance normal to the panel.

#### Debris Range

Kulesz, et al.,<sup>24</sup> used similitude theory to organize a data base and performed a statistical analysis on scaled debris range. The report includes a plot of cumulative probability versus range, R, and also nondimensional range, R, (range divided by square root of average presented debris area, A) for three energy levels which are reproduced here as Figures 3 and 4. These curves allow one to predict the percentage of concrete from an R/C structure that will travel a certain distance. The report noted that the three curves on Figures 3 and 4 are nearly parallel. This could indicate that it may be possible to derive a scale factor from the energy ratios and magnitude which is related to the mean of the distribution.

Ahlers<sup>25</sup> compiled a data base for a very wide range of accidental and test explosions and made linear and quadratic curve fits for the data base, including maximum debris distance versus yield, energy scaled ( $W^{1/3}$ ) maximum distance versus yield, and maximum debris distance versus impulse. The correlation coefficient for the curve fits tended to be low (0.7 or less); however, this may be due to the very wide range of data used for the fits. The data base will be discussed later.

Analytical methods for predicting debris range incorporate equations of motion and a set of assumed initial conditions which can include concrete fragment mass, launch angle, drag coefficient, velocity, lift coefficient, and attack angle. Various authors give relationships between debris range and velocity. These studies were discussed earlier. Those methodologies which apply for R/C concrete (i.e., make no assumptions such as shape or density) are listed in Table 10.

#### Distribution

Kulesz, et al.,<sup>24</sup> give a methodology for generating a hypothetical missile map using Figures 2 and 3 and the procedure given in Table 11. This procedure assumes all weights are distributed log normally in a given interval of range. Ahlers<sup>25</sup> studied the distribution of debris from the Pantex accident noted earlier. The reference included plots of square feet/concrete fragment and square feet/pound of debris versus range. This analysis appears to have assumed concentric rings of equal area about the charge for the ground area term. However, as the reference points out, the debris pattern was directional. Hence, using the area of a whole ring instead of the part of the ring containing debris will give lower ground area per number or pound of debris. This reference also includes plots of square feet per concrete fragment versus ground range for numerous accidents of a wide range of structural types (light-frame construction, R/C, and earth-covered igloo magazines). Merz, et al.,<sup>28</sup> discuss R/C debris distribution and the results of 1/10 scale model test for above-ground storage magazines and includes these conditions:

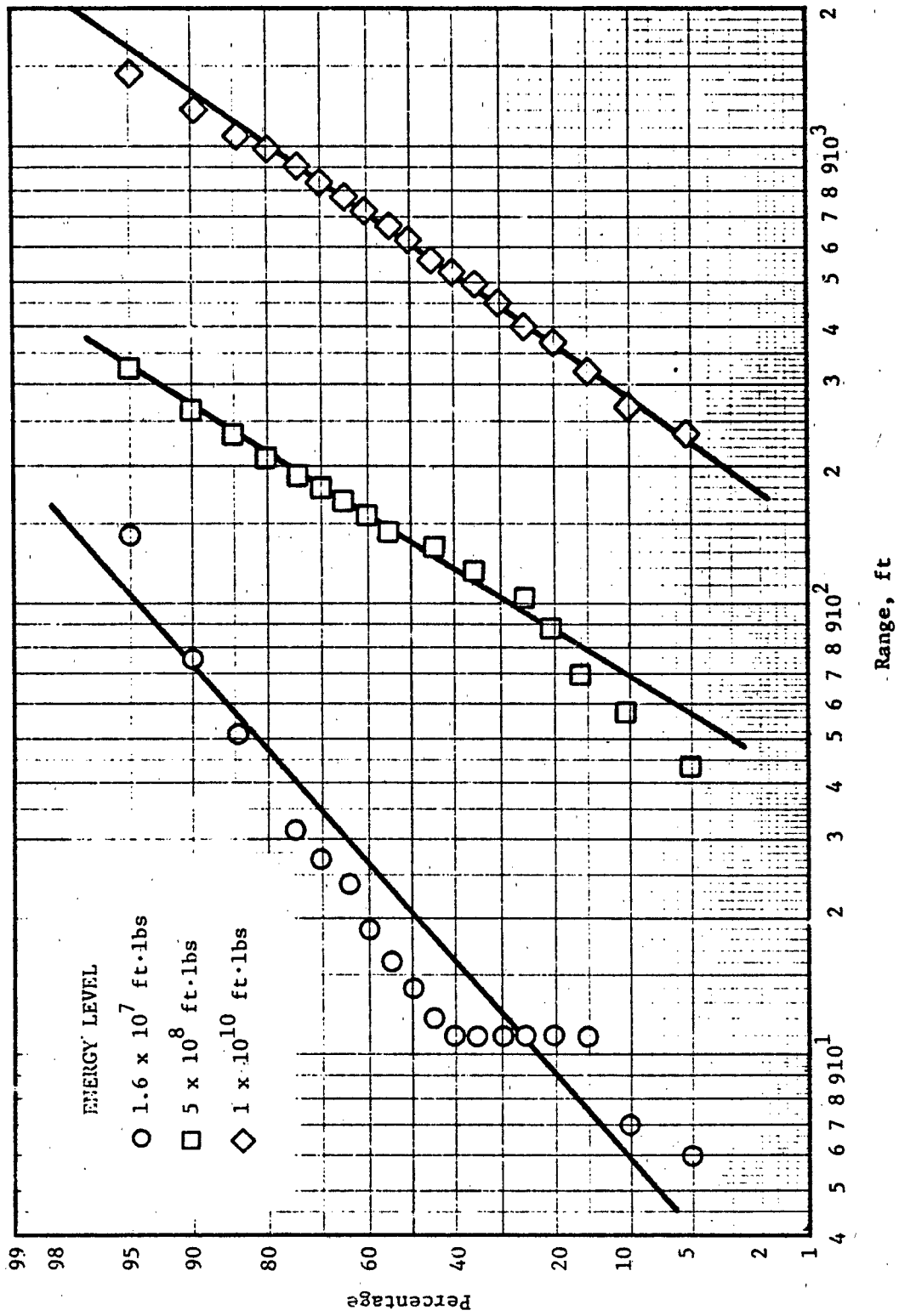


FIGURE 3. CUMULATIVE PROBABILITY DISTRIBUTION, DEBRIS RANGE (FT)

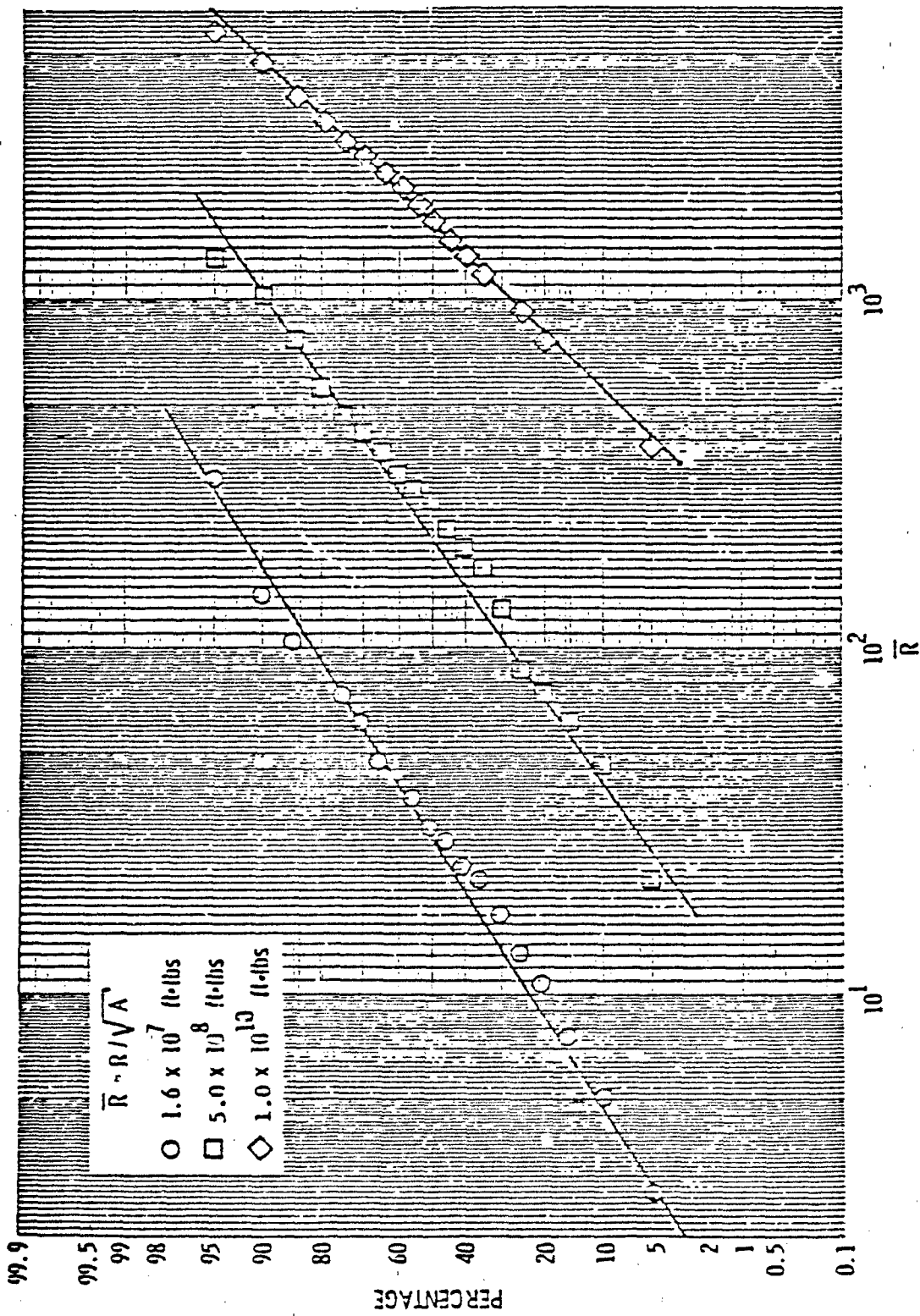


FIGURE 4. DEBRIS CUMULATIVE PROBABILITY DISTRIBUTION, NONDIMENSIONAL RANGE,  $\bar{R}$

TABLE 10. METHODOLOGY FOR PREDICTION OF DEBRIS RANGE

PARAMETER	METHODOLOGY	LIMITS of APPLICABILITY	DESIGNATION	REFERENCE
Range (As a function of velocity)	$v = V \exp(-R/L)$ <p>where: <math>v</math> = velocity  <math>R</math> = range  <math>L</math> = distance in which fragment velocity drops to 1/e of its initial value, <math>V</math></p> $L = \frac{2(k^2 m)^{1/3}}{C_D \rho}$ <p><math>k</math> = shape factor  <math>m</math> = mass  <math>\rho</math> = air density  <math>C_D</math> = drag coefficient</p>	Constant Drag No Gravity		(25)
Solutions to Equations of Motion	$\ddot{x} + 3v\dot{x} + g \sin \alpha = 0$ $\ddot{y} + 8v\dot{y} + g \cos \alpha = 0$ <p>where: <math>\bar{x}</math> and <math>\bar{y}</math> are local coordinates tangent and normal to trajectory  <math>v</math> = speed in path  <math>g</math> = acceleration of gravity  <math>\alpha</math> = angle between <math>\bar{x}</math> axis and horizontal  <math>\beta</math> = aerodynamic drag coefficient</p> <p>solutions:</p> $\bar{x}_0 = \{\log(1+u)\}/\beta$ $\dot{\bar{x}}_0 = v_0/(1+u)$ <p>where <math>u = 8v_0 t</math></p> $\bar{x}_p = -(g/2)t^2 \sin \alpha (8u/3)/(1+u)$ $\bar{y} = \frac{(-g/2)t^2 \cos \alpha}{2} [(u(1+u/2) - \log(1+u))]$ $\dot{\bar{x}}_p = \frac{-gt \sin \alpha}{(1+)^2} [1+u(1+u/3)]$ $\dot{\bar{y}} = -gt \cos \alpha (1+u/2)/(1+u)$	Gravity Free Solution		(17)
				(17)

TABLE 10. (CONT.)

PARAMETER	METHODOLOGY	LIMITS OF APPLICABILITY	DESIGNATION	REFERENCE
Solutions to Equations of Motion (con't)	Global Displacements:			(21)
	$\Delta x = \bar{x} \cos \alpha - \bar{y} \sin \alpha$ $\Delta y = \bar{x} \sin \alpha + \bar{y} \cos \alpha$	$t \ll (8g)^{-1/2}$		
	Rotation of Trajectory Tangent			
	$\alpha = \tan^{-1} \left( \frac{\dot{y}}{\dot{x}} \right)$			
	$\ddot{x} = - \frac{A_D C_D \rho}{2m} v_x^2 \cos \alpha$ $\ddot{y} = -g - \frac{A_D C_D \rho}{2m} v_y^2 \sin \alpha$	No Lift		(18)
	where: $\rho$ = air density $g$ = acceleration of gravity $A_D$ = drag area $C_D$ = drag coefficient $\alpha$ = angle between horizontal and tangent to trajectory $v_x, v_y$ = velocity components $m$ = mass			
	$\ddot{x} = - \frac{A_D C_D \rho}{2m} (\dot{x}^2 - \dot{y}^2) \cos \alpha$ $- \frac{A_L C_L \rho}{2m} (\dot{x}^2 + \dot{y}^2) \sin \alpha$ $\ddot{y} = -g - \frac{A_D C_D \rho}{2m} (\dot{x}^2 + \dot{y}^2) \sin \alpha$ $+ \frac{A_L C_L \rho}{2m} (\dot{x}^2 + \dot{y}^2) \cos \alpha$	Life and Drag	FRISS Equations	(18)
	where: $A_L$ = lift area $C_L$ = lift coefficient Other symbols as above.			

TABLE 11. METHODOLOGY OF PREDICTING DEBRIS DISTRIBUTION<sup>24</sup>

A procedure for estimating the number of debris missiles of a given mass interval which will fall within a given distance from an explosion inside a building is as follows:

1. Estimate  $W_B$  = total destroyed weight of the building (portion of the building which has fragmented). This estimate will depend mainly upon the amount of explosive stored or machined in the building at any given time and the building structure and shape.
2. Using the weight distribution in Figure 2, obtain the average weight of debris from the explosion,  $W_a$ , by reading it off the appropriate curve at the 50th percentile. The total number of debris fragments from the explosion is then

$$N_f = \frac{W_B}{W_a}$$

3. Using the range distribution in Figure 3, take equal percentage increments (0-10%, 10-20%, etc.) or equal range increments (0-10 ft, 10-20 ft, etc.) and find the number of debris fragments  $N_{f1}$ , in each increment. (If equal percentage increments were taken, the number of debris fragments in each increment is, of course, the same.)

TABLE 11. (CONT.)

4. Again using the weight distribution in Figure 2, determine the percentage of debris in a particular weight interval. The total numbers in each range interval have already been calculated (Step 3). Thus, the number of debris of a particular weight in a particular range interval (distance out from the source) can be determined. The major assumption made in this procedure is that all weights are distributed log normally in a given interval of range. Since we could find no correlation between weight and range for a given energy level, and since weight is log normally distributed over each energy level (which covers the entire range), there is no reason to assume that weight is not log normally distributed within a given range increment.

- o Debris dispersion in R/C buildings is dependent on building shape. In the direction normal to walls there is a greater number of concrete fragments with larger range than out from corners.
- o The more strength and ductility in a structure, the more directional the dispersal is in the surface normal directions. The model magazines were reinforced concrete which represented ductile construction of considerable strength and the failure of the magazines were similar to a chamber pressure failure, with forces acting perpendicularly on the four walls. The initial shock waves did not contain enough energy to fail the structure.
- o Merz suggests that, because of the relatively flat trajectories of fragments, distributions should not be measured by number of concrete fragments per ground area, but number of concrete fragments transversing a plane vertical to the ground and parallel to a surface. This is because debris presents a hazard along its entire path and not just where it eventually lands.
- o Merz also points out that for the model tests and many full-scale instances, the debris presents the predominate hazard in an accident of this type.

#### Final Velocity

Final velocity of debris fragments can be predicted using equations of motion, the initial conditions and solving for conditions at impact. These equations are given in Table 10.

#### Hazards Analysis

Moseley and Whitney<sup>27</sup> combined methodologies in several of the above discussed categories for a prediction of a debris hazard for an explosion in an R/C structure. The object of the project was to investigate several analytical methods of predicting blast and fragment hazards from an accidental explosion inside a Norwegian aircraft shelter. This work was in support of model tests being conducted in Norway. The steps taken for the fragment analysis included:

- o Determination of debris fragment size and initial trajectory angle. Films of model tests were reviewed to obtain predominate launch angles and relationship between debris fragment sizes and location on structure. Trajectories were found to be approximately normal to the surface. Debris sizes were found to be small, close to the off-centered (in the building) charge and a wide range of sizes, including entire surfaces, away from the charge location.
- o Determination of initial velocity consisted of calculating velocity from both shock loading and quasi-static pressures. Shock velocity,  $V_i$ , was calculated using Equation (4). Quasi-static velocity was calculated using the program CYLIN. The velocities computed using both shock and quasi-static loads appeared to compare well with the model tests. The structure was overloaded severely in these tests.

- o Debris range was determined using the program FRISB. Input was concrete fragment sizes and mass, and corresponding velocities as determined above. Launch angles were predominately normal to the surfaces, but also included some off-normal launch angles indicated by films. The code was run considering only drag forces, then repeated considering both lift and drag forces. These calculations led to determination of maximum concrete fragment ranges as a function of direction around the shelter. Comparison with the results of the test data are incomplete pending further test and data reduction.

#### Data Bases

Several reports include the bulk data or indicate where bulk data for R/C debris may exist. The data bases available include:

- o Kulesz, et al.,<sup>24</sup> include debris data from six structures obtained from DDESB accident reports. The data include estimated yield, individual debris weight, and individual debris range.
- o Reference 25 contains a large collection of accident data which include amount of explosive, maximum debris distance, assumed applied impulse, and  $W^{1/3}$ -scaled debris distance and impulse. Also the reference includes a table of data from the Pantex accident including individual debris size, mass, and range. Number of concrete fragments, total mass of debris, average debris weight, and individual debris mass are given for ground range increments in this reference.
- o References 27 and 28 indicate data bases for model tests are available, however, do not include the data in these reports.
- o Reference 26 includes the data base for debris from scale models of dividing walls. This includes number of concrete fragments recovered for several mass ranges, average mass for each range, average distance for each mass range, total number of concrete fragments, and concrete fragment shape. The reference includes a model analysis and plots of scaled data.
- o Edmunds<sup>29</sup> has debris data for brick walls which fail under instantaneously applied static loads. This includes quantity, weight, and distance of individual debris.

## CHAPTER 3

## ACCEPTABLE HAZARD HANDLING ARC CRITERIA

Currently, manufacturing, storage, or handling of high explosives in quantities between 68 and 13,600 kg (150 and 30,000 lb) is regulated by the Explosive Safety Quantity Distance Criteria established by the DDESB. These criteria define the Acceptable Hazard Handling Arc as 381 m (1250 ft). Exemptions may be granted for those cases where approved analysis or testing has been conducted. In this case, the acceptable hazard handling arc for an explosion event is defined by the minimum range at which both the blast overpressure and the fragment hazard criteria are satisfied. The criteria are as follows:

1. the blast overpressure is less than 6.89 kPa (1.0 psi), and
2. the number of hazardous fragments entering a given region is less than 1.0 hazardous fragment per  $55.7 \text{ m}^2$  ( $600 \text{ ft}^2$ ) of ground surface area. A fragment is considered hazardous when it has an impact energy equal to or in excess of 80J (58 ft-lb).

During this program we attempted to discover the basis for the above criteria. We did not identify the original source, but we believe the 80J (58 ft-lb) refers to a 50 percent injury (50 percent fatality) level of a combat soldier, and the  $55.7 \text{ m}^2$  ( $600 \text{ ft}^2$ ) refers to 100 times the ground surface covered by one prone soldier. In Reference 30, a review of different criteria for hazardous fragments was presented. These different criteria are summarized in Table 12.<sup>31,32</sup> Two of the criteria are based on the kinetic energy at impact, while the other criterion is based on impact momentum. Interestingly enough, the last three criteria are all less conservative than the standard 80J (50 ft-lb) criteria. This is shown in Table 13, where allowable velocities for fragments with masses of 0.025, 0.1 and 0.4 kg (0.055, 0.22, and 0.90 lb) are summarized for all four criteria. If the last three criteria were used instead of the 80J (58 ft-lb) criteria, then larger acceptable hazard arcs would be derived.

The reason for this discussion is to emphasize that different definitions for a hazardous fragment exist in the literature, and for some situations a different criterion than 80J (58 ft-lb) of energy may be more appropriate. Indeed a more rational approach to specifying hazard arcs would be to specify the fragment energy as a function of the "target." As an example, different hazardous fragment energies could be derived for a specified level of:

TABLE 12. HAZARDOUS FRAGMENT CRITERIA

<u>Criterion</u>	<u>Definition</u>	<u>Reference</u>	<u>Casualty Level</u>
A	K.E. = 80J	Wide use	
B	$\frac{K.E.}{D} = 2.5 \times 10^4 N$	Netherlands <sup>30</sup>	Penetration of 37 mm of poplar wood
C	$M^{0.4} V = 27.1 \text{ kg}^{0.4} \text{ m/s}$	German, 1965 <sup>31</sup>	
D	$\frac{MV}{A} = 2.0 \times 10^4 \frac{\text{kg}}{\text{m}^2}$	U.S., 1951 <sup>32</sup>	

- K.E. - fragment kinetic energy  
M - fragment mass  
V - fragment velocity  
A - average fragment presented area  
D - characteristic fragment length

TABLE 13. ALLOWABLE VELOCITIES FOR CERTAIN MASSES USING THE HAZARDOUS FRAGMENT CRITERIA

Criterion	Allowable Velocities (m/ε) for Fragment Masses of		
	0.025 kg	0.1 kg	0.4 kg
A	80	40	20
B*	190	120	75.8
C	119	68.1	39.1
D*	204	132	83.1

\* Assuming spherical, steel fragments

1. human casualty,
2. damage to nearby buildings (concrete structures), and
3. damage to nearby ships (steel structures).

However, for safety evaluations, the human casualty level would probably always override the damage levels for buildings and ships. Correspondingly the area used in the estimation of the fragment flux should also correspond to the appropriate presented area for a human, a building, or a ship. In the estimation of areas, the presented area should correspond to the frontal area for low trajectory fragments, or ground surface area for high trajectory fragments. For safety evaluations, the soldiers position should be standing (not prone as is now considered)--for this case, then, the vulnerable target area for low trajectory debris is greater than for high trajectory debris. The use of more specific definitions for hazardous fragment flux would result in more credible safe handling arcs.

#### A GENERAL METHOD FOR PREDICTING THE FRAGMENT AND DEBRIS ENVIRONMENT

The general method for predicting the fragment and debris environment resulting from an accidental explosion is given in flow chart form in Figure 5. The method is general and can be applied to an explosion of a weapon in the open field or to an explosion inside a building. For the case of an explosion in a building, the methodology is applied separately for the fragments and the debris, and the results are combined in the last step to define the hazard arc. The method can conceptually be applied to situations where no data or limited data are available by substitution of engineering estimates for the various parameters in the problem definition phase.

The methodology presented in this interim report parallels a similar methodology developed by J. M. Ward<sup>33</sup> for predicting and subsequently analyzing the fragment hazard associated with the accidental detonation of weapons, specifically a pallet load of Mk 82 bombs. His methodology, which is an application of concepts developed by F. B. Porzel<sup>34</sup> for NESIP, was developed for the special case of an explosion in the open field. This method provides for both high- and low-launch angle fragments. This distinction is important in the establishment of acceptable hazard arcs. In this report, we have included this important concept in the estimation of fragment hazards for both fragments and debris missiles.

#### Assumptions

Several assumptions were made in the preparation of this flow chart. These assumptions are:

1. There is a uniform distribution of fragments or debris missiles with respect to launch angle.
2. At any launch angle, there is a uniform distribution of fragment or debris mass.

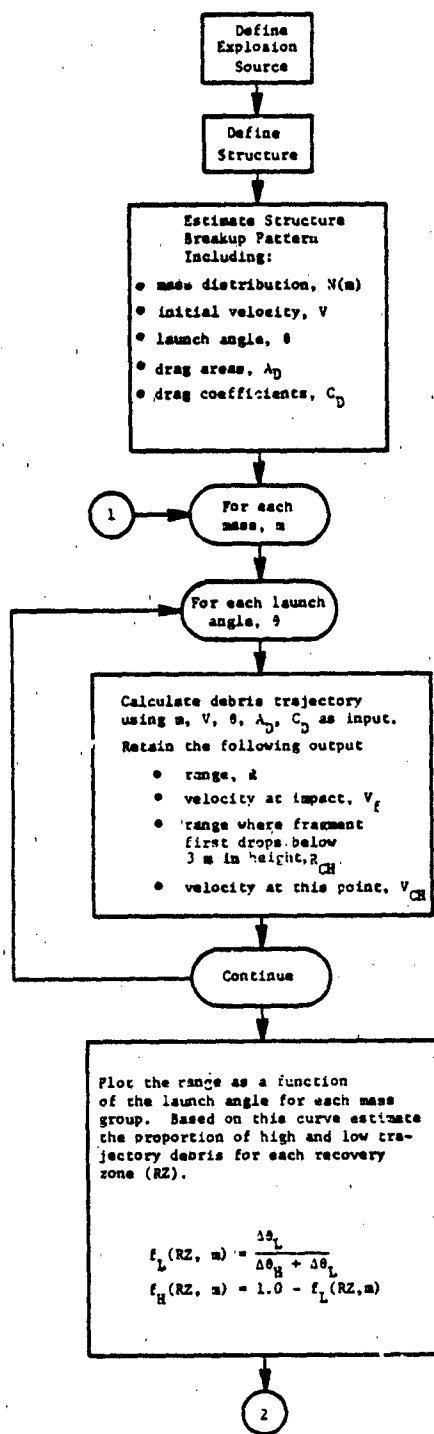


FIGURE 5. FLOW CHART FOR PREDICTING THE FRAGMENT AND DEBRIS ENVIRONMENT AROUND EXPLOSIONS

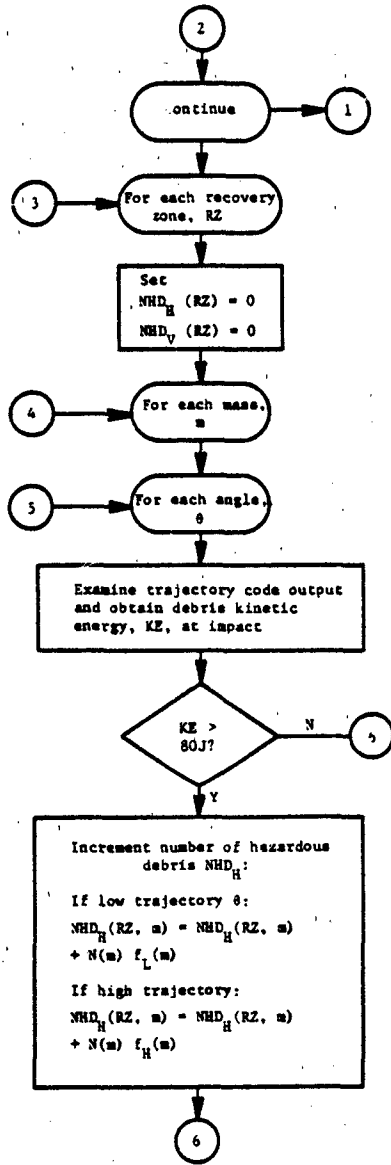


FIGURE 5. (CONT.)

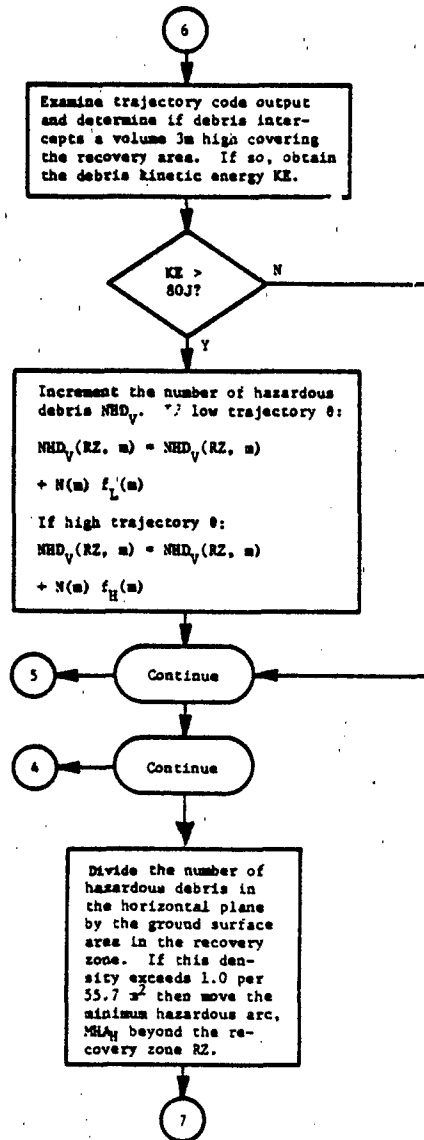


FIGURE 5. (CONT.)

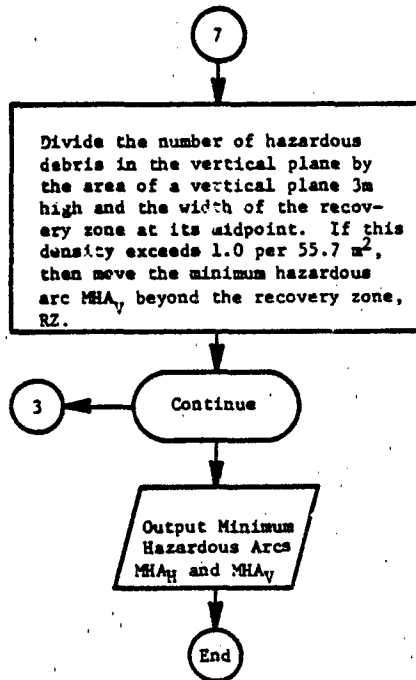


FIGURE 5. (CONT.)

3. The fragments or debris have the same initial velocity.
4. The fragments or debris missiles exhibit drag and no lift. The drag area is approximated from a simple function of the fragment mass. The function is derived from measurements of the fragment presented area for a small sample of fragments. The drag coefficient is chosen according to the fragment shape. Drag coefficients for tumbling cubes or for shell fragments are used in the absence of specific fragment shape information.

The first three assumptions, which are related, are made to simplify the problem formulation. It is realized that in practice uniform distributions are not likely to be encountered. However, the inclusion of nonuniform distributions (where they can be derived) would require Monte-Carlo simulations in order to arrive at a reasonable solution. For some situations, such as the off-center explosion of a charge within a building, the assumption of a constant initial velocity may not be appropriate. In this case, it is possible to use this methodology individually for, as an example, each of the four walls and the roof, and to superimpose the results in the last stage of the method. The last assumption refers to the method of calculation used to estimate the debris trajectory. Drag coefficients and areas for stable orientation solids are used in the trajectory calculations, since little information is available for equivalent drag coefficients for tumbling objects.

#### APPLICATION OF THE METHOD

##### Problem Definition

The fragment/debris environment prediction methodology presented in Figure 5 consists of four parts. The first and most difficult part to calculate consists of the problem definition. Where data are available, this phase, although tedious, presents little problem. Where no data are available, a considerable amount of engineering judgement is required to define adequately and accurately the requisite input parameters. The specific parameters which must be defined in the initial part of the methodology are:

1. the mass distribution--generally presented in the Mott format:
 
$$N(m > M) = N_0 \exp(-m/m_0)^\lambda$$
2. the initial velocity of the fragments or the debris
3. the range of launch angles--for example debris missiles from a reinforced concrete wall preferentially emanate normal to the original plane of the wall. Thus the range of launch angles can be fairly narrow.
4. the fragment/debris drag areas and coefficients--generally tumbling cubes and shell shapes are selected for the fragments, and drag coefficients are taken from standard tables. The drag areas are estimated from a simple relationship of presented area as a function of the fragment mass. For debris, other shapes may be

more appropriate; for example, concrete rubble might be represented by tumbling cubes or spheres.

5. the range distribution--the number of fragments/debris per recovery zone broken down by mass,  $N = f(R,m)$ , determined experimentally.\*

In this section the methodology will be illustrated using data collected in some recent experiments conducted at SwRI.<sup>26</sup> In these tests, reinforced concrete panels were overloaded by bare explosive charges placed at small scaled distances from the panel. In each test, the debris was recovered, and the recovery location, mass, shape, and physical dimensions were recorded. The test, presented as an example in this report, is summarized in Table 14. A missile map for this test is given in Figure 6, and a mass distribution is given in Figure 7. The maximum velocity measured in the high-speed films was 23.5 m/s (77 fps). The number of concrete fragments collected in the six recovery areas marked on the missile map is summarized in Table 15.

The range of launch angles assumed by the debris missiles was established based on the missile map given in Figure 6. Assuming that the debris is ejected in a circularly symmetric pattern, the range of launch angles is the same as the range of the debris spray angle. This assumption was verified, at least approximately by the high-speed films taken during the test. It was noted in the films that the preferential debris launch angle in this test was normal to the original plane of the wall panel, which is in conflict with the assumption of a uniform distribution of debris missiles with respect to launch angle. Nonetheless, for the purposes of illustrating the methodology, the range of launch angles used in this example problem was taken to be -20 to +80 degrees. Each debris missile was assumed to have an initial height of 9 inches, the height of the charge above the ground. This represents another simplification for the purpose of this example problem. For the test, of course, the initial height varied from ground level to the top of the panel.

The final input, which was necessary to demonstrate the methodology, was debris drag or presented area. To generalize the effects of different debris shapes (pancake or chunky type) and mode of flight for tumbling concrete fragments, average areas were determined for each debris mass recovered by computing the equivalent volume of the debris, using the three orthogonal dimensions corresponding somewhat to width, length, and thickness, and assuming the debris missile was a rectangular solid. This leads to the following expression for the drag area:

$$A = (L \times W \times T)^{2/3} \quad (5)$$

The areas calculated using Equation (5) were then plotted as a function of debris mass as shown in Figure 8. The equation of this line, the percent standard deviation and the multiple correlation coefficient, R, are included on

\*This parameter is considered as an input variable only if there are data available. When test data are available then the analytical procedure described is a procedure for analyzing the recovered fragment/debris data.

TABLE 14. GENERAL SUMMARY FOR A TYPICAL DIVIDING WALL TEST

<b>PANEL CHARACTERISTICS</b>	
PANEL SPAN	0.46 M
REBAR DIAMETER	2.11 MM
REBAR COVER	6.35 MM
CONCRETE COMPR. STR.	35.43 MPA
PANEL THICKNESS	55.6 MM
REBAR SPACING	25.4 MM
NO. EDGES SUPPORTED	3
<b>CHARGE CHARACTERISTICS</b>	
CHARGE TYPE	C-4
CHARGE WEIGHT	453.60 GM
REFL. IMPULSE	5.17 KPA-S
INITIATOR	M-6
STANDOFF DISTANCE	0.147 M
CHARGE HEIGHT	0.152 M

**FRAGMENT CHARACTERISTICS**

SOURCE	TYPE	NO. FRAGS RECOVERED	MASS (GM)		RANGE (M)	
			LG	AVG	LG	AVG
RED		79	48.06	7.01	24.15	8.54
WHITE		57	27.51	9.65	25.79	12.59
BLUE		21	39.75	8.20	10.82	3.27
GREEN		8	42.75	7.42	8.26	4.93
INTERIOR		75	121.95	10.05	14.14	4.18
ACCEPTOR		10	18.14	8.29	3.26	1.80
-----						
<b>SHAPE</b>						
	PANCAKE	156	121.95	9.38	25.79	6.74
	CHUNKY	94	48.06	7.55	24.15	8.29
-----						
<b>TOTAL</b>		250	121.95	8.69	25.79	7.32

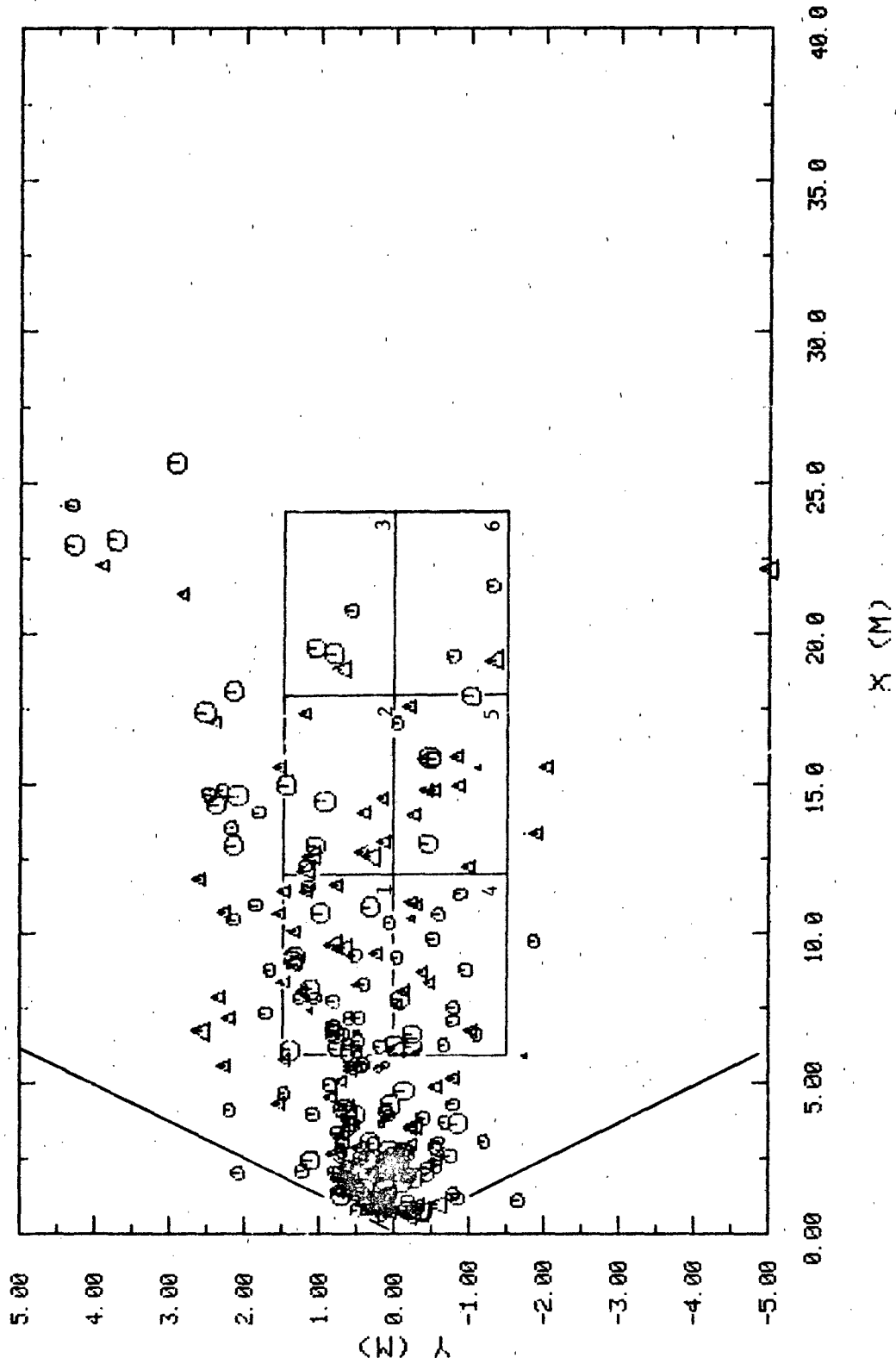


FIGURE 6. MISSILE MAP FOR A TYPICAL DIVIDING WALL TEST

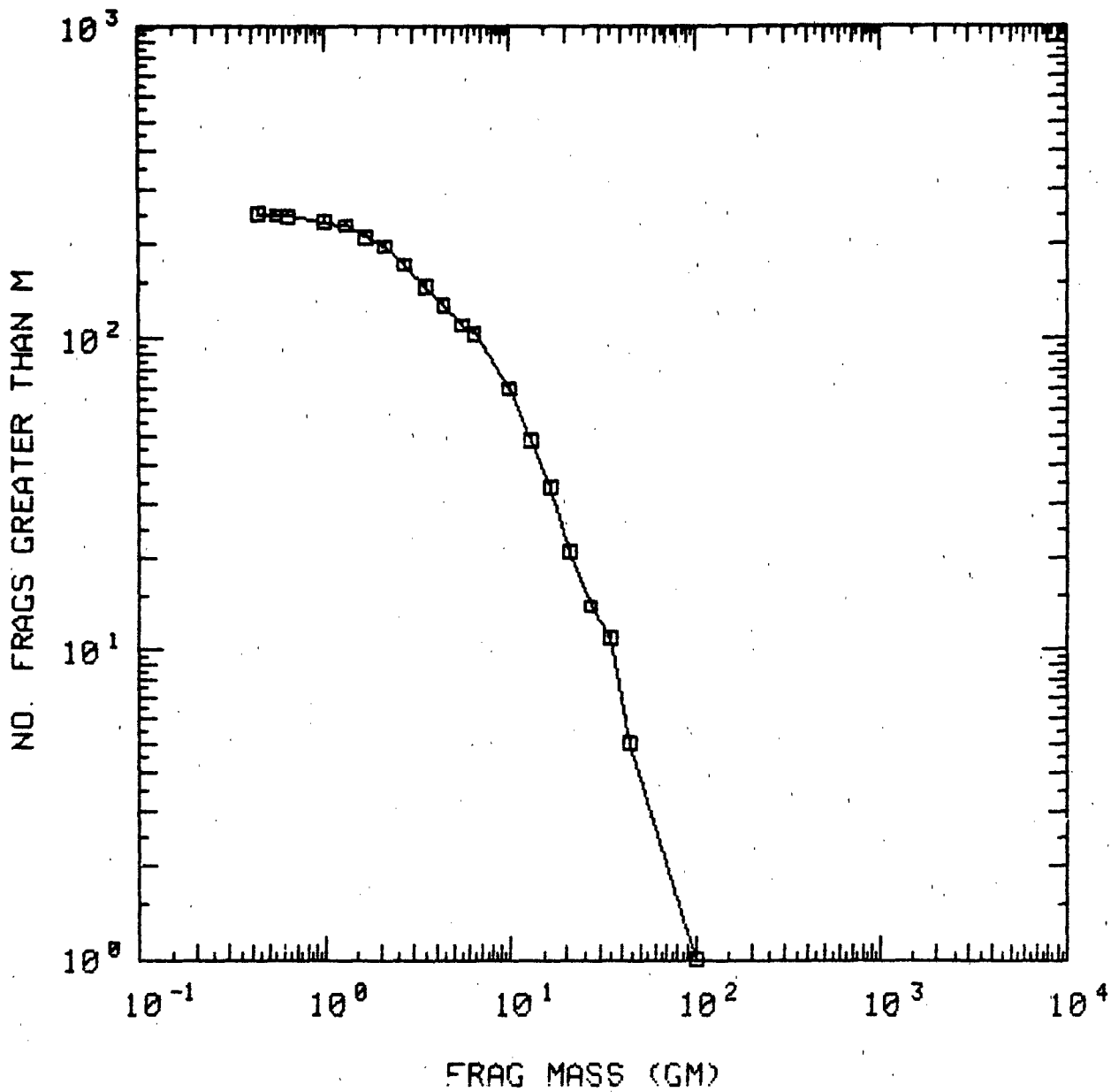


FIGURE 7. MASS DISTRIBUTION FOR A DIVIDING WALL TEST

TABLE 15. NUMBER OF CONCRETE FRAGMENTS RECOVERED BY MASS IN THE SIX RECOVERY ZONES

Mass Interval (gm)	Number of Debris Missiles Recovered in Zone					
	1	2	3	4	5	6
0.0 - 0.9	4	0	0	1	1	0
0.9 - 4.5	20	3	0	17	8	0
4.5 - 27.0	13	9	4	4	4	3
27.0 - 90.0	1	0	0	1	0	0

the graph in Figure 8. Using this fitted equation, drag areas could be determined for all masses considered in the analysis. An average drag coefficient of 0.9 was used for all debris in this analysis since they were mostly chunky in shape and 0.9 is the average between the drag coefficient for a face-on and edge-on cube.

#### Hazard Arc Definition

**General.** In this report, two criteria for defining debris as hazardous to personnel are discussed. The traditional criterion considers debris hazardous if it strikes the ground surface with more than 80J (58 ft-lb) of kinetic energy. This criterion applies to prone personnel. Another criterion considers debris hazardous at a specific point if it passes through a vertical plane with more than 80J (58 ft-lb). This criterion applies to standing personnel and, therefore, the height of the vertical plane is set at 3 m (9.8 ft).\* The following subsection will describe the methodology which will be used to calculate debris densities in the horizontal and vertical planes around an explosive source. This methodology requires that the ground surface around the explosion source be divided into recovery zones. The horizontal debris density in each recovery area is calculated as the number of hazardous debris elements that land in that zone divided by its ground surface area. The vertical debris density corresponding to that recovery area is calculated as the number of hazardous debris elements that cross any vertical plane 3 m (9.8 ft) high in the recovery zone. One such vertical plane is shown schematically in Figure 9. A recovery area is considered unsafe for personnel if the hazardous debris density in either the vertical or horizontal plane exceeds one hazardous debris element per 55.7 m<sup>2</sup> (1/600 ft<sup>2</sup>).

**Debris Density in the Horizontal Plane.** The hazardous debris in the horizontal plane is determined by examining the debris which land in each recovery area in a test. For each recovery location there are two trajectory solutions which could explain the observed debris range: a high and a low trajectory. This distinction is important since the input energies associated with these two trajectory solutions can be remarkably different. For this reason it is necessary to determine the ratio of high trajectories to low trajectories per recovery area. To accomplish this, typical or representative

\*The height of an average man plus a 50 percent safety margin.

PANCAKE AND CHUNKY FIT

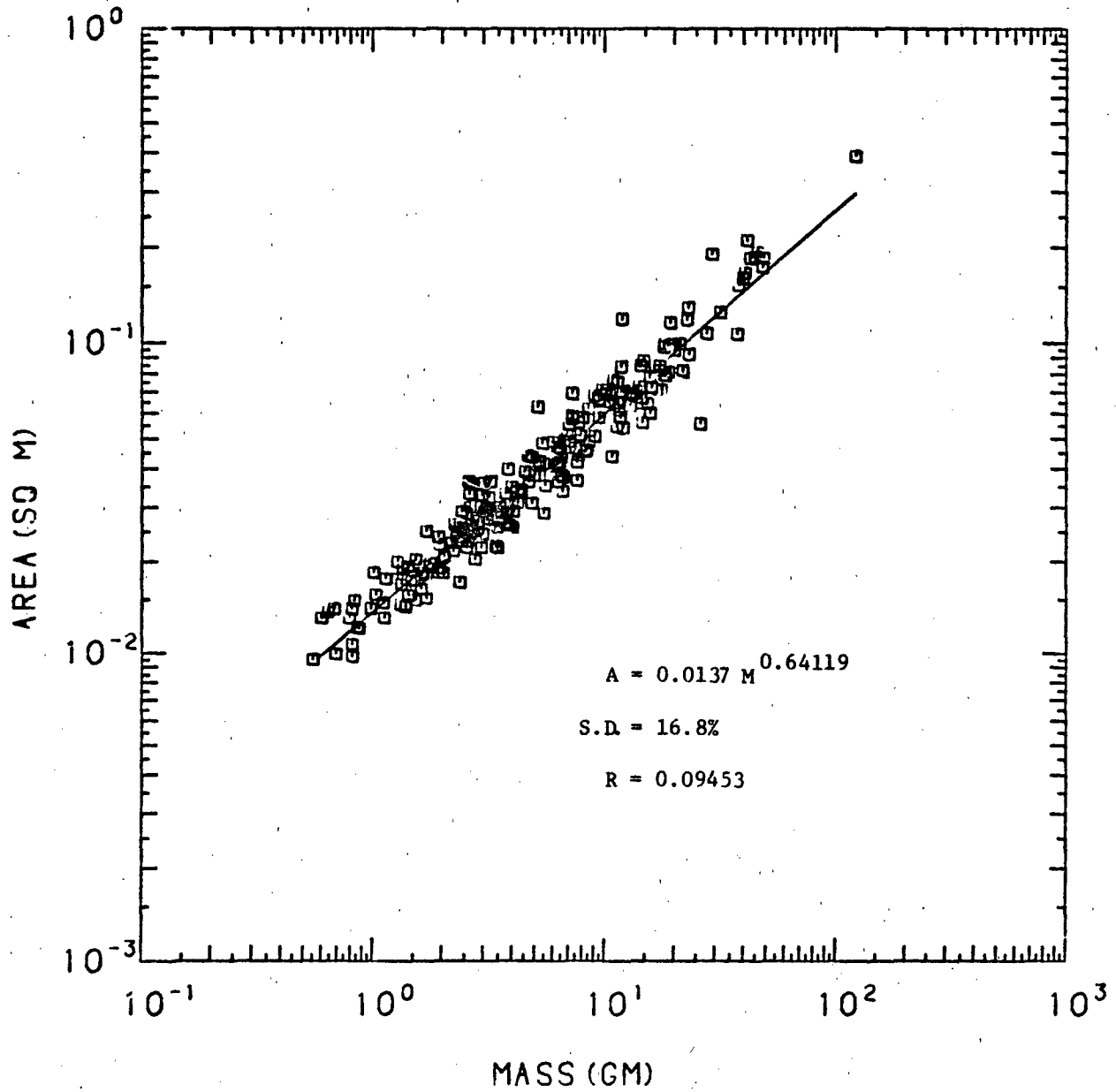


FIGURE 8. DRAG AREA ESTIMATION CURVE FOR CONCRETE FRAGMENTS

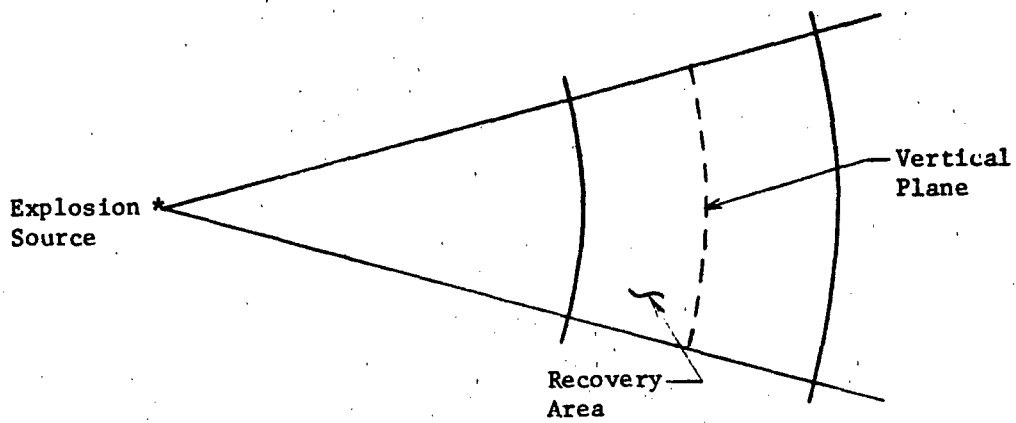


FIGURE 9. DEFINITION OF VERTICAL PLANE USED TO ESTIMATE THE VERTICAL DEBRIS DENSITY

masses and launch angles are selected and the debris range is calculated using a standard trajectory code.\* In this illustrative example, the calculations were performed for:

masses: 0.9, 4.5, 27.0, 90 gm (0.002, 0.01, 0.06, 0.20 lb)

launch angles: -20 to 80 degrees in 10 degree increments

initial velocity: 23.5 m/s (77.1 fps)

drag area: determined from Figure 8 and the debris mass

By systematically varying the launch angles, it is possible to define the maximum possible range as a function of the launch angle for each mass group. One such plot is given in Figure 10. This figure is used to define the low trajectories, in this case all trajectories, resulting from a launch angle less than 42 degrees. Similarly high trajectories are defined as having launch angles greater than 42 degrees.

Figure 10 can be used to establish the proportion of low to high trajectory debris with a mass of 90 gm (0.20 lb) recovered in a particular zone. Consider recovery zone 5 which is 12 to 18 m (20 to 40 ft) downrange. Debris with a mass of 90 gm (0.20 lb) could have landed in this recovery zone if it was launched at an initial angle between 6.7 and 10 degrees or between 76.7 and 81.7 degrees. The range of possible low trajectory launch angles is called  $\Delta\theta_L$  and is  $10 - 6.7$  or 3.3 degrees wide. The range of high trajectory angles is  $\Delta\theta_H$ , which for this case is 5.0 degrees wide. The percentage of low trajectory debris elements in the recovery area is then defined as:

$$F_L = \frac{\Delta\theta_L}{\Delta\theta_L + \Delta\theta_H} = 0.398 \quad (6)$$

The percentage of high trajectory debris elements is then:

$$F_H = 1.0 - F_L = 0.602 \quad (7)$$

Once the proportion of high and low angle trajectories are known for each mass group, the number of hazardous debris in the recovery zone can be calculated. This is accomplished by examining the trajectory code output for each representative mass and an average high trajectory launch angle,  $\theta_H$ . If the kinetic energy of this case exceeds the 80J (58 ft-lb) criterion, then the number of hazardous debris elements in that recovery area is incremented by:

$$N_H = N_H + N(m) \cdot f_H(m) \quad (8)$$

\*At SwRI, the trajectory code used is FRISB, which was developed under a NASA contract.<sup>23</sup>

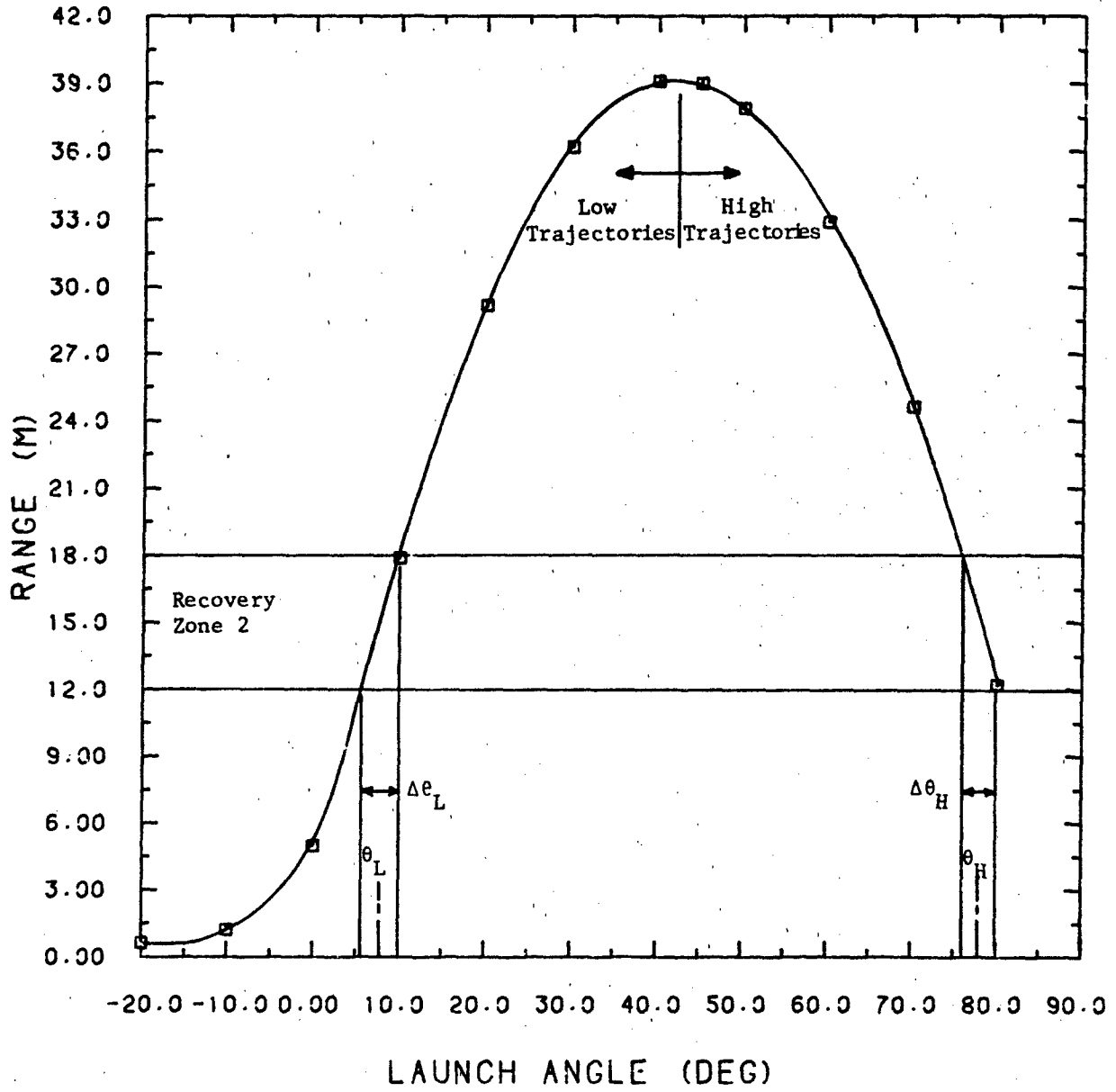


FIGURE 10. MAXIMUM RANGE ENVELOPE FOR 90 GM (0.20 LB) DEBRIS

where

$N_H$  = number of hazardous debris elements

$N(m)$  = number of debris elements with a mass  $m$  found in the recovery zone

$f_H(m)$  = percentage high trajectory debris elements with a mass  $m$  in the recovery zone

Similarly, the contribution of low angle trajectory debris of the specific mass group to the total number of hazardous debris in the recovery can be estimated by examining the trajectory code output again for each representative mass and an average low trajectory launch angle,  $\theta_L$ . Whenever the impact kinetic energy of one of these cases exceeds the kinetic energy criterion, then the number of hazardous debris in that recovery area is incremented by:

$$N_H = N_H + N(m) \cdot f_L(m) \quad (9)$$

The methodology for the calculation of the hazardous debris density was applied to the dividing wall test data. The results of these calculations are summarized in Table 16. For each of the six recovery zones, the four representative masses and the high and low angles ( $\theta_L$  and  $\theta_H$ ), the code was examined and the debris kinetic energy at impact was calculated. Using a properly scaled hazard criterion of 0.37J (0.27 ft-lb),\* the number of hazardous debris elements was determined for each recovery zone. The hazardous debris density was calculated and normalized to 55.7 m<sup>2</sup> (600 ft<sup>2</sup>). The results summarized in Table 16 indicate that the minimum hazard arc is beyond recovery zones 3 and 6 or more than 24 m (78 ft) from ground zero (see Figure 6).

It should be noted that for some classes of events, the hazard criterion (horizontal plane) will be satisfied at points close to ground zero, but will not be satisfied at large distance from ground zero. This result can be obtained

\*The dividing wall test program was conducted at 1/6 scale. Well established laws of scaling require that energies scale as the geometric scale factor cubed. Thus the energy criterion of 80J (58 ft-lb) becomes 0.37J (0.27 ft-lb). The range that a debris missile travels is not properly scaled in the model tests since the gravity field was not increased by the geometric scale factor (1/6) in the tests. This means the model scale range observations are of the same magnitude as those observed in full scale. Therefore, the debris density of 1/55.7 m<sup>2</sup> (1/600 ft<sup>2</sup>) is appropriate. Note that, neglecting drag, the range of a debris element is:

$$R = \frac{V_o^2 \sin 2\theta}{g} + V_o \sqrt{\frac{2d}{g}}, \quad d \text{ is the initial height of the debris.}$$

In these experiments, the velocity,  $V_o$ , and the gravity,  $g$ , were held constant and the initial height of the debris was properly scaled. If we consider debris emerging from the ground surface ( $d = 0$ ), the model and full-scale ranges are identical. However, for proper scaling, the model ranges should be modified to account for the scale change of 1/6 for the second term in this range equation.

TABLE 16. CALCULATIONS OF THE HAZARDOUS DEBRIS DENSITY IN THE HORIZONTAL PLANE

Recovery Zone	$\theta_L$ or $\theta_H$ (deg)	$f_L$ or $f_H^†$	Mass (gm)	$V_f$ (m/s)	$KF_f$ (J)	N(m)	$N_H$
1	3.7	1.0	0.9	15.2	0.105	4	-
			4.5	18.0	0.734	20	20
			27.0	20.2	5.6	13	13
			90.0	21.3	20.7	1	1
			Total $N_H$ in Zone 1				
Hazardous Density *						204	
2	8.5	0.398	0.9	12.5	0.071	0	-
			4.5	15.5	0.546	3	1.19
			27.0	18.4	4.62	9	3.58
			90.0	19.9	18.0	0	-
	79.2	0.602	0.9	8.9	0.036	0	-
			4.5	11.4	0.292	3	-
			27.0	14.7	2.92	9	5.42
			90.0	16.7	12.6	0	-
	Total $N_H$ in Zone 2						10.2
	Hazardous Density						61.1
3	13.2	0.542	0.9	10.9	0.054	0	-
			4.5	13.8	0.434	0	-
			27.0	16.9	3.91	4	2.17
			90.0	18.7	15.9	0	-
	74.0	0.458	0.9	10.5	0.050	0	-
			4.5	13.5	0.410	0	-
			27.0	16.6	3.72	4	1.83
			90.0	18.3	15.1	0	-
	Total $N_H$ in Zone 3						4.00
	Hazardous Density						24.0

TABLE 16. (CONT.)

Recovery Zone	$\theta_L$ or $\theta_H$ (deg)	$f_L$ or $f_H$ †	Mass (gm)	$V_f$ (m/s)	KE <sub>f</sub> (J)	N(m)	N <sub>H</sub>		
4	3.7	1.0	0.9	15.2	0.105	1	-		
			4.5	18.0	0.734	17	17		
			27.0	20.2	5.6	4	4		
			90.0	21.3	20.7	1	1		
			Total N <sub>H</sub> in Zone 4						22
Hazardous Density						132			
5	8.5	0.398	0.9	12.5	0.071	1	-		
			4.5	15.5	0.546	8	3.18		
			27.0	18.4	4.62	4	1.59		
			90.0	19.9	18.0	0	-		
	79.2	0.602	0.9	8.9	0.036	1	-		
			4.5	11.4	0.292	8	-		
			27.0	14.7	2.92	4	2.41		
			90.0	16.7	12.6	0	-		
			Total N <sub>H</sub> in Zone 5						7.18
			Hazardous Density						43.1
6	13.2	0.542	0.9	10.9	0.054	0	-		
			4.5	13.8	0.434	0	-		
			27.0	16.9	3.91	3	1.63		
			90.0	18.7	15.9	0	-		
	0.458	0.458	0.9	10.5	0.050	0	-		
			4.5	13.5	0.410	0	-		
			27.0	16.6	3.72	3	1.37		
			90.0	18.3	15.1	0	-		
			Total N <sub>H</sub> in Zone 6						3.00
			Hazardous Density						18.0

\* Number of hazardous debris divided by  $9.29 \text{ m}^2$  ( $100 \text{ ft}^2$ ) ground surface area and normalized to  $55.7 \text{ m}^2$  ( $600 \text{ ft}^2$ )

† In this illustrative example, the  $f_L$  and  $f_H$  used correspond to the 90 gm (0.20 lb) debris element. In practice, separate estimates for  $f_L$  and  $f_H$  should be made for each mass and range group.

when the debris missiles emerge predominately with launch angles close to the optimum value for maximum range. Thus the safety analyst must be careful to analyze the full range of plausible launch angles.

Debris Density in the Vertical Plane. The debris density calculations for the vertical plane parallel those for the horizontal plane. The difference is that the debris velocity and its vertical height as it crosses a vertical plane are used (instead of the range and the velocity at impact) in the determination of whether it is hazardous. In practice, all combinations of the representative debris masses and the representative launch angles are used in the trajectory calculations. As each debris element crosses the recovery area, its velocity and height are noted. If the debris height is less than 3 m (9.8 ft), and the debris kinetic energy exceeds 80J (58 ft-lb) then that piece of debris is considered hazardous and the number of hazardous debris in that recovery zone is incremented according to:

$$N_v = N_v + F_L(m)N(m) \quad (10)$$

where

$N_v$  = number of hazardous debris in the vertical plane

$F_L(m)$  = percentage low trajectories for a mass group  
(see Equation (6))

$N(m)$  = number of debris elements with mass,  $m$ , which landed  
in the recovery zone being considered

When all of the debris has been accounted for, the hazardous debris density in the vertical plane is estimated by dividing  $N_v$  by the area of the vertical plane at the midspan of the recovery area. A recovery area is considered unsafe for personnel if the hazardous debris areal density exceeds  $1/55.7 \text{ m}^2$  ( $1/600 \text{ ft}^2$ ).

As an illustrative example, consider again the dividing wall test data. Trajectory calculations were performed for the same masses and launch angles considered for the horizontal debris density estimates. In this case the trajectory code was modified to print out the debris velocity and height as it crossed vertical planes at the midpoint of the recovery areas located at 9, 15, and 21 m (30, 50, and 70 ft) downrange (see Figure 6). These calculations are summarized in Table 17. Using the scaled hazardous kinetic energy of 0.37J (0.27 ft-lb), the number of hazardous debris missiles per recovery plane was calculated and the hazardous debris densities were compared to  $1/55.7 \text{ m}^2$  ( $1/600 \text{ ft}^2$ ). The comparison shown at the bottom of Table 17 indicates that the minimum hazard arc from the vertical plane calculations is less than 21 m (70 ft). Since this arc is less than that for the horizontal plane calculations, the overall safety arc is controlled by the horizontal plane calculations. It should be noted that these findings resulted because the vertical plane calculations considered the plane located at the midspan of each of the six recovery zones, not at the close-in boundary of the recovery area sector. In practice, the hazard arc based on the vertical plane calculations will control the definition of the minimum acceptable hazard arc.

TABLE 17. NUMBER OF HAZARDOUS DEBRIS IN THE VERTICAL PLANE

$\theta$ (deg)	$\theta_L$ (1)	mass (gm)	Velocity (m/s) of the Debris Across Plane at (2)			$N_v$ (m)	$N_H$ at Each Recovery Plane		
			9m	15m	21m		9m	15m	21m
3.7 (Zone 1)	1.0	0.9	-(3)	-	-	4	-	-	-
		4.5	-	-	-	20	-	-	-
		27.0	20.2	-	-	13	13	-	-
		90.0	21.2	-	-	1	1	-	-
8.5 (Zone 2)	0.398	0.9	-	-	-	0	-	-	-
		4.5	17.3	-	-	3	1.19	-	-
		27.0	-	18.3	-	9	-	3.53	-
		90.0	-	20.0	-	0	-	-	-
13.2 (Zone 3)	0.542	0.9	-	-	-	0	-	-	-
		4.5	-	14.3	-	0	-	-	-
		27.0	-	-	-	4	-	-	-
		90.0	-	-	18.7	0	-	-	-
						Zone 1	Zone 2	Zone 3	
						Number of Hazardous Debris	15.19	3.53	0
						Debris Density <sup>(4)</sup>	182.0	42.4	0
3.7 (Zone 4)	1.0	0.9	-	-	-	1	-	-	-
		4.5	-	-	-	17	-	-	-
		27.0	20.2	-	-	4	4	-	-
		90.0	21.2	-	-	1	1	-	-
8.5 (Zone 5)	0.398	0.9	-	-	-	1	-	-	-
		4.5	17.3	-	-	8	3.18	-	-
		27.0	-	18.3	-	4	-	1.59	-
		90.0	-	20.0	-	0	-	-	-
13.2 (Zone 6)	0.542	0.9	-	-	-	0	-	-	-
		4.5	-	14.3	-	0	-	-	-
		27.0	-	-	-	3	-	-	-
		90.0	-	-	18.7	0	-	-	-
						Zone 4	Zone 5	Zone 6	
						Number of Hazardous Debris	8.18	1.59	0
						Debris Density (4)	98.2	19.1	0

(1) Only the low launch angles were considered in this example. In actual application the full range of plausible initial launch angles should be considered.

(2) In this illustrative example, the debris, kinetic energy and height were checked only at the midspan of each recovery area. In practice, the debris energy and height should be checked at all positions over the recovery zone. In effect then, the method calls for checking the kinetic energy for every particle which has a trajectory which intercepts a volume 3 m (9.8 ft) high and encompassing the entire recovery zone.

(3) No velocity is given if the debris missile did not pass through the vertical recovery plane.

(4) <sup>a</sup> Number of debris elements divided by 4.65 m<sup>2</sup> (50 ft<sup>2</sup>) vertical recovery area and normalized to 55.7 m<sup>2</sup> (600 ft<sup>2</sup>).

## CHAPTER 4

## DEBRIS HAZARDS METHODOLOGY DEVELOPMENT PLAN

When an explosion occurs within a building, structural collapse can occur and hazardous debris can be hurled towards other occupied areas. The mechanisms which control the debris formation are complex and vary widely for different types of structures and different parameters associated with the explosive contained inside. In order to approach the problem of deriving prediction methodologies for debris hazards, the first step must be to identify the important physical parameters which have an effect on debris characteristics. Identification of these parameters will allow one to organize the steps to be taken in an investigation of debris hazards.

Debris characteristics are defined in this report as the number of debris fragments, debris mass, shape, size, velocity, launch angle, range, and spray angle. These debris characteristics are controlled by the structural details of the building and the applied internal loads. The structural details depend upon the type of building considered and from what portion of the structure the debris originates. The internal loads are dependent upon the charge size, shape, location, and orientation within the structure. Also the effect of charge casing, when present, can affect the internal loading.

## STRUCTURAL PARAMETERS

Debris emanating from a building due to an accidental internal explosion is controlled by a number of parameters related to the structural details of the building. Various types of buildings\* are used to house ordnance items including reinforced concrete (laced and unlaced), concrete masonry construction, and steel construction. These different types of buildings would each present different classes of hazards depending on the failure pattern. This wide range of construction types would necessitate a very broad research effort to identify debris hazard methodologies. In order to maintain a smaller research effort and to concentrate on the type of construction which is expected to be the most prevalent for ordnance handling, a generic debris donor structure should be selected. This report will concentrate on reinforced concrete structures. This is not to say that hazards do not exist for structures other than reinforced concrete.

\*The contributions from equipment and furnishings inside the building are not considered.

Past experience has shown that the main debris hazard from explosions inside reinforced concrete buildings originates from the walls. This may not be true of all building shapes; however, many buildings will have flat roofs from which the debris is projected upward. The debris will fall on or very near the original site. In contrast, wall debris will be projected large distances. In addition, the wall debris emanates primarily in a direction normal to the original wall surface. This is shown in Figure 11. By concentrating on wall debris, the number of permutations of possible debris conditions to be studied is reduced.

A reinforced concrete wall can be either of laced or unlaced construction. Laced construction is typically used in the design of a structure to withstand the applied blast loading. The specific intent in the design of a laced reinforced concrete wall is to control the collapse and breakup of the wall. Some debris may occur in the form of backface spall or scabbing. For occupied areas exposed to these debris sources, it is standard practice to provide protection in the form of spall plates. For these reasons a laced reinforced wall shall not be considered in this report. Any further reference to reinforced concrete will pertain to unlaced construction unless otherwise noted.

The following is a description of the type of structure considered in this report. Typically, the wall is rigidly attached on two or more edges with equal reinforcing running in both the horizontal and vertical directions and on both faces of the wall. The concrete cover over the rebar conforms to American Concrete Institute (ACI) requirements, 0.019 meters (0.75 in.) for inside surfaces and 0.038 meters (1.5 in.) for exterior surfaces.

Other structural conditions could have an effect on reinforced concrete debris formation. Wall reinforcement can be tied into the floor, roof, or walls to form various boundary conditions (fixed, simple, or free). The type of wall boundary conditions will control the yield line formation which, in turn, affects debris formation. The amount of tie in rebar and wall thickness at the perimeter will determine whether the wall fails due to support reactions or in bending. Also, stirrup design will govern whether or not the main flexural rebar is allowed to develop its full bending resistance without premature failure in shear. The differences in types of failure (support reaction, shear, or bending) could cause differences in debris characteristics. As will be suggested in Chapter 5, the model test series will include a test fixture with a support frame in which the debris forming wall will be held. The number of sides of the wall to be supported in the frame can be varied. For the investigation suggested in this report only fixed boundary conditions should be considered at this time. As discussed, shear reinforcement could have an effect on debris formation. Incorporating shear rebar into the model panels to be discussed in Chapter 5 would be costly. Hence, it is suggested that shear design not be considered for the initial investigation discussed in this report. If a more detailed test series is considered at a later date, then shear design can be investigated along with other parameters not included in the initial test series. It should be noted that if full-scale tests were conducted, incorporation of shear reinforcing into the test panels would also be costly and a scale model panel including shear rebar would still be less expensive.

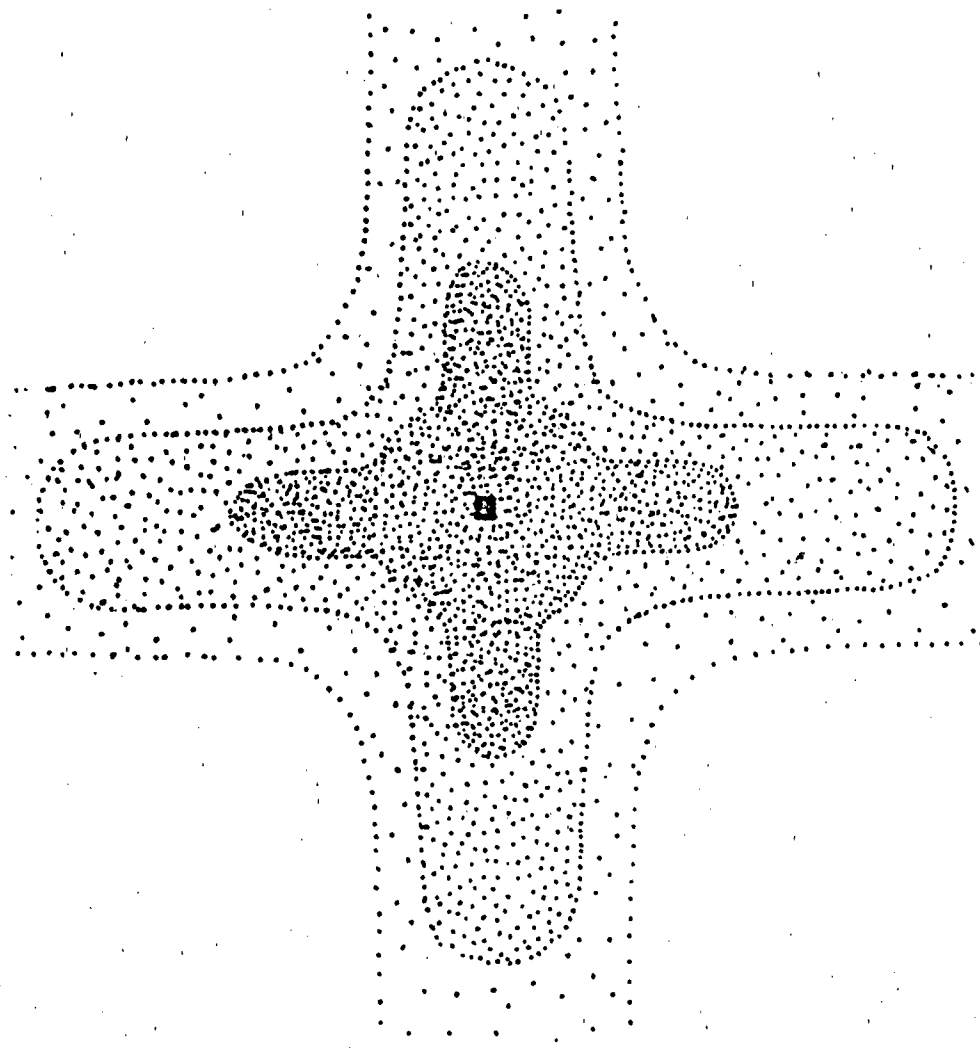


FIGURE 11. DRAWING OF MEASURED DEBRIS DENSITY OF BUILDING AND CRATER MATERIAL DURING MODEL TESTS

For the reinforced concrete wall described above, the parameters to be considered further which can be identified as controlling the debris characteristics include the following:

- o Concrete compressive strength
- o Aggregate size
- o Concrete density
- o Wall dimensions (height, width, thickness)
- o Rebar diameter
- o Rebar spacing
- o Rebar/concrete adhesion
- o Rebar yield and ultimate strength
- o Boundary conditions, i.e., wall restraints

These parameters and their relationship between each other and debris characteristics are discussed in the section entitled "Parameter Relationship."

#### BLAST AND FRAGMENT LOAD PARAMETERS

The formation of reinforced concrete debris due to an internal explosion is affected by the applied loading which is a function of charge size, location, and the presence of casing. Shock strength increases with decreasing charge standoff and increasing charge size. Charges close to the wall but off-center in the room will have a shock reverberation pattern which will be dominated by the first reflection. Charges centered in the room will have secondary reflections which are also important. The charge size and importance of secondary shock reflections can affect whether the structure will respond impulsively, dynamically, quasi-statically, or under reverberation. The charge size and location within the structure are hence identified as important parameters controlling debris formation. Room volume affects the quasi-static phase of an explosion and is also considered an important blast parameter. Vent area is not considered here because this is usually compared to wall area, and wall collapse should occur before substantial venting for large charge weights.

The shape of the explosive will have an effect on the forcing function. High explosives can be in boxes, cylindrical containers, or in stacks of munitions of a variety of shapes. Except for munitions, nonspherical containers are expected to be compact (i.e., L/D approximately 1) for ease of handling. Munitions stacked in an array are expected to be in a compact arrangement. To consider all possible permutations of charge shape would be expensive, particularly when a spherical or compact cylindrical (L/D = 1) shape can reasonably represent many shapes typically encountered.

Whether a charge is cased or uncased will have an effect on the loading applied to the wall surface. The casing will affect the blast loading and can become a source of fragment impact on the wall surface. To limit the type of casing to be studied from the variety of casings available, it is suggested that only steel casing should be considered.

The density of the explosive material can have an effect on the loading on the wall surface. If the same mass of explosive is packaged in bulk form, a different blast field is expected, given an explosion, as compared with that in pressed form. Differences are also expected for explosives which are packaged as individual quantities in a stack (although each is in pressed form) compared with a single pressed unit of the same overall shape. The worst case loading will be expected from the compact, pressed explosive and will be considered under this report.

In summary, the explosive parameters to be considered further which are identified as important in debris formation of reinforced concrete walls are:

- o Explosive mass
- o Explosive location within the enclosed structure
- o Room volume (affects quasi-static phase)
- o Explosive shape (only compact shape will be considered)
- o Casing effects (shock interaction and jetting effects of warheads)
- o Explosive density (only pressed explosive will be considered)

#### PARAMETER RELATIONSHIP

The parameters previously identified as being important to debris formation from reinforced concrete walls can be related to debris characteristics (mass, shape, size, velocity, trajectory, quantity, range, and distribution) through the use of similarity methods. Similarity is a powerful tool for organizing parameters into terms (called pi terms) which are physically significant to the problem under study. The validity and usefulness of similitude analysis is well documented in the literature and has been applied to a wide range of physical problems including those similar to this debris problem (Reference 34 includes an excellent overview of similitude analysis). Under a previous study, a similitude analysis for explosive fracturing of a dividing wall was developed.<sup>26</sup> The parameters considered in this report are similar to those studied in Reference 26, however, enough differences exist that a separate similitude analysis was necessary. The results of Reference 26, however, were used as a guideline. Similitude (or model) analysis is typically used in conjunction with model or scaled tests. A model test series will be suggested and discussed in Chapter 5 for a debris hazard study.

The pi terms derived using the parameters identified in the development of the model analysis and the debris characteristics to be measured are given in Tables 18, 19, and 20. The tables are arranged according to parameters to be varied in the model tests, those to remain constant, and the parameters to be measured. The reason for varying some and not others is discussed in Chapter 4. Tables 18 through 20 include important parameters, symbols, and dimensions (force F, time T, and length L). Below the tables are the nondimensional pi terms corresponding to the above parameters. The nondimensional terms were organized to reflect physically significant relationships thought to be of importance. Concrete compressive strength is combined with wall dimensions (which govern the amount of concrete in compression during bending) to relate a strain energy to charge energy. The yield and ultimate strengths of the

TABLE 18. PARAMETERS TO BE VARIED DURING MODEL TESTING

<u>Parameter</u>	<u>Symbol</u>	<u>Dimension</u>
Wall Thickness	X	L
Rebar Diameter	D	L
Rebar Spacing (horizontal = vertical)	S	L
Charge Energy	W	FL
Charge Location in Room		
height above floor	h	L
distance from wall	r	L
distance from nearest sidewall	l	L
Charge Casing Thickness	d	L

$$\Pi_1 = \frac{\sigma_c XLH}{W}$$

Note: L, H, and R are defined  
in Table 19

$$\Pi_2 = D/X$$

$$\Pi_3 = S/X$$

$$\Pi_4 = h/H$$

$$\Pi_5 = r/R$$

$$\Pi_6 = l/L$$

$$\Pi_7 = \frac{d^3 \sigma_c}{W}$$

TABLE 19. PARAMETERS TO BE HELD CONSTANT DURING MODEL TESTING

<u>Parameter</u>	<u>Symbol</u>	<u>Dimension</u>
<b>Room Size</b>		
height	H	L
distance from debris forming wall to back wall	R	L
distance from side wall to side wall	L	L
<b>Aggregate Size</b>	a	L
<b>Concrete Density</b>	$\rho_c$	$FT^2/L^4$
<b>Concrete Compressive Strength</b>	$\sigma_c$	$F/L^2$
<b>Rebar Density</b>	$\rho_s$	$FT^2/L^4$
<b>Rebar Yield Strength</b>	$\sigma_y$	$F/L^2$
<b>Rebar Ultimate Strength</b>	$\sigma_u$	$F/L^2$
<b>Gravity</b>	g	$L/T^2$
<b>Standard Air Pressure</b>	$p_o$	$F/L^2$
<b>Strain Rate</b>	$\dot{\epsilon}$	$L/L/T$

$$\Pi_8 = H/V^{1/3} \quad (\text{where } V = HRL = \text{room volume})$$

$$\Pi_9 = R/V^{1/3}$$

$$\Pi_{14} = \sigma_u / \sigma_y$$

$$\Pi_{10} = L/V^{1/3}$$

$$\Pi_{15} = \frac{g M \lambda}{W}$$

$$\Pi_{11} = a/x$$

$$\Pi_{16} = \frac{p_o V}{W}$$

$$\Pi_{12} = \rho_c / \rho_s$$

$$\Pi_{17} = \dot{\epsilon} T$$

$$\Pi_{13} = \frac{\sigma_y DS (LH)^{1/3}}{W}$$

Note: M is defined in Table 20

TABLE 20. MEASURED PARAMETERS OR DEBRIS CHARACTERISTICS

	<u>Symbol</u>	<u>Dimension</u>
Launch Angle	$\theta$	-
Spray Angle	$\phi$	-
Debris Velocity	$v$	L/T
Debris Mass	$M$	$FT^2/L$
Debris Size		
length	$\alpha_1$	L
width	$\alpha_2$	L
thickness	$\alpha_3$	L
Debris Range	$Z$	L
Debris Quantity	$N$	-

$$\Pi_{18} = \theta$$

$$\Pi_{19} = \phi$$

$$\Pi_{20} = \frac{v^2 M}{W}$$

$$\Pi_{21} = \frac{M}{\rho_c \sqrt{HL} X S}$$

$$\Pi_{22} = \frac{(\alpha_1 \alpha_2 \alpha_3) \rho_c}{M}$$

$$\Pi_{23} = \frac{Zg}{v^2}$$

$$\Pi_{24} = N$$

rebar are treated similarly. Rebar spacing, rebar diameter, and aggregate size are combined with wall thickness which for these parameters is considered to be the most important length term. Charge location within the room is combined with the corresponding major room dimension (i.e., charge height above floor room height). Room volume, charge weight, and atmospheric pressure are combined relating quasi-static pressure. The parameters in Table 20 are also arranged with similar parameters to form pi terms. Velocity is squared and combined with mass to form a kinetic energy which is then ratioed with the charge energy. Mass is combined with concrete density and debris mass (which thereby relates debris size back to wall dimensions). Debris range is related to gravity and velocity squared.

All of the pi terms discussed above are suggested. Rearrangement of terms can be made if more suitable relationships are found.

#### SCALING LAWS FOR REINFORCED CONCRETE MODEL

Using the method of similarity, it is possible to derive the scale factors for all parameters in a replica model. A replica model is one in which both the prototype and the model structure are made from the same materials. In a replica model all geometric dimensions (lengths, thickness, etc.) are scaled down by the same factor  $\lambda$ . All angles, densities, strengths, strains, and the number of debris/fragments generated will be invariant or the same as in full scale. Time and impulse in the model will scale with the geometric scale factor  $\lambda$ . Mass of debris and energy in the explosive charge will scale as  $\lambda^3$ . Strain rate and acceleration due to gravity will scale as  $\lambda^{-1}$ .

The scale factors for the explosive loading and subsequent breakup of the reinforced concrete wall are summarized in Table 21. All parameters listed in Tables 18 to 20 will be scaled properly except acceleration due to gravity, debris range, and strain rate. The failure to scale gravity, which should be  $\lambda$  times greater in the model, is important only in the trajectory of the debris generated by the explosion. Since the initial launch angle, initial velocity, and debris mass are properly scaled, it should be possible to calculate the equivalent full-scale ranges using these initial conditions measured in model scale experiments. The failure to scale strain rate properly arises because strain is invariant and time scales as  $\lambda$ . Thus strain rates in the model will be  $\lambda$  times larger than those in the prototype. This is not as catastrophic as it seems because steel and concrete are not strongly sensitive to strain rate. The ratio of "dynamic strength" to static strength for these materials is roughly linear with respect to the logarithm of the strain rate. In an explosion, strain rates in the steel elements and in the concrete may vary from  $10^{-1}$  to 100/sec. Over this range those materials may have an increase in "dynamic strength" from 1.1 to 1.8 times the static strength. In a 1/10th scale model the strain rates in a similar explosion may be  $10^0$  to 1000/sec. The "dynamic strength" increase in the model may then be on the order of 1.2 to 2.4 times the static strength. From this discussion it can be seen that strain rate effects between the model and prototype structure are real; however, these effects probably will be difficult to discern given the usual scatter inherent in this type of testing.

TABLE 21. MODEL LAW FOR DIVIDING WALL FRAGMENTATION

<u>Parameter</u>	<u>Replica Scaling Law</u>
Lengths	$\lambda$
Angles	1.0
Densities	1.0
Strengths, moduli	1.0
Poisson's ratio	1.0
Strains	1.0
Strain Rate	$\lambda^{-1}$
Velocities	1.0
Acceleration (gravity)	$\lambda^{-1}$
Mass	$\lambda^3$
Reinforcement ratio	1.0
Explosive energy	$\lambda^3$
Pressure	1.0
Impulse	$\lambda$
Time	$\lambda$
Number of fragments	1.0

## NUMERICAL RANGE OF PARAMETERS TO BE INVESTIGATED

As discussed in the previous section, it is suggested that the parameters listed in Table 18 be varied during model testing. The parameters in Table 19 will be held constant for all tests. The reason these parameters are held constant is because the effect of their variation on debris formation for structures of interest is expected to be less significant (except for room dimensions) than parameters listed in Table 18. The parameters in Table 19 are also somewhat constant in typical construction, i.e., aggregate size, concrete density, and rebar strengths do not vary greatly in common construction. The number of permutations can be greatly reduced by holding these parameters constant. Consideration of a constant room size is strictly an economical decision. The model test setup to be discussed in Chapter 5 is envisioned to be a reusable structure (except for the debris forming wall), and it is economically desirable to maintain a constant room size.

The range over which the parameters in Table 18 are to be varied was chosen to reflect that expected to be found in existing structures. The ranges are given in Table 22. A survey of existing structures was not made for use in determining the range of variance in the table, but, these values were chosen for what past experience has shown to be typical. Any disagreement with these values can be incorporated by expanding or contracting the range of parameters to be considered as listed in the table

TABLE 22. FULL-SCALE RANGE OF VARIATION TO BE APPLIED TO PARAMETERS  
IN TABLE 18 DURING MODEL TESTING

Wall thickness	0.3 - 0.46 meters (12 - 18 in.)
Explosive mass	150 - 4500 kg (330 - 10,000 lb <sub>TNT</sub> )
Casing (one thickness)	Bare or cased
Charge Position in room	
height above floor	0 - 1/3 room height
distance from wall	varied
distance from sidewall	centered
Rebar size	#5 - #8
Rebar spacing	0.15 - 0.46 m (6 - 18 in.)

## CHAPTER 5

## RECOMMENDED MODEL TESTS

To better define the debris characteristics of reinforced concrete buildings and walls exposed to blast loading, it is recommended that a small scale study be initiated. The use of model tests can provide a large data base at a reduced cost compared to full-scale testing. With the use of the similitude analysis discussed in Chapter 4 the effect of the various parameters on debris formation can be studied using model test data. Model testing is widely used for problems similar to debris hazards. Modeling is well understood and documented in the literature (References 35 and 36) where the validity of properly managed model tests are unquestioned. The model used for testing should simulate the prototype as closely as possible for all important physical parameters. These conditions are easily satisfied except for the gravity term which unfortunately does not scale. This handicap only affects the range of the debris, i.e., the range term does not scale properly. All other measured parameters, however, do scale. During model testing several parameters will be varied. The overall test program can be performed as a series of small test programs where one or two of the parameters will be varied with the remaining parameters held constant. At time of completion of the first series of tests, another series would be initiated with a different set of parameters varied. For validation of the small scale tests, several model scales including full scale should be investigated. Table 23 outlines a series of tests designed to provide accurate and reliable fragment/debris data for reinforced concrete structures subjected to internal loads. As mentioned earlier, when the final selection of the donor system is made, the test plan and corresponding model test series can be organized in a manner similar to that discussed here.

## SCALE MODEL ENCLOSURE

It is suggested that the tests to be performed on reinforced concrete walls make use of a scale-model enclosure. This enclosure would consist of a reusable concrete base slab (to which a frame or fixture for use in supporting the roof and walls would be attached), a blowout roof, and three frangible walls. The fourth wall will be the test wall. The test wall will be made of reinforced concrete and would be supported on either one or three sides by the reusable support frame.

SwRI fabricated 1/6 scale model reinforced concrete walls for a program funded by ARRADCOM, entitled "Explosive Fragmentation of Dividing Walls."<sup>26</sup> In fabricating the model walls, 14 gauge steel wire was used to simulate the reinforcing bars. The wire was chosen to have equivalent strength properties of the rebar being modeled, and the gauge of the wire was a scaled equivalent of

TABLE 23. PRELIMINARY TEST PLAN

Test Series	Wall Thickness	Charge Wt.	Bare or Cased	Standoff Distance	Charge Location	Rebar Diam	Percent Rebar	Rebar Spacing	Scale
1	Constant	Constant	Constant	Constant	Constant	Constant	Constant	Constant	Constant
2	Varied	"	"	"	"	"	"	"	"
3	Constant	Varied	"	"	"	"	"	"	"
4	"	Constant	Varied	"	"	"	"	"	"
5	"	"	Constant	Varied	"	"	"	"	"
6	"	"	"	Constant	Varied	"	"	"	"
7	"	"	"	"	Constant	Varied	"	"	"
8	"	"	"	"	"	Constant	Varied	"	"
9	"	"	"	"	"	"	Constant	Varied	"
10	"	"	"	"	"	"	Constant	Constant	Varied

Full Scale	0.3-0.46m	150 - 4500kgTNT	Varied	Varied	Centered 1/3 Height	0.015 - 0.0254m	Varied	0.15-0.46m	Constant
1/3rd Scale	0.1-0.15	50-1500	"	"	"	0.0053 - 0.0085	"	0.075 - 0.23	"
1/6th Scale	0.05-0.077	25-750	"	"	"	0.0027 - 0.0042	"	0.0375 - 0.115	"
1/12th Scale	0.025-0.038	12.5-375	"	"	"	0.00133 - 0.002	"	0.019 - 0.0575	"

Full Scale	12-18 in.	330 - 10000 lbTNT	Varied	Varied	Centered 1/3 Height	0.625 - 1.0 in.	Varied	6-16 in.	Constant
1/3rd Scale	4-6.00	11.1-370.4	"	"	"	0.125 - 0.33	"	2.67-4	"
1/6th Scale	2-3.00	1.4-46.3	"	"	"	0.062 - 0.167	"	1.34-2	"
1/12th Scale	1-1.50	0.4-5.8	"	"	"	0.031 - 0.08	"	0.67-1	"

the rebar size. Because rebar is not smooth and bonding to concrete is important, the wire was crimped to incorporate this feature in the model. Rebar was located in both the horizontal and vertical direction without lacing. Molds for the concrete walls were fabricated into a rectangular plywood frame which was designed to be reusable. The frame had a series of holes on the side which held the rebar in its proper place. Concrete was poured into the model such that a layer of concrete covered the rebar on both faces. SwRI recommends this type of fabrication process for use in the proposed program if small scale models are used. For larger scale models actual rebar is available for use in fabrication of the test wall. The smallest rebar available commercially is No. 2 bar; however, it is only obtainable in plain round. This limits the scale of the model if actual rebar is to be used.

The frangible walls and roof can be fabricated of light yet sturdy material such as plywood or pressboard. The frangible panels would be supported in such a way that they would remain in place long enough to reflect the shock waves generated by the explosion. This would subject the test wall to a realistic forcing function. The frangible panels can be covered by dirt to simulate a full-scale mass if uncovered frangible wall response is determined to be too rapid. The dirt can be heaped against and on the model or poured between two panels of proper spacing to obtain the correct scaled mass. When the frangible walls and roof (either dirt covered or uncovered) do fail, the fact that they are made of light materials will eliminate hazardous debris.

The test wall should be color coded on both the front and back face. It is suggested that at least four colors be used on each face. To identify sections of the test wall, small number labels should be glued on the wall in an array within each colored area. Previous model tests have incorporated this color coding and labeling scheme with success.<sup>26,27</sup> The tests should be made with the wall facing a debris recovery pit which is a sand bed large enough to receive all expected debris.

#### INSTRUMENTATION

It is suggested that both real time and high-speed cameras be used to record the event. The cameras can be placed at the model end of the recovery pit in order to record the debris immediately after the explosion. A ruled background panel can be used to serve as a backdrop for the camera recordings. Ruled lines on the panel will give a reference frame in the film. This type of setup was used with the model tests described in Reference 26. Figure 12 is an example of this kind of test setup.

Pressure gauges can be located on the test enclosure floor if a record of the blast environment is desired. Because the test wall will collapse, no pressure history recordings can be made of the wall surface itself. Blast measurements can be made if a steel panel, designed not to fail, is placed in the test frame with an attached array of blast gauges. This type of test setup is referred to as a loads model. A minimum of five gauges evenly spaced on the plate is suggested. In addition to those on the plate, blast gauges should be located on the floor (in the same location as for debris model) for use as reference gauges. The loads model would require a series of tests which include all charge sizes and locations. A comparison of the pressure histories from

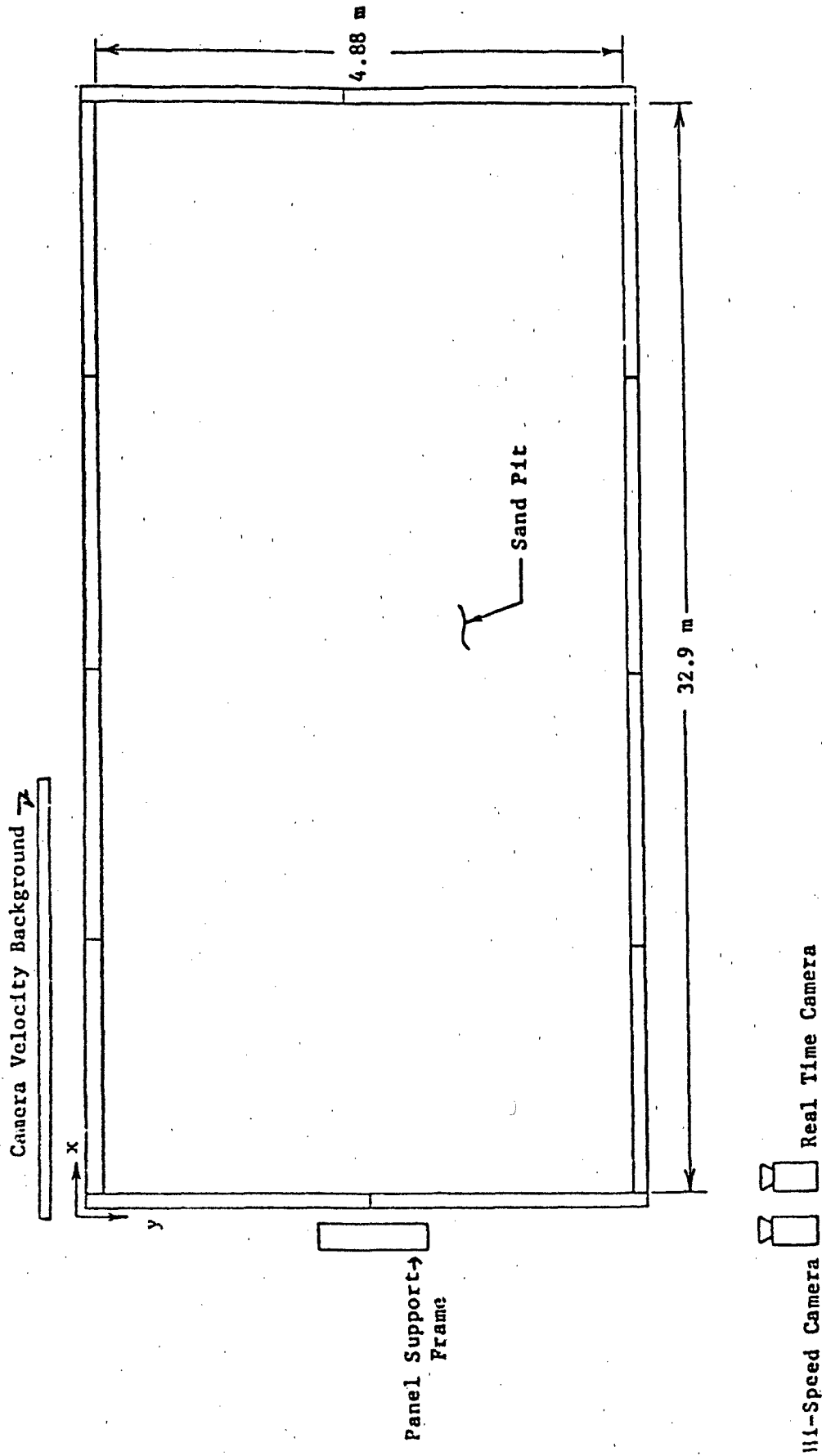


FIGURE 12. TEST SETUP

reference gauges (on the floor) could be made between a corresponding loads test and debris test. This would allow determination of whether the applied loads to the wall are similar.

#### DEBRIS DATA TO BE RECORDED

Measurements made for each debris test should include the recorded values corresponding to the parameters identified in Table 21 for a reinforced concrete wall. Other debris donors would have similar characteristics to be measured. Debris mass and dimensions should be measured. The presented area can be estimated in two ways. The best method consists of an icosahedron gauge which uses photodetectors to measure the "shadow" of the debris in each of 16 different orientations. The 16 different readings are averaged to yield an "effective presented area." Unfortunately this device is quite expensive and only two such units are in existence. A simple and cheaper method consists of measuring three orthogonal dimensions (L, W, T) of the debris. From these readings an "effective presented area" is estimated as  $(L \times W \times T)^{2/3}$ .

Debris range should be measured and recorded. An attempt should be made to locate the origin of the debris on the wall through use of the color coding and numbering system. Debris trajectory and velocity may be obtained from high-speed film recordings and perhaps flash techniques or breakwire systems. The number of debris particles per test should be recorded. If very small debris makes this difficult, then debris above a certain size can be counted. The number of debris elements recovered versus distance from the test wall can be measured. The number of debris particles versus debris mass can be counted. These parameters can be obtained from what is commonly called a missile map which includes debris location, total number of debris, and debris size.

#### ADDITIONAL TESTS IN SUPPORT OF MODEL TESTS

In Chapter 4 the important parameters affecting debris characteristics were discussed. One of the parameters which affect debris range is gravity ( $\pi_{23}$ , Table 20), which is not properly scaled. In order to determine a full scale range, additional analysis of the test data is required. Using the debris, velocity, mass, shape, launch angle, and spray angle, a corresponding range can be determined using existing trajectory solutions. The only missing parameter is a proper drag coefficient and debris presented area.

Since there is no method for predicting the drag coefficient or the drag area for tumbling debris, it is common practice to assume a stable orientation for the debris missile, calculate the drag areas for this orientation, and obtain  $C_D$  from handbooks or standard references. In addition, values for  $C_D$  are given for only a limited number of orientations, i.e., edge-on, side-on, etc.<sup>37</sup> Coefficients for other debris missile orientations such as  $10^\circ$  off-normal,  $20^\circ$  off-normal, etc., are not available. In reality, debris missiles will have any of numerous orientations including tumbling. Test data covering a range of debris orientations would be very useful to obtain a prediction model. This will require an experimental program varying the orientation and rate of tumble of typical debris fragments. This type of program could be performed using debris missiles with known dimensions fired out

of an air gun with a certain orientation, and at a known launch angle and initial velocity. The range traveled by the missile could be recorded and compared to that predicted by the standard trajectory codes. By varying the initial debris orientation, the resultant debris range could be corrected to account for the drag of the missile. A similar analysis could be performed for tumbling debris by introducing a tumbling medium and then changing the tumbling rate.

## CHAPTER 6

## ANALYSIS OF TEST DATA

Test data collected as discussed in Chapter 5 should be part of a parametric study aimed at developing methodologies for the reasonable prediction of hazards associated with debris from blast loaded reinforced concrete walls. Proper analytical models would be useful as input to the NOHARM program for use in debris hazard predictions. Generalization of experimental results is difficult due to the response dependence on fabrication and explosive parameters. To date there are no established prediction equations for calculating the effect that various parameters have on concrete wall break-up.

In Reference 26 a model analysis was used to design the scale model tests and to interpret the test results. Based on the limited tests conducted on this program, preliminary prediction models were formed for greatest debris velocity, longest debris range, number of debris elements, and largest recovered mass as a function of the scaled total impulse applied to the wall. Examples of the types of results for dividing walls supported on three sides are given in Figures 13 through 16. Although these results are not directly applicable to the situation of a naval munition exploding within a structure, these results are indicative of the type of empirical analysis which is possible.

Thus far, the analysis which can be performed on maximum responses obtained in the tests has been presented. A similar analysis can be performed on statistical distributions of measured data. For example, consider the case of the mass of the debris fragments collected in the dividing wall tests.<sup>26</sup> In these experiments all significant debris generated was collected and weighed. The mass distributions were prepared by choosing mass intervals which were approximately log linearly distributed. The number of debris missiles with a mass greater than the specified mass intervals was counted. Using these data, plots similar to the one given in Figure 17 were prepared. The data from several tests were plotted in Figure 18. In this case, the various curves represent different explosive loadings applied to the wall. Of course, the top curve represents the most highly loaded wall, and the bottom curve represents the wall with the lowest loadings. Each of the curves has a similar shape which suggests that it should be possible, through proper selection of dimensionless ratios, to correlate empirically all of the mass distributions into a single curve.<sup>28</sup>

The above are suggestions of the type of analysis that can be performed with the test data. Similar analyses are expected in conjunction with the actual test series. The use of similarity analysis provides a powerful tool in development of prediction methodologies. The data accumulated will have to be reduced for use in NOHARM and should be formatted as required by the methodologies described in Chapter 3.

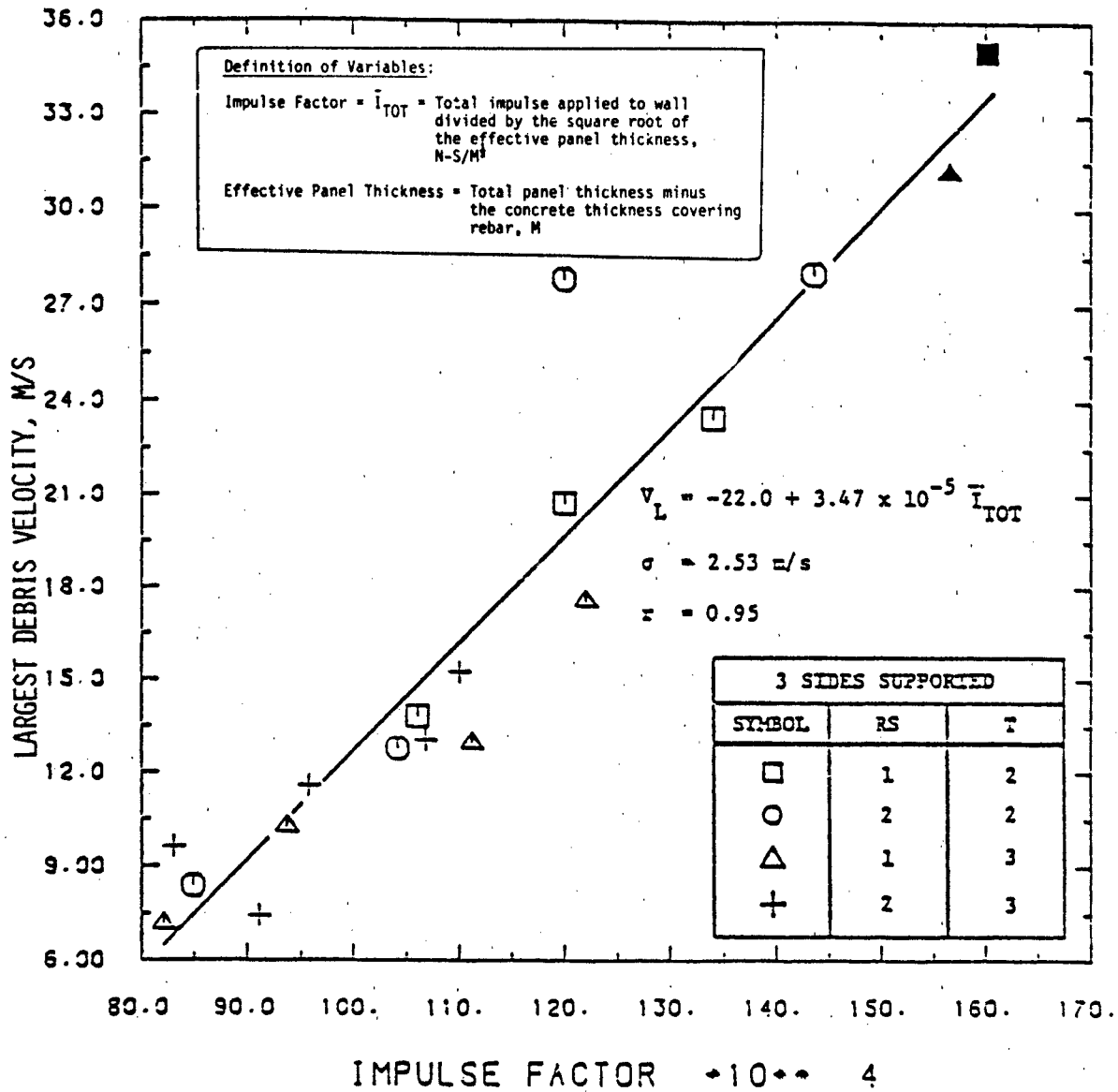


FIGURE 13. THE LARGEST DEBRIS VELOCITY AS A FUNCTION OF THE IMPULSE FACTOR FOR THREE-SIDE-SUPPORTED PANELS<sup>26</sup>

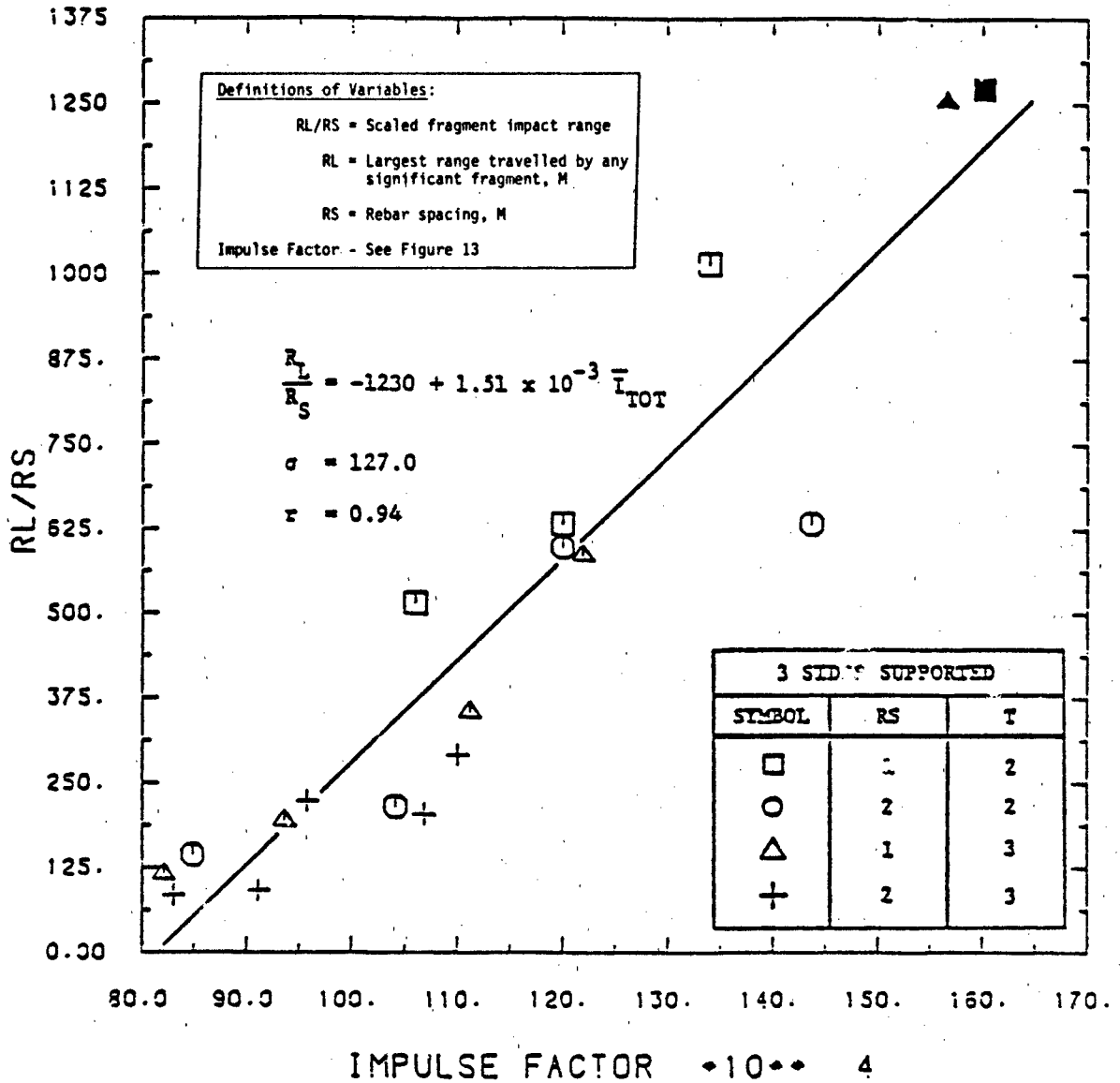


FIGURE 14. THE LARGEST DEBRIS RANGE AS A FUNCTION OF THE IMPULSE FACTOR FOR THREE-SIDE-SUPPORTED PANELS<sup>26</sup>

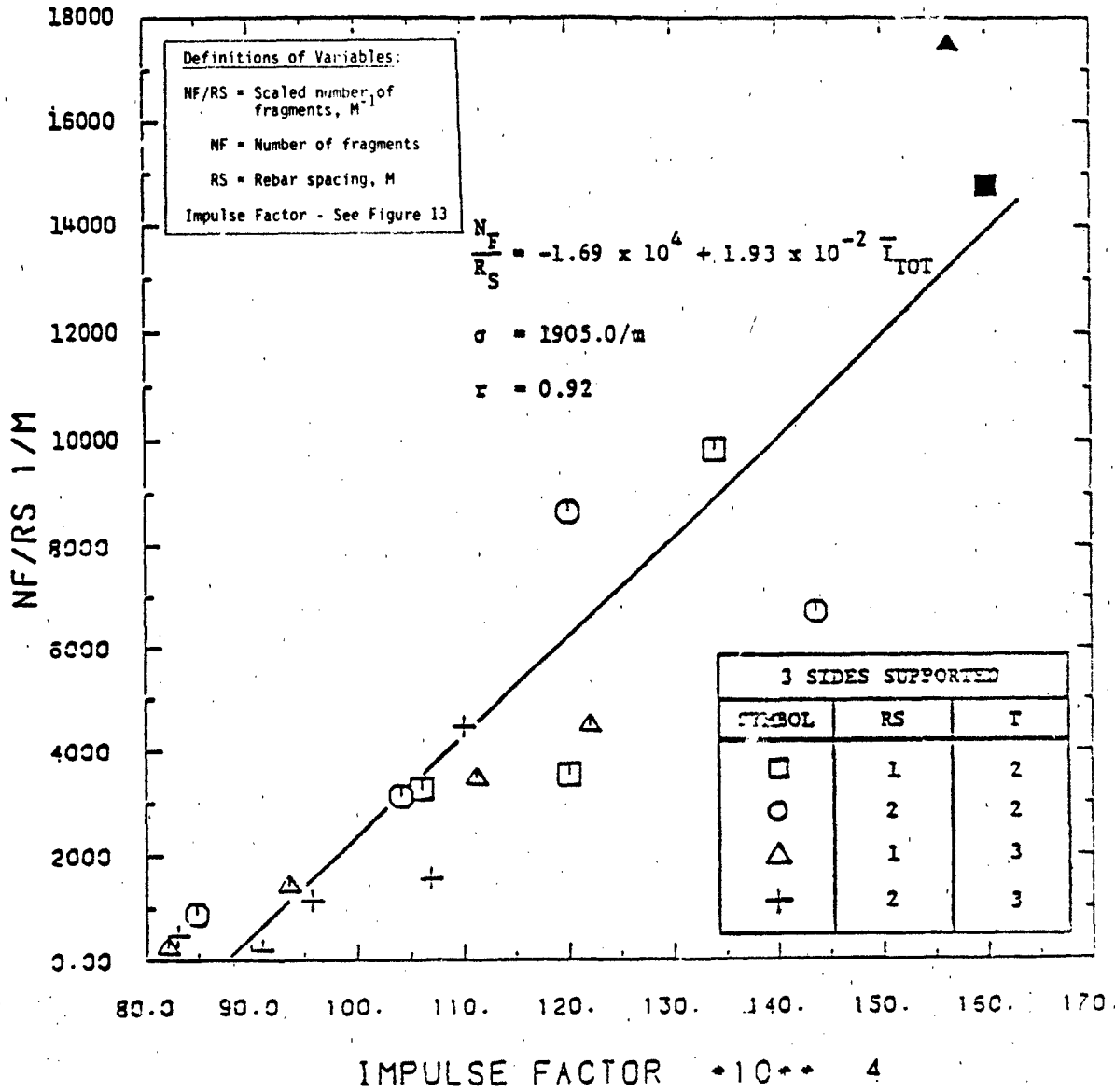


FIGURE 15. NUMBER OF DEBRIS MISSILES PRODUCED AS A FUNCTION OF THE IMPULSE FACTOR FOR THREE-SIDE-SUPPORTED PANELS<sup>26</sup>

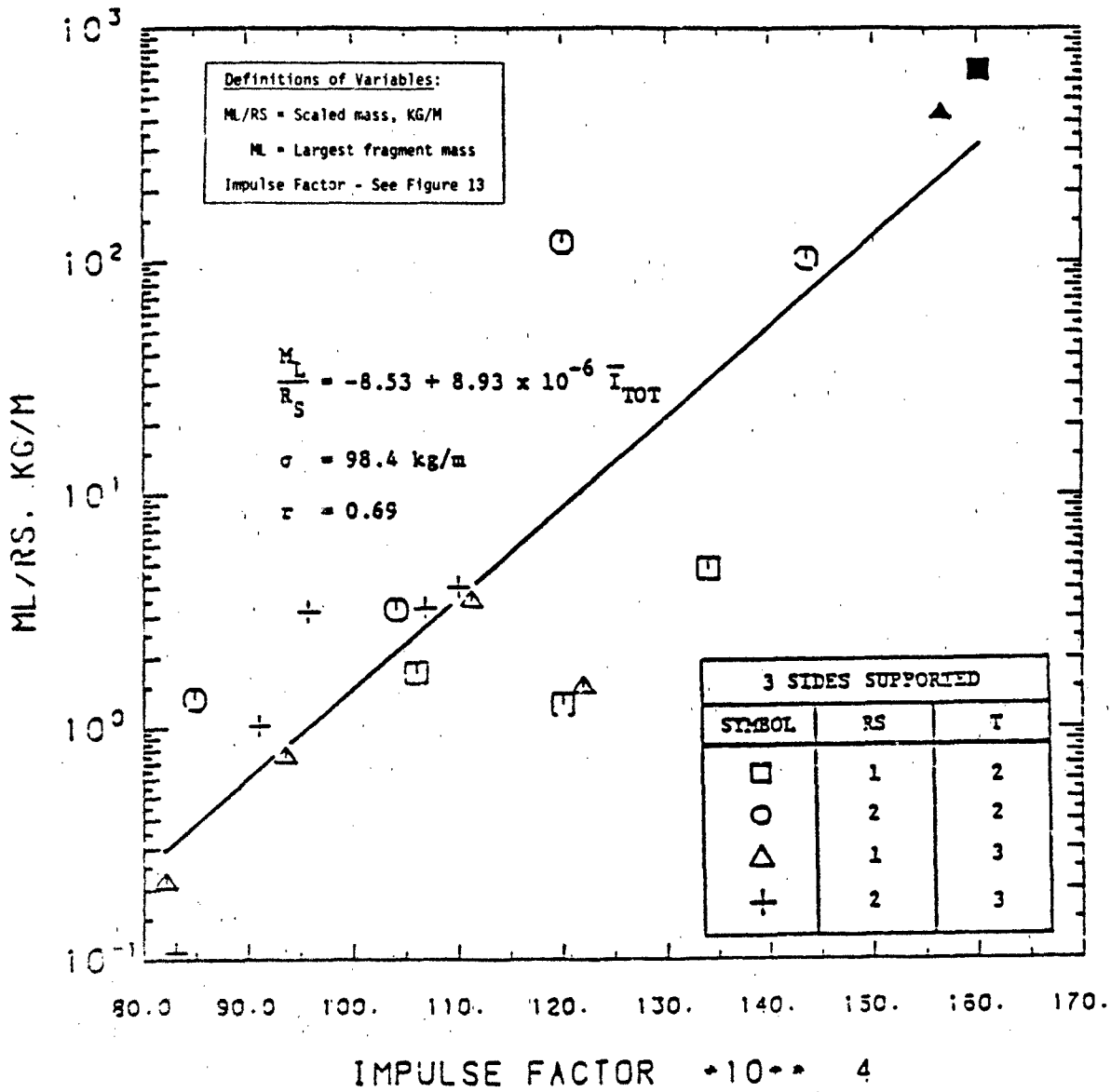
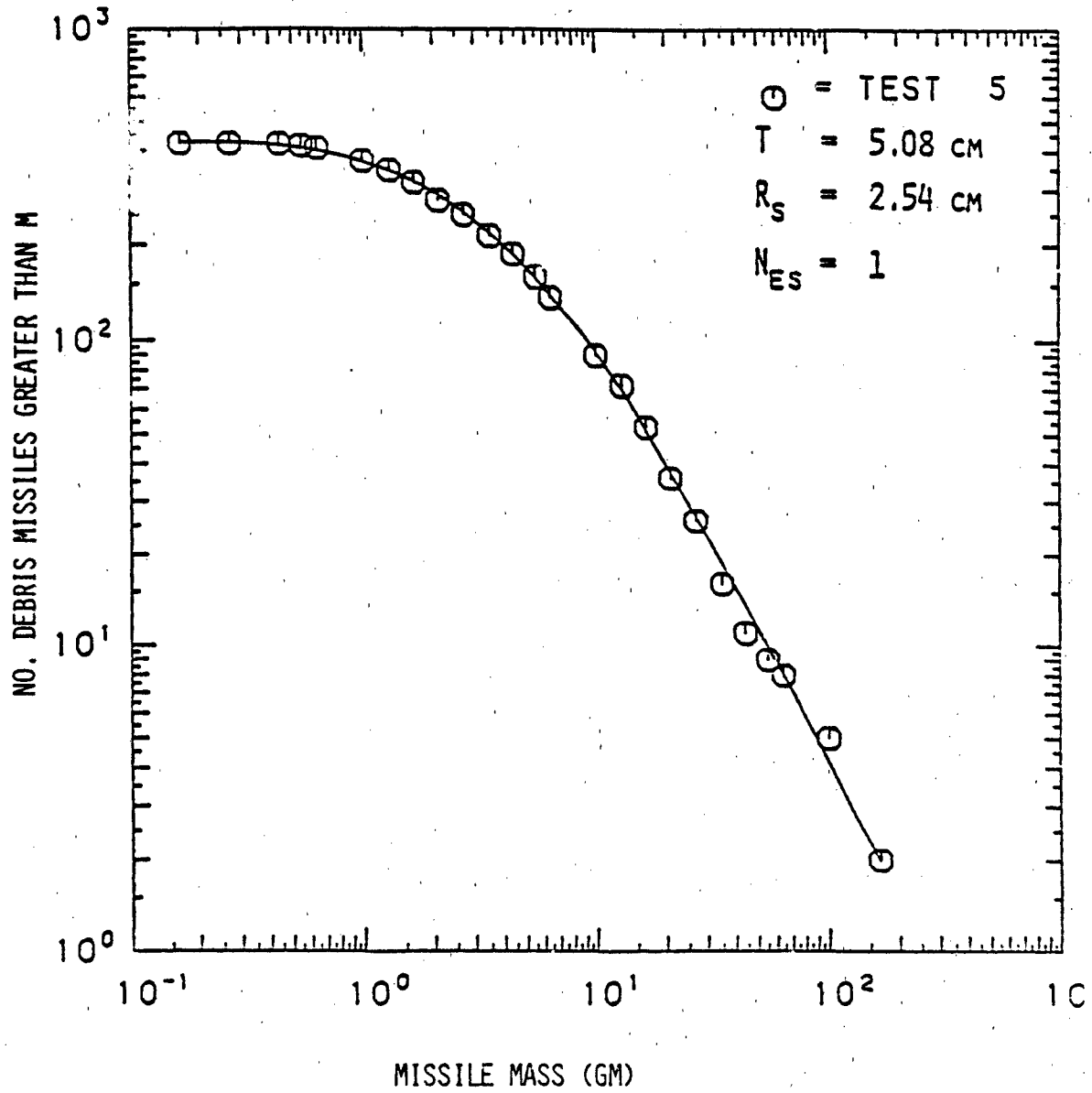


FIGURE 16. LARGEST RECOVERED MASS AS A FUNCTION OF THE IMPULSE FACTOR FOR THREE-SIDE-SUPPORTED PANELS<sup>26</sup>

## COMBINED DISTRIBUTION FOR TEST SERIES 1W

FIGURE 17. DEBRIS MASS DISTRIBUTION FOR A CANTILEVERED WALL<sup>26</sup>

COMBINED DISTRIBUTION FOR TEST SERIES 4S

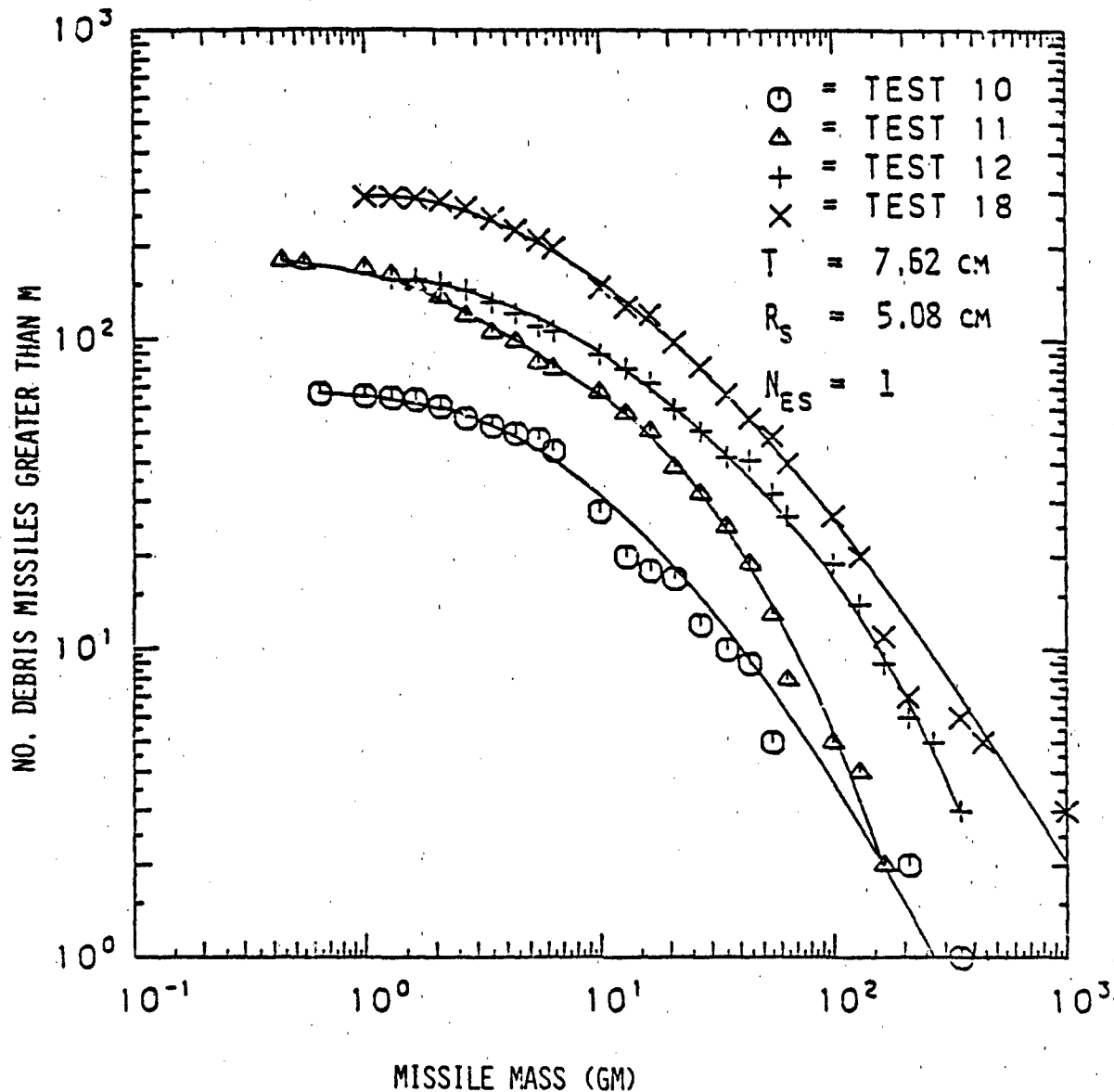


FIGURE 18. DEBRIS MASS DISTRIBUTION FOR CANTILEVERED DIVIDING WALLS AS A FUNCTION OF BLAST LOADING<sup>26</sup>

## REFERENCES

1. Hekker, L. J., and Pasman, H. J., "Statistics Applied to Natural Fragmenting Warheads," Proceedings of the Second International Symposium on Ballistics, American Defense Preparedness Association, 1975.
2. Randers-Pehrson, G., "An Improved Equation for Calculating Fragment Projection Angles," Proceedings of the Second International Symposium on Ballistics, American Defense Preparedness Association, 1976.
3. Structures to Resist the Effects of Accidental Explosions, Department of the Army TM-5-1300, Department of the Navy Publication NAVFAC P-397, Department of the Air Force Manual AFM 88-22, U.S. Army, Navy, and Air Force, Jun 1969.
4. Eriksson, L., and Arvidsson, T., "A Study of the Fragmentation of Cylindrical Shells of Four Carbon Steels," International Conference on Fracture, 3rd Proc., Munich, Germany, Apr 1973.
5. Johnson, C., and Moseley, J. W., Preliminary Warhead and Terminal Ballistics Handbook, NWL TR No. 1821, Mar 1964.
6. Sternberg, H. M., Fragment Weight Distributions from Naturally Fragmenting Cylinders Loaded with Various Explosives, NOLTR 73-83, 12 Oct 1972.
7. Krauklis, P., and Bedford, A. J., "Fragmentation Data Analysis: 1. Computer Program for Mass and Number Distributions and Effects of Errors on Mass Distributions," Australian Defense Scientific Service, Maribyrnong, Australia, Report 549, Nov 1974.
8. Porzel, F., Petes, J., Tondo, D., Smith, C., Freund, D., and Swisdak, M., Naval Explosives Safety Improvement Program, (NESIP): Summary and Status through 30 Jun 1976, NSWC TR 81-27, Mar 1981.
9. Jacobs, Sigmund, J., The Gurney Formula: Variations on a Theme by Lagrange, NOLTR 74-86, Jun 1974.
10. "Static Fragmentation Tests of High-Explosive Munitions," U.S. Army Test and Evaluation Command, Test Operations Procedure, 31 Jan 1980.

## REFERENCES (Cont.)

11. Lacher, E. B., "ZONE, a Computer Program for Reducing Test Arena Data to Zone Data for Fragmenting Warheads," Tech. Memo 203A, Picatinny Arsenal, Mar 1972.
12. Suppressive Shields Structural Analysis and Design Handbook, Report No. HNNDM-1110-1-2, U.S. Army Corps of Engineers, Huntsville Division, Huntsville, AL, Nov 1977.
13. Zaker, T. A., "Trajectory Calculations in Fragment Hazard Analysis," Thirteenth Explosives Safety Seminar, San Diego, CA, Sep 1971.
14. Schreyer, H. L., and Romesberg, L. E., "Analytical Model for High Explosive Munitions Storage," Mechanics Research Inc., Albuquerque, NM, Jun 1970.
15. Ramsey, R. T., Powell, J. G., Jr., and Smith, W. D., III, "Fragment Hazard Investigation Program," Eighteenth Explosives Safety Seminar, San Antonio, TX, Sep 1978.
16. Fugelso, L. E., and Rathmann, C. E., "Effect of Earth Cover on Far-Field Fragment Distribution," Department of Defense Explosives Safety Board, Washington, DC, Dec 1973.
17. Baker, et al., Workbook for Estimating Effects of Accidental Explosions in Propellant Ground Handling and Transport Systems, NASA Contractor Report 3023, Aug 1978.
18. Klein, P. F., "Fragment and Debris Hazards," Technical Paper 12, Department of Defense Explosives Safety Board, Washington, DC, Jul 1975.
19. Fugelso, L. E., Weiner, L. M., and Schiffman, T. H., Explosion Effects Computational Aids, Final Report GARD Project No. 02-1540, Jun 1972.
20. Connor, J. G., Jr., "Accidental Torpedo Detonation in Submarine Tender Workshops," Nineteenth Explosives Safety Seminar, Los Angeles, CA, Sep 1980.
21. Swisdak, M. M., Jr., "Determination of Safe Handling Arcs Around Nuclear Attack Submarines," Nineteenth Explosives Safety Seminar, Los Angeles, CA, Sep 1980.
22. Kulesz, J. J., Moseley, P. K., and Baker, W. E., Fragment and Blast Hazards from Explosions in a Tender Torpedo Workshop, SwRI report for David Taylor Naval Ship Research and Development Center, Bethesda, MD, 6 Nov 1978.
23. Baker, W. E., Kulesz, J. J., Ricker, R. E., Bessey, R. L., Westine, P. S., Parr, V. B., and Oldham, G. A., Workbook for Predicting Pressure Wave and Fragment Effects of Exploding Propellant Tanks and Gas Storage Vessels, NASA Contractor Report 134906, Sep 1977.

## REFERENCES (Cont.)

24. Kulesz, J. J., Moseley, P. K., and Parr, V. B., "Prediction of Debris Weight and Range Distributions from Accidental Explosions Inside Buildings," Southwest Research Institute, San Antonio, TX, DAC87-79-C-0091, paper presented at Nineteenth Explosives Safety Seminar, Los Angeles, CA, Sep 1980.
25. Ahlers, E. B., Debris Hazards: A Fundamental Study, IIT Research Institute, Chicago, IL, IITRI Report No. 8231, DASA-1362 (no date).
26. Vargas, L. M., Hokanson, J. C., and Rindner, R. M., "Explosive Fragmentation of Dividing Walls," Southwest Research Institute, San Antonio, TX, prepared for ARRADCOM, SwRI Project No. 02-5793, Aug 1980.
27. Moseley, P. K., and Whitney, M. G., "Blast and Debris from an Accidental Explosion Inside a No weg'an Aircraft Shelter," Southwest Research Institute, San Antonio, TX, prepared for Norwegian Defense Construction Service, SwRI Project No. 02-5881, Feb 1981.
28. Merz, H. A., "Debris Hazards from Explosions in Above Ground Magazines," Basler and Hofmann Consulting Engineers, Zurich, Switzerland, paper presented at Nineteenth Explosives Safety Seminar, Los Angeles, CA, Sep 1980.
29. Edrunds, J. E., "Experiments to Determine Debris Formation from Corrugated Steel and Brick Walls," URS Research Company, Burlingame, CA, for the Office of Civil Defense, URS 751-4, Jan 1970.
30. Schellings, A. A. J., Mechanisms for Evaluation of Fragmentation, Volume II - Fragment Ballistics, Report No. TL-1968-20, of the Technological Laboratories of the Netherlands (TNO) Oct 1968, (In Dutch, translation by Dr. W. E. Baker, Southwest Research Institute, Dec 1980).
31. Schwarz, B. D., "Feststellung der Wirkung im Ziel von Spillor - Spreng-munition," Brief dr. Zwarg 664061, Koblenz BWB - WM IV 4-Az: 90-13-00-30 (30), Nov 1965.
32. Sterne, T. E., "Criteria for Incapacitation by Fragments," BRL Tech Note 556, Nov 1951.
33. Ward, J. M., "Blast/Fragment Hazards Associated with the Accidental Detonation of a Mark 82 Bomb Pallet," Presented at the Nineteenth Explosives Safety Seminar, Los Angeles, CA, Sep 1980.
34. Porzel, F. B., "Technology Base of the Navy Explosives Safety Improvement Program," Nineteenth Explosives Safety Seminar, Los Angeles, CA, Sep 1980.
35. Baker, W. E., Westine, P. S., and Dodge, F. T., Similarity Methods in Engineering Dynamics: Theory and Practice of Scale Modeling, (Rochelle Park, NJ:, Hayden Book Company, Inc., Jan 1973).

REFERENCES (Cont.)

36. Cohen, E., and Dobbs, N., "Models for Determining the Response of Reinforced Concrete Structures to Blast Loading," Annals of the New York Academy of Sciences, 152, Art. 1, Oct 1968, pp. 810-828.
37. Hoerner, S. F., Fluid-Dynamics Drag, Published by the Author, Midland Park, NJ, 1958.
38. Justrow, "Theorie der Splitterwirkung von Granaten, Wurfminen und ähnlichen Sprengkörpern," Techn. u. Wehrmacht 24 (1921) 202, 241, Table 3.

NSWC TR 85-114

APPENDIX A  
BIBLIOGRAPHY

AD/AS Workshop MK-48 Fragment Test, TERA Report NMT/TERA No. TD-79-1134, BB-U, Contract No. N00123-78-C-0745, prepared for Naval Surface Weapons Center, 5 Nov 1979.

Ahlers, E. B., "Fragment Hazard Study," Minutes of the Eleventh Explosives Safety Seminar, Memphis, TN, Sep 1969.

Ahlers, E. B., "Fragment Behavior Discussions for Storage of Ammunition and Explosives," Minutes of the Eleventh Explosives Safety Seminar, Vol. I, pp. 343-348, Memphis, TN, Sep 1969.

Ahlers, E. B., "Debris Hazards, A Fundamental Study," IIT Research Institute Project No. 8231, DASA-1362 (no date).

Anderson, C. A., "Internal Blast Loading of Scale-Model Explosive-Processing Bays," Minutes of the Eleventh Explosives Safety Seminar, Memphis, TN, Sep 1969.

Arya, R., Dobbs, N., Ammar, A., Weissman, S., and Price, P., Blast Capacity Evaluation of Belowground Structures, ARRADCOM, Contractor Report ARLCD-CR-77006, May 1977.

Baker, et al., Workbook for Estimating Effects of Accidental Explosions in Propellant Ground Handling and Transport Systems, NASA Contractor Report 3023, Aug 1978.

Baker, W. E., Kulesz, J. J., Westine, P. S., Cox, P. A., and Wilbeck, J. S., A Manual for the Prediction of Blast and Fragment Loadings on Structures, DOE/TIC-11268, SwRI Final Report for U.S. Army Corps of Engineers, Huntsville Division, Huntsville, AL, Jun 1980.

Baker, W. E., Parr, V. B., Bessey, R. L., and Cox, P. A., Assembly and Analysis of Fragmentation Data for Liquid Propellant Vessels, NASA Report CR-134538, Contract NA53-16009, Jan 1974.

Baker, W. E., Westine, P. S., Kulesz, J. J., Wilbeck, J. S., and Cox, P. A., A Manual for the Prediction of Blast and Fragment Loadings on Structures, prepared for U.S. Department of Energy, DOE/TIC-11268, Nov 1980.

Barnett, Ralph L., Costello, James F., and Feinstein, David I., "Debris Formation and Translation," IIT Research Institute, IITRI Project M6103, Nov 1966.

Barnett, Ralph L., and Hermann, Paul C., "Fragmentation of Reinforced Concrete Slabs," IIT Research Institute, IITRI Project No. J6107, Oct 1968.

Base Fragment Velocities of Service Navy Projectiles, Report No. 1201, U.S. Naval Proving Ground, Dahlgren, VA, Nov 1953.

Basler and Hofmann, Model Experiments for Above-Ground Powder Magazines, Part I. Design and Execution, Report B-952-2, Nov 1979.

Basler and Hofmann, Model Experiments for Above-Ground Powder Magazines, Part II. Data and Photo Documentation, Report B-952-2, Aug 1979.

Basler and Hofmann, Model Experiments for Above-Ground Explosive Magazines, Part III. Evaluation and Results, Report B-952-4, Mar 1980.

Char, W. T., "Simplified Approach for Design of Buildings Containing Accidental Explosions," Minutes of the Eighteenth Explosives Safety Seminar, San Antonio, TX, Sep 1978.

Cohen, E., and Dobbs, N., "Design Procedures and Details for Reinforced Concrete Structures Utilized in Explosive Storage and Manufacturing Facilities," Annals of the New York Academy of Sciences, Vol. 152, Art. 1, Oct 1968.

Cohen, E., and Dobbs, N., "Models for Determining the Response of Reinforced Concrete Structures to Blast Loads," Annals of the New York Academy of Sciences, Vol. 152, Art. 1, Oct 1968.

Connor, Joseph G., Jr., "Accidental Torpedo Detonation in Submarine Tender Workshops," Nineteenth Explosives Safety Seminar, Los Angeles, CA, Sep 1980.

Davis, J. O., "A Predesign Analysis Technique for Reinforced Concrete Structures," Minutes of the Sixteenth Explosives Safety Seminar, Hollywood, FL, Sep 1974.

Draper E., and Watson, R. R., Collated Data on Fragments from Stacks of High Explosive Projectiles, Directorate of Safety, London, England, Report No. TM-2/70, Mar 1970.

Edmunds, James E., Experiments to Determine Debris Formation for Corrugated Steel and Brick Walls, URS Research Company, Burlingame, CA, Report URS-751-4, Jan 1970.

Eriksson, L., and Arvidsson, T., "A Study of the Fragmentation of Cylindrical Shells of Four Carbon Steels," International Conference on Fracture, 3rd Proc., Munich, Germany, Apr 1973.

Feinstein, D. I., "Fragmentation Hazard Evaluations and Experimental Verification," Minutes of the Fourteenth Explosives Safety Seminar, New Orleans, LA, Sep 1974.

Feinstein, D. I., "Fragment Hazard Study: Grading and Analysis of 155 mm Yuma Test Fragments," IITRI for DOD Explosives Safety Board, Oct 1972.

Feinstein, D. I., Fragmentation Hazards to Unprotected Personnel, Department of Defense Explosives Safety Board, Report No. IITRI J6176, Jan 1972.

Feinstein, D. I., and Nagaoka, H. H., Fragmentation Hazard Study, Phase III. Fragment Hazards from Detonation of Multiple Munitions in Open Stores, IIT Research Institute, Report No. J6176, Aug 1977.

Feinstein, D. I., and Nagaoka, H. H., "Fragmentation Hazards to Unprotected Personnel," Minutes of the Thirteenth Explosives Safety Seminar, San Diego, CA, Sep 1971.

Fragmentation of Double Sleeve Warhead No. 141, Report No. 1083, U.S. Naval Proving Ground, Dahlgren, VA, Feb 1953.

Fragmentation Test of 3/50 Rod Projectiles, EX 26 MOD 1 and EX 27 MOD 1, Report No. 1079, U.S. Naval Proving Ground, Dahlgren, VA, Jan 1953.

Fragmentation Test of Notched Ring Warhead No. 139, Report No. 997, U.S. Naval Proving Ground, Dahlgren, VA, Jul 1952.

Fragmentation Test of Rod Expelling Warhead No. 134, Report No. 972, U.S. Naval Proving Ground, Dahlgren, VA, May 1952.

Fragmentation Testing of Dual Initiated 3.5 Warhead No. 144, Report No. 1140, U.S. Naval Proving Ground, Dahlgren, VA, Jun 1953.

Frigiola, J. A., An Evaluation of the Protective Devices' Bomb Handling System, Naval Explosive Ordnance Disposal Facility, TR-145, Mar 1973.

Fugelso, L. E., Weiner, L. M., and Schiffman, T. H., Explosion Effects Computational Aids, Final Report GARD Project No. 02-1540, Jun 1972.

Fugelso, L. E., and Rathmann, C. E., Effect of Earth Cover on Far-Field Fragment Distribution, Department of Defense Explosives Safety Board, Final Report GARD Project No. 1577, Dec 1973.

Fullwood, R., et al., Fragment Environment Modeling for STS Launch Accidents, AFWL-TR-79-167, Air Force Weapons Laboratory, Kirtland Air Force Base, NM, Jun 1980.

Gabrielson, B. L., Response of Wall Panels Subjected to Blast Loading, Reprint 1399, ASCE National Structural Engineering Meeting, Baltimore, MD, Apr 1971.

Gabrielson, B., Wilton, C., and Kaplan, K., "Response of Arching Walls and Debris From Interior Walls Caused by Blast Loading," URS Research Company, URS 7030-23, Feb 1975.

Greenspon, J. E., "An Approximate Nondimensional Representation of the THOR Equations," J. G. Engineering Research Association, Oct 1976.

Gurney, R. W., The Initial Velocities of Fragments from Bombs, Shells and Grenades, BRL Report No. 405, Sep 1943.

Healey, John J., and Weissman, Samuel, "Primary Fragment Characteristics and Impact Effects in Protective Design," Sixteenth Explosives Safety Seminar, Hollywood, FL, Sep 1974.

Hekker, L. J., and Pasman, H. J., "Statistics Applied to Natural Fragmenting Warheads," Proceedings of the Second International Symposium on Ballistics, American Defense Preparedness Association, 1975.

Jacobs, Sigmund J., "The Gurney Formula: Variations on a Theme by Lagrange," Naval Ordnance Laboratory, White Oak, MD, Jun 1974.

Karpp, R. R., and Predebon, W. W., "Calculations of Fragment Velocities from Naturally Fragmenting Munitions," BRL Memorandum Report No. 2509, Jul 1975.

Keenan, W. A., and Tancreto, J. E., "Blast Environment from Fully and Partially Vented Explosions in Cubicles," CEL, NCBC, Port Hueneme, CA, Feb 1974.

Kot, C. A., and Pap, J., "Spalling of Concrete Walls Under Blast Load," Transactions of the Fourth International Conference on Structural Mechanics in Reactant Technology, San Francisco, CA, 15-19 Aug 1977.

Kot, C. A., and Turula, P., Air Blast Effects on Concrete Walls, Argonne National Laboratory, Report No. ANL-CT-76-50, Jul 1976.

Johnson, C., and Moseley, J. W., Preliminary Warhead and Terminal Ballistics Handbook, NW TR No. 1821, Mar 1964.

Krauklis, P., and Bedford, A. J., Fragmentation Data Analysis: 1. Computer Program for Mass and Number Distributions and Effects of Errors on Mass Distributions, Australian Defence Scientific Service, Maribyrnong, Australia, Report 549, Nov 1974.

Kulesz, J. J., Moseley, Patricia K., and Parr, V. B., "Prediction of Debris Weight and Range Distributions from Accidental Explosions Inside Buildings," Southwest Research Institute, Nineteenth Explosives Safety Seminar, Los Angeles, CA, Sep 1980.

Lacher, E. B., "ZONE, a Computer Program for Reducing Test Arena Data to ZONE Data for Fragmenting Warheads," Tech. Memo 2034, Picatinny Arsenal, Mar 1972.

Leondi, Michael F., "Dynamic Modeling of Post Failure Conditions of Reinforced Concrete Subjected to Blast," ARRADCOM, LCWSL, Dover, NJ, Mar 1979.

Levy, S., Rindner, R., Saffian, L., Wachtell, S., Cohen, E., Dede, M., and Dobbs, N., Full and Model Scale Tests of Bay Structure, Technical Report No. 4168, Picatinny Arsenal, Feb 1971.

Melichar, J. F., "A Preliminary Investigation of Analytic Debris Estimation Procedures," URS Research Co, No. DAH-20-69-C-0135, Feb 1970.

Merz, Hans A., "Debris Hazards from Explosions on Above-Ground Magazines," Nineteenth Explosives Safety Seminar, Los Angeles, CA, Sep 1980.

Merz, Hans A., "The Effects of Explosions in Slightly Buried Concrete Structures," Proceedings of Fifth International Symposium on Military Applications of Blast Simulation, Stockholm, Sweden, May 1977.

Mullins, R. K., and Baker, C. F., "Interim Report on Use of Steel Fibers in Concrete Slab Construction to Resist Spall Caused by High-Explosive Blast Effects," Lawrence Livermore Laboratory, 7 Sep 1979.

Pittman, J. F., Blast and Fragments from Superpressure Vessel Rupture, NSWC/WOL/TR 75-87, Feb 1976.

Porzel, Francis B., "Design of Lightweight Shields, Against Blast and Fragments," Minutes of the Seventeenth Explosives Safety Seminar, Vol II, Denver, CO, 14-16 Sep 1976.

Porzel, F., Petes, J., Tondo, D., Smith, C., Freund, D., and Swisdak, M., Naval Explosives Safety Improvement Program (NESIP): Summary and Status through 30 Jun 1976, NSWC TR 81-27, Mar 1981.

Porzel, Francis B., "Technology Base of the Navy Explosives Safety Improvement Program," Nineteenth Explosives Safety Seminar, Los Angeles, CA, Sep 1980.

Powell, J. G., and Smith W. D., III, "Fragment Hazard Investigation Program (Large-Scale Detonation Tests)," Naval Surface Weapons Center, Oct 1978.

Proctor, J. F., "A Review of Methods of Predicting Concrete Penetration by Postulated Reactor Plant Missiles," Naval Surface Weapons Center, 25 Jul 1975.

Ramsey, Richard T., Powell, Joseph G., Jr., and Smith, William D., III, "Fragment Hazard Investigation Program," Eighteenth Explosives Safety Seminar, San Antonio, TX, Oct 1978.

Randers-Pehrson, G., "An Improved Equation for Calculating Fragment Projection Angles," Proceedings of the Second International Symposium on Ballistics, American Defense Preparedness Association, 1976.

Randers-Pehrson, Glenn, Karpp, R. R., Anderson, C. E., Jr., and Blishche, H. J., "Shortfrag Users Guide," Memorandum Report ARBRL-MR-03007, Mar 1980.

Rinehart, J. S., Stress Transients in Solids, Hyperdynamics, Santa Fe, NM, 1975.

Schippers, J., "Estimation of Explosion Damage to Urban Structures in the Netherlands," Minutes of the Eighteenth Explosives Safety Seminar, San Antonio, TX, Sep 1978.

Shelly, S. O., Vulnerability and Lethality Testing Systems (VALTS), Armament Development and Test Center, ADTC-TR-72-127, Dec 1972.

Schellings, A. A. J., "Mechanisme En Evaluering Van Verscherving, Part I: Literature Survey," Technologisch Laboratorium RVO-TNO, Rijswijk, 1969.

Schellings, A. A. J., "Mechanisme En Evaluering Van Verscherving, Part II: Scherfballistiek - 1," Technologisch Laboratorium RVO-TNO, Rijswijk, Oct 1968.

Schellings, A. A. J., "Mechanisme En Evaluering Van Verschering, Part III: Scherfballistiek - 2, " Technologisch Laboratorium RVO-TNO, Rijswijk, Nov 1968.

Shreyer, H. L., and Romesberg, L. E., "Analytical Model for High Explosive Munitions Storage," Mechanics Research Inc., Albuquerque, NM, Jun 1970.

Sliter, G. E., "Assessment of Empirical Concrete Impact Formulas," Journal of the Structural Division, ASCE, May 1980.

Static Fragmentation of 8/55 FCL (VT) Projectiles MK 25 MOD 1 With Experimental VT Fuses, Report No. 974, U.S. Naval Proving Ground, Dahlgren VA, May 1952.

Static Fragmentation Tests of High-Explosive Munitions, U.S. Army Test and Evaluation Command, Test Operations Procedure, 31 Jan 1980.

Sten, Goran, The Effect of Fragmenting Warheads Against Ground Targets When the Terrain Gives Some Protection, Part 1: A Probabilistic Treatment Based on a Random Terrain Model and a Partly Random Model of the Target and the Warhead, FOA Report C 20120-D4(D5, D5), Stockholm, Jun 1976.

Sternberg, H. M., Computation of Weight, Velocity and Angular Distributions of Fragments from Naturally Fragmenting Weapons, NOLTR 74-77, 17 Jul 1974.

Sternberg, H. M., Fragment Weight Distributions from Naturally Fragmenting Cylinders Loaded with Various Explosives, NOLTR 73-83, 12 Oct 1972.

Steves, B. F., Callahan, H. L., and Hill, W. V., "Design of a Small Explosive Loaded Storage Building," Minutes of the Eleventh Explosives Safety Seminar, Memphis, TN, Sep 1969.

Structures to Resist the Effects of Accidental Explosions, Department of the Army Technical Manual, TM 5-1300, Department of the Navy Publication NAVFAC P-397, Department of the Air Force Manual AFM 88-22, U.S. Army, Navy, and Air Force, Jun 1969.

Swisdak, M. M., Jr., "Determination of Safe Handling Arcs Around Nuclear Attack Submarines," Nineteenth Explosives Safety Seminar, Los Angeles, CA, Sep 1980.

Suppressive Shields Structural Analysis and Design Handbook, Report No. HNDM-11110-1-2, U.S. Army Corps of Engineers, Huntsville Division, Huntsville, AL, Nov 1977.

Thurston, R. S., and Mudd, W. L., "Spallation Criteria for Numerical Computations," LASL, Sep 1968.

U.S. Army Corp of Engineers, Overpressure Effects on Structures, Report No. HNDTR-75-23-ED-SR, Reissued 1 Apr 1979.

Vargas, L. M., Hokanson, J. C., and Rindner, R. M., Explosive Fragmentation of Dividing Walls, SwRI prepared as ARRADCOM Contractor Report ARLCD-CR-81018, AD-E400-670, Jul 1980.

Wachtell, S., "Comparison of Blast Response-Scaled Versus Full-Sized Concrete Structures," Annals of the New York Academy of Sciences, Oct 1968.

Walsh, B. E., "Control of Explosively-Induced Fracture in Fragmenting Munitions," Fourth Tewksbury Symposium, Melbourne, Australia, Feb 1979.

Waterman, Thomas E., Fire Laboratory Tests -- Phase III. Fire in Blast-Initiated Debris External to Shelters, IIT Research Institute, Report No. IITRI-J6217, Feb 1973.

Ward, J., "Blast/Fragment Hazards Associated with the Accidental Detonation of a MK82 Bomb Pallet," Nineteenth Explosives Safety Seminar, Los Angeles, CA, Sep 1980.

Willoughby, A. B., Wilton, C., Gabrielsen, B. L., and Zaccor, J. V., "A Study of Loading Structural Response and Debris Characteristics of Wall Panels," URS Research Company, Burlingame, CA, Jul 1969.

Wilton, Chuck, Gabrielson, B. L., and Kaplan, Kenneth, "Failure Strengths of Wall Panels Under Explosive Loading," Minutes of the Fifteenth Explosives Safety Seminar, Vol. I, San Francisco, CA, Sep 1973.

Zabel, P. H., and Kuhn, W. J., "Computer Model for Fragmentation Threat from a High Explosive Shell," TFD-73-634, B-2 Division, Rockwell Int., AD-B-043-158, 24 Oct 1973.

Zaker, T. A., "Computer Program for Predicting Casualties and Damage from Accidental Explosions," Department of Defense Explosives Safety Board, Technical Paper No. 11, Washington DC, May 1975.

Zaker, T. A., "Trajectory Calculations in Fragment Hazard Analysis," Thirteenth Explosives Safety Seminar, San Diego, CA, Sep 1971.

Zaker, T. A., "Fragment and Debris Hazards," Technical Paper 12, Department of Defense Explosives Safety Board, Washington, DC, Jul 1975.

## DISTRIBUTION

	<u>Copies</u>		<u>Copies</u>
Chief of Naval Material		Commander	
Attn: MAT-08T2	1	Naval Electronic Systems Command	
MAT-08L	1	Attn: ELEX-03A	1
Department of the Navy		ELEX-9053	1
Washington, DC 20360		Naval Electronic Systems	
		Command Headquarters	
Chief of Naval Operations		Washington, DC 20360	
Attn: NOP-411	1	Commander	
NOP-411F	1	Naval Facilities Engineering	
NOP-621C	1	Command	
NOP-622C	1	Attn: Code 032E	1
NOP-987	1	Code 09M22C	1
NOP-983	1	Naval Facilities Engineering	
Department of the Navy		Command Headquarters	
Washington, DC 20350		Alexandria, VA 22332	
Chief of Naval Research		Commander	
Attn: ONR-102	1	Naval Sea Systems Command	
ONR-412	1	Attn: SEA-06H	1
ONR-420	1	SEA-62R	1
ONR-432	1	SEA-64	1
ONR-460	1	SEA-64E	1
ONR-463	1	SEA-09G32	1
ONR-465	1	SEA-99612	1
800 N. Quincy Street		Naval Sea Systems Command	
Arlington, VA 22217		Headquarters	
Office of Naval Technology		Washington, DC 20362	
800 N. Quincy Street		Officer in Charge	
Arlington, VA 22217	1	Civil Engineering Laboratory	
Commander		Naval Construction Battalion Center	
Naval Air Systems Command		Attn: W. Keenan	5
Attn: AIR-00D4	1	L. Huang	5
AIR-03B	1	J. Tancreto	1
AIR-03C	1	Port Hueneme, CA 93043	
AIR-09E	1	Library of Congress	
AIR-09E3	1	Attn: Gift and Exchange Division	4
AIR-350	1	Washington, DC 20540	
AIR-516C	1		
Naval Air Systems Command			
Headquarters			
Washington, DC 20361			

## DISTRIBUTION (Cont.)

	<u>Copies</u>		<u>Copies</u>
Commanding Officer Naval Research Laboratory Attn: Technical Information Center Washington, DC 20375	1	Commander Naval Ocean Systems Center San Diego, CA 92152	1
Commander David W. Taylor Naval Ship Research and Development Center Bethesda, MD 20084	1	Commanding Officer Naval Ordnance Missile Test Facility White Sands Missile Range, NM 88002	1
Naval Ship Research and Development Center Attn: Library Underwater Explosions Research Division Portsmouth, VA 23709	1	Commanding Officer Naval Ordnance Station Attn: Technical Library Indian Head, MD 20640	1
Commander Naval Weapons Center Attn: Code 3687 China Lake, CA 93555	1	Commanding Officer Naval Ordnance Station Louisville, KY 40214	1
Commander Naval Air Development Center Warminster, PA 18974	1	Commanding Officer Naval Ordnance Test Unit Cape Canaveral Air Force Station, FL 32920	1
Commanding Officer Naval Air Engineering Center Lakehurst, NJ 08733	1	Commander Naval Safety Center Naval Air Station Norfolk, VA 23511	1
Commanding Officer Naval Coastal Systems Center Attn: Technical Library Panama City, FL 32407	1	Commanding Officer Naval Ship Weapons Systems Engineering Station Port Hueneme, CA 93043	1
Commanding Officer Naval Explosive Ordnance Disposal Facility Attn: Technical Library Indian Head, MD 20640	1	Commanding Officer Naval Undersea Warfare Engineering Station Keyport, WA 98345	1
Officer in Charge Naval Mine Engineering Facility Yorktown, VA 23691	1	Commanding Officer Naval Underwater Systems Center Newport, RI 02840	1
		Commanding Officer Naval Weapons Station Charleston, SC 29408	1

## DISTRIBUTION (Cont.)

	<u>Copies</u>		<u>Copies</u>
Commanding Officer Naval Weapons Station Colts Neck, NJ 07722	1	Headquarters U.S. Army Munitions Command Attn: Library Dover, NJ 07801	1
Commanding Officer Naval Weapons Station Concord, CA 94520	1	Chief of Engineers Attn: DAEN-ASI-L DAEN-RDZ-A DAEN-SQZ-A	1 1 1
Commanding Officer Naval Weapons Station Seal Beach, CA 90740	1	Department of the Army Washington, DC 20314	
Commanding Officer Naval Weapons Station Attn: Research and Development Division Yorktown, VA 23691	1	Director U.S. Army Engineering Waterways Experiment Station Attn: Library P. O. Box 65 Vicksburg, MS 39180	1
Commanding Officer Naval Weapons Support Center Crane, IN 47522	1	Director U.S. Army Material Command Field Safety Activity	
Commander Pacific Missile Test Center Pt Mugu, CA 93042	1	Attn: Library Charlestown, IN 47111	2
Director Strategic Systems Project Office Department of the Navy Washington, DC 20376	1	Commanding Officer Aberdeen Research and Development Center Attn: Technical Library Aberdeen, MD 21005	1
Commandant of the Marine Corps Attn: MC-OT00 MC-LMW-50 Navy Department Washington, DC 20380	1 1	Commanding Officer U.S. Army Armament Research and Development Command Attn: Technical Library Dover, NJ 07801	1
Commanding General U.S. Army Material, Development and Readiness Research Command Attn: Technical Library DRCDE DRCSE 5001 Eisenhower Avenue Alexandria, VA 22333	1 1 1	Commanding General U.S. Army Natick Research and Development Command Attn: Library Natick, MA 01762	1
		Headquarters Air Force Systems Command Andrews Air Force Base Attn: Technical Library Washington, DC 20331	1

## DISTRIBUTION (Cont.)

	<u>Copies</u>		<u>Copies</u>
Directorate of Safety Headquarters Eastern Space and Missile Center Attn: SEM Patrick Air Force Base, FL 32925	1	Defense Technical Information Center Cameron Station Alexandria, VA 22314	12
Commander Air Force Weapons Laboratory Kirtland Air Force Base Albuquerque, NM 87117	1	Director of Defense Research and Engineering Attn: Technical Library Washington, DC 20330	1
Commander Armament Development and Test Center Attn: DLOSL, Technical Library Eglin Air Force Base, FL 32542	1	Chairman Department of Defense Explosives Safety Board Attn: DDESB-KT Room 856C Hoffman Bldg. 1 2461 Eisenhower Avenue Alexandria, VA 22331	1
Commander Air Force Cambridge Research Laboratories L. G. Hanscom Field Attn: Library Bedford, MA 01730	1	Director Defense Nuclear Agency Attn: Technical Library Washington, DC 20305	1
OGAMA Hill Air Force Base Attn: Code MME Ogden, UT 84401	1	Commander Field Command Defense Nuclear Agency Attn: FCTOH Kirtland Air Force Base, NM 87115	1
Commander Headquarters Air Force Inspection and Safety Center Attn: SEV Norton Air Force Base, CA 92409	1	TERA New Mexico Institute of Mining and Technology Socorro, NM 87801	1
Chairman USAF Nonnuclear Munitions Safety Board Attn: AD/SES Eglin Air Force Base, FL 32542	1	Kaman Tempo 2560 Huntington Avenue Alexandria, VA 22303	1
Commander Air Force Logistics Command Attn: A E. Adams Wright-Patterson Air Force Base, OH 45433	1	Hercules Incorporated Box 98 Magna, UT 84044	1
		IIT Research Institute Attn: Technical Library H. Napodensky 10 West 35th Street Chicago, IL 60616	1 1

## DISTRIBUTION (Cont.)

Copies

## Southwest Research Institute

Attn: J. Hokanson	5
L. Vargas	5
M. Whitney	5
T. Moseley	5
J. Cardinal	5

8500 Culebra Road  
San Antonio, TX 78206

## Internal Distribution:

R (J. Frasier)	1
R10 (J. Proctor)	1
R10 (D. Price)	1
R11	1
R12	1
R13 (C. Dickinson)	1
R14 (M. Marshall)	1
R15	1
R15 (M. Swisdak)	5
R15 (Smith)	1
R15 (V. Moore)	1
R16 (H. Haiss)	1
R121 (M. Stosz)	1
R122 (L. Roslund)	1
N41 (J. Ebbets)	1
N42 (J. Cascio)	1
N43 (F. Maillie)	1
E231	9
E232	3